DTRA-TR-00-6

Technical Report

Advanced Regional Array Studies

Approved for public release; distribution is unlimited.

September 2001

Prepared for:
Defense Threat Reduction Agency
8725 John J. Kingman Road, MS-6201
Ft. Belvoir, VA 22060-6201

DSWA01-97-C-0128

Tormod Kvaerna

Prepared by:

NORSAR
P.O. Box 51
N-2027 Kjeller, Norway

DESTRUCTION NOTICE:

Destroy this report when it is no longer needed.
Do not return to sender.

PLEASE NOTIFY THE DEFENSE THREAT REDUCTION AGENCY, ATTN: ADM, 8725 JOHN J. KINGMAN ROAD, MS-6201, FT BELVOIR, VA 22060-6201, IF YOUR ADDRESS IS INCORRECT, IF YOU WISH IT DELETED FROM THE DISTRIBUTION LIST, OR IF THE ADDRESSEE IS NO LONGER EMPLOYED BY YOUR ORGANIZATION.

DISTRIBUTION LIST UPDATE

This mailer is provided to enable DTRA to maintain current distribution lists for reports. (We would appreciate you providing the requested information.)

- ☐ Add the individual listed to your distribution list.
- ☐ Delete the cited organization/individual.
- ☐ Change of address.

Note:
Please return the mailing label from the document so that any additions, changes, corrections or deletions can be made easily. For distribution cancellation or more information call DTRA/ADM

NAME: _____

ORGANIZATION: _____

OLD ADDRESS	NEW ADDRESS
_____	_____
_____	_____
_____	_____

TELEPHONE NUMBER: ( ) _____

DTRA PUBLICATION NUMBER/TITLE	CHANGES/DELETIONS/ADDITIONS, etc.) *(Attach Sheet if more Space is Required)*
_____	_____
_____	_____
_____	_____

DTRA or other GOVERNMENT CONTRACT NUMBER: _____

CERTIFICATION of NEED-TO-KNOW BY GOVERNMENT SPONSOR (if other than DTRA):

SPONSORING ORGANIZATION: _____

CONTRACTING OFFICER or REPRESENTATIVE: _____

SIGNATURE: _____

CUT HERE AND RETURN

DEFENSE THREAT REDUCTION AGENCY
ATTN: ADM
8725 John J. Kingman Road, MS-6201
Ft Belvoir, VA 22060-6201

DEFENSE THREAT REDUCTION AGENCY
ATTN: ADM
8725 John J. Kingman Road, MS-6201
Ft Belvoir, VA 22060-6201

REPORT DOCUMENTATION PAGE		Form Approved OMB No. 0704-0188

1. AGENCY USE ONLY (*Leave blank*)	2. REPORT DATE	3. REPORT TYPE AND DATES COVERED
	010900	Technical 970904-990930

4. TITLE AND SUBTITLE

Advanced Regional Array Studies

5. FUNDING NUMBERS

C - DSWA 01-97-C-0128
PE - 4630
PR - CD
TA - CD
WU - DH64934

6. AUTHOR(S)

Tormod Kvaerna

7. PERFORMING ORGANIZATION NAME(S) AND ADDRESS(ES)

NORSAR
Post Box 51
N-2027 Kjeller, Norway

8. PERFORMING ORGANIZATION REPORT

684

9. SPONSORING/MONITORING AGENCY NAME(S) AND ADDRESS(ES)

Defense Threat Reduction Agency
8725 John J. Kingman Road, MS-6201
Fort Belvoir, VA 22060-6201

TDCN/Dainty

10. SPONSORING/MONITORING AGENCY REPORT NUMBER

DTRA-TR-00-6

11. SUPPLEMENTARY NOTES

This work was sponsored by the Defense Threat Reduction Agency under RDT&E RMC code B 4630 D CD CD 64934 C340 25904D.

12a. DISTRIBUTION/AVAILABILITY STATEMENT

Approved for public release; distribution is unlimited.

12B. DISTRIBUTION CODE

13. ABSTRACT (Maximum 200 words)

We have addressed the problem of optimizing the site-specific seismic threshold monitoring method in order to achieve the highest possible automatic monitoring capability of particularly interesting areas, such as the Novaya Zemlya testing area, and the Indian and Pakistani test sites. For the Novaya Zemlya test site, where a regional monitoring network is available, we obtain a monitoring capability varying between m_b 2.0 and 2.5 during normal noise conditions. Based on data from the teleseismic network observing the Indian and Pakistani tests of 1998, we obtain a monitoring capability in the range m_b 2.8-3.0 for these test sites.

In order to fully automate the site-specific threshold monitoring method, we have developed an automatic explanation facility for analysis of the threshold traces. In this way threshold peaks caused by events located outside the target region can be discarded from further analysis.

14.SUBJECT TERMS

Seismology
Threshold Monitoring
Surface Waves
Test Sites

15.NUMBER OF PAGES

94

16. PRICE CODE

17. SECURITY CLASSIFICATION OF THIS PAGE	18. SECURITY CLASSIFICATION OF REPORT	19. SECURITY CLASSIFICATION OF ABSTRACT	20. LIMITATION OF ABSTRACT
UNCLASSIFIED	UNCLASSIFIED	UNCLASSIFIED	SAR

CLASSIFIED BY:

N/A since Unclassified

DECLASSIFY ON:

N/A since Unclassified

13. ABSTRACT (Continued)

We have also extended the site-specific threshold monitoring method to process surface waves. An important results of this study is the demonstration of the significant benefits of using a shorter period band (8-12 seconds) instead of the traditional processing band (17-24 seconds) for processing surface waves at regional disturbances during an aftershock sequence.

Table of Contents

Figures

Tables

Section 1
Summary

Continuous seismic threshold monitoring is a technique that has been developed over the past several years to assess the upper magnitude limit of possible seismic events that might have occurred in a geographical target area. The method provides continuous time monitoring at a given confidence level, and can be applied in a site-specific, regional or global context.

We address the problem of optimizing the site-specific approach in order to achieve the highest possible automatic monitoring capability of particularly interesting areas. **Section 2** addresses the application of the method to cases where a *regional* monitoring network is available. We have in particular analyzed events from the region around the Novaya Zemlya (NZ) nuclear test site to develop a set of optimized processing parameters for the arrays SPITS, ARCES, FINES, and NORES. From analysis of the calibration events we have derived values for beamforming steering delays, filter bands, short-term average (STA) lengths, phase travel-times (P and S waves), and amplitude-magnitude relationships for each array. By using these parameters for threshold monitoring of the Novaya Zemlya testing area, we obtain a monitoring capability varying between m_b 2.0 and 2.5 during normal noise conditions.

The advantage of using a network, rather than a single station or array, for monitoring purposes becomes particularly evident during intervals with high global seismic activity (aftershock sequences), high seismic noise levels (wind, water waves, ice cracks) or station outages. For a selected two-month time period (November-December 1997), all time intervals with network magnitude thresholds exceeding m_b 2.5 were visually analyzed, and we found that all of these threshold peaks could be explained by teleseismic, regional, or local signals from events outside the Novaya Zemlya testing area. We could therefore conclude within the confidence level provided by the method that no seismic event of magnitude exceeding 2.5 occurred at the Novaya Zemlya test site during this two-month time interval.

As an example of particular interest in a monitoring context, we apply optimized threshold processing of the SPITS array for a time interval around the 16 August 1997 m_b 3.5 event in the Kara Sea. We show that this processing enables us to detect a second, smaller event from the same site (m_b 2.6), occurring about 4 hours later. This second event was not defined automatically by standard processing.

Section 3 addresses the application of the optimized site-specific threshold monitoring method to regions covered by a *teleseismic* or a *combined regional-teleseismic* network. We apply the method to the Indian and Pakistani nuclear test sites, and show results during the periods of nuclear testing by these two countries in May 1998. Since the coverage by regional stations in these areas is poor, an optimized approach requires the use of selected, high-quality stations at teleseismic distances.

To optimize the threshold monitoring of these test sites, we use as calibration events either one of the nuclear explosions or a nearby earthquake. From analysis of the calibration events we derive values for array beamforming steering delays, filter bands, short-term averages (STA) lengths, phase travel-times (P waves), and amplitude-magnitude relationships for each station. By applying these parameters, we obtain a monitoring capability of both test sites that is in the range m_b 2.8-3.0 using teleseismic

stations only. When including the nearby Nilore station to monitor the Indian tests, we show that the threshold can be reduced by about 0.4 magnitude units. In particular, we demonstrate that the Indian tests on 13 May 1998, which were not detected by any known seismic station, must have corresponded to a magnitude (m_b) of less than 2.4.

We also discuss the effect of a nearby aftershock sequence on the monitoring capability for the Pakistani test sites. Such an aftershock sequence occurred in fact on the day of the last Pakistani test (30 May 1998), following a large (m_b 5.5) earthquake in Afghanistan located about 1100 km from the test site. We show that the threshold monitoring technique has sufficient resolution to suppress the signals from these interfering aftershocks without significantly affecting the true peak of the nuclear explosion on the threshold trace.

The research described in **Section 4** has focused on the development of a fully automatic peak explanation facility for analysis of the magnitude threshold traces. There are often instances when the monitoring threshold is temporarily increased because of signals from events located outside the region of interest. For complete monitoring, we have until recently manually investigated the cause of these threshold peaks. The procedure used has been to compare the time intervals of the short duration threshold peaks to event and signal detection information found in standard event bulletins or signal detection lists. If a threshold peak could confidently be associated with an event located outside the target area, we considered it highly unlikely that another event simultaneously took place within the target area.

The purpose of the automatic peak explanation facility is to minimize the need for manual classification of the threshold peaks such that manual analysis will only be necessary when events within the actual target region occur. Although the focus is the Novaya Zemlya test site, the method will be directly applicable to any geographical areas like the other underground nuclear test sites.

The first step in an automatic analysis of the threshold traces is to identify significant threshold peaks. In order to accommodate both undulations in the long-term background noise level and noise variability, we have developed a peak detection method based on estimates of the noise variance and the long-term trend of the threshold trace. For the NZ test site, the peak detection threshold is typically around m_b 2.0. Secondly, we have developed a procedure for association of network threshold peaks with arrivals detected at each individual station. If we can confidently state that these arrivals originated outside the target area, the corresponding threshold peak can reasonably be discarded from further consideration.

For arrivals detected at array stations, the estimated azimuth and apparent velocity can effectively be used as criteria for sorting out arrivals originating outside the target area. An additional criterion for sorting out non-critical arrivals is a confident association with an event located outside the target area. Such phase associations are currently available in the PIDC Reviewed Event Bulletin (REB) and the NORSAR automatic regional bulletin.

Section 5 is entitled "Continuous assessment of upper limit M_S ". It describes a new application of the continuous seismic threshold monitoring technique (TM) to long-period data, for the purpose of obtaining a continuous assessment of surface wave magnitude (M_S). We present initial results from investigating the relation between PIDC station magnitudes and STA based estimates calculated from bandpass filtered data, as well as a case study with monitoring of surface waves from a mining area on

the Kola peninsula during and after a M_S 7.6 earthquake in Turkey.

An important result of this study is the demonstration of the significant benefits of using a shorter period band (8-12 seconds) instead of the traditional processing band (17-24 seconds) for processing surface waves at regional distances during an after-shock sequence. In this study, we have used the three IMS arrays ARCES, NOA and SPITS, and applied a site-specific technique to investigate the threshold trace during a large earthquake sequence. A natural follow-up of this work would be to include additional long-period and broadband IMS stations for the same time interval, in order to assess the improvements in monitoring capability when using a network with better azimuthal coverage.

As in the short period case, there is a trade-off between optimizing the TM process for site-specific studies and developing a more general TM application for global surface wave monitoring. Among the main issues is the sharpness of the beam lobe, which depends upon the filter setting, the STA time windows and the tolerance for travel-time deviations. Another issue is the need for regional corrections, which may be greater than in the short-period case. For example, the significant difference between oceanic, continental and combined oceanic-continental paths are important for surface wave propagation, but have little or no counterpart in analyzing short-period P and S waves.

Section 6 provides advice on how the methods developed under the current contract can be integrated into the processing pipelines at the PIDC. In 1998 NORSAR released a global variant of the Threshold Monitoring (TM) method to be used for continuous assessment of event detection capability of the CTBT International Monitoring System (IMS). The system is currently running within the continuous processing pipelines at both the International Data Center (IDC) in Vienna, Austria, and the Prototype International Data Center (PIDC) in Arlington, VA, USA. Our recommendations are building on the developments made and the experience gained during the implementation of the global TM system.

Section 2
Optimized Threshold Monitoring of the Novaya Zemlya Test Site

2.1 Introduction.

Continuous seismic threshold monitoring (TM) is a technique that has been developed at NORSAR over the past decade to monitor a geographical area continuously in time. Data from a network of arrays and single stations are combined and "steered" toward a specific area to provide an ongoing assessment of the upper magnitude limit of seismic events that might have occurred in that area.The basic principles have been described by Ringdal and Kværna (1989, 1992), who showed that this method could be useful as a supplement to event detection analysis. Recently, Kværna and Ringdal (1999) have shown the potential of using the TM method for global network capability estimation.

The main purpose of the TM technique is to highlight instances when a given threshold magnitude is exceeded, thereby helping the analyst to focus on those events truly of interest in a monitoring situation.The analyst can then apply traditional tools in detecting, locating and identifying the source of the disturbance. The capability achieved by the threshold monitoring method is in general dependent upon the size of the target area, and it is convenient to consider three basic approaches:

Site-specific threshold monitoring: A seismic network is focused on a small area, such as a known test site. As discussed in this paper, this narrow focusing enables a high degree of optimization, using site-station specific calibration parameters and sharply focused array beams.

Regional threshold monitoring: Using a dense geographical grid, and applying site-specific monitoring to each grid point, threshold contours for an extended region are computed through interpolation. In contrast to the site-specific approach, it is usually necessary to apply regionally averaged attenuation relations, and the monitoring capability will therefore not be quite as optimized.

Global threshold monitoring: Using a global seismic network, and taking into account that phase propagation time is up to several tens of minutes, global travel-time and attenuation tables are applied, possibly with regional corrections, with a much coarser geographical grid than in the regional approach.

A main goal of the current contract has been to further develop the site-specific approach. by optimizing the monitoring capabilities for a given target site, using calibration events to optimize parameters such as bandpass filters, beam steering parameters, and window lengths for short term averaging. We thus aim at utilizing the *full resources* of the monitoring network to focus on a specific target site in order to enable monitoring of this target site with as high a capability as the network and available calibration information will allow. We will in this section address the case of a regional monitoring network, with special application to the Novaya Zemlya (NZ) test site.

The area around Novaya Zemlya is characterized by generally low natural seismicity. However, during the last decades a few small events have been observed and several studies have been conducted to locate and characterize these events (e.g., Marshall et al.,(1989); Ringdal (1997); Ringdal et al., 1997). Some of these events were only detected at the regional arrays operated by NORSAR.

We show that threshold monitoring using this network can be used to achieve a high capability for continuous monitoring of this site.

2.2 Method Description.

2.2.1 Generating the Threshold Trace.

Let us assume that a network of seismic stations is available for monitoring a specified target site. For simplicity of presentation, we will assume that these are all array stations, able to provide phase velocity and back-azimuth information for detected signals. Extension to the single-station case is straightforward. The stations can be located either at regional or teleseismic distances.

Following Ringdal and Kværna (1989), let us consider a network of seismic stations (i=1,2....,N) and a number of seismic phases (j=1,2,...,M). For a seismic event of magnitude m_b=m an estimate $\hat{m}_{ij}$ of m is given by

$$\hat{m}_{ij} = \log S_{ij} + b_j(\Delta, h) \tag{1}$$

where S_{ij} is a measurement of the signal amplitude of the *j-th* phase at the *i-th* station and $b_j(\Delta, h)$ is a distance-depth correction factor for the *j-th* phase.

In standard formulas for magnitude, the measured amplitude S_{ij} is usually estimated as A/T, i.e., amplitude of ground displacement divided by dominant signal period. In our case, we will use the short-term average (STA) at the expected signal arrival time as a measurement of signal amplitude, so that $STA_{ij} = S_{ij}$. The value is measured on an array beam or a single channel filtered in an appropriate frequency band.

Traditionally, relation (1) is defined only for the time window corresponding to a detected seismic event. We will now consider the right-hand side of (1) as a continuous function of time. Define the threshold parameter $a_{ij}(t)$ as follows:

$$a_{ij}(t) = \log STA_{ij}(t) + b_j(\Delta, h) \tag{2}$$

Equation (2) represents a function which can be considered as a continuous representation of the upper magnitude limit for a hypothetical seismic event at a given geographical location (target region). It coincides with the event magnitude estimate if an event occurs at that site. The function is, by definition, tied to a specific station and a specific phase.

The threshold parameter traces are then time-aligned in accordance with the expected travel-time of the considered phase, such that the time reference for all threshold parameter traces is the origin time at the target region. For each time sample we obtain a network-based representation of the upper magnitude limit by considering the function:

$$g(m, t) = 1 - \prod_{i,j}\left(1 - \Phi\left(\frac{(m - a_{ij}(t))}{\sigma_{ij}}\right)\right) \tag{3}$$

where m is event magnitude, σ_{ij} is the standard deviation of the assumed magnitude distribution for the i-th station and j-th phase, and Φ denotes the standard (0,1) normal distribution function. This network-based representation assumes statistical independence among the different station/phase observations, and the function g(m,t) is discussed in more detail by Ringdal and Kværna (1989).

The function $g(m, t)$ is the probability that a given (hypothetical) seismic event of magnitude m at time t would generate signals that exceed the observed noise values at at least one station of the network. For a given t, the function $g(m, t)$ is a monotonically increasing function of m, with values between 0 and 1. A 90 per cent upper limit at time t is defined as the solution to the equation

$$g(m, t) = 0.90 \tag{4}$$

The solution is a function of t, which we will denote $m_{T90}(t)$. We call this the *threshold trace* for the network and target region being considered.

It is important to interpret the 90 per cent limit defined above in the proper way. It should not be considered as a 90 per cent network detection threshold, since we have made no allowance for a signal-to-noise ratio which would be required in order to detect an event, given the noise values. Rather, the computed level is tied to the actually observed noise values and to the fact that any hypothetical signal must lie below these values. Our 90 per cent limit represents the largest magnitude of a possible hidden event, in the sense that above this limit, there is at least a 90 per cent probability that one or more of the observed noise values would be exceeded by the signals of such an event.

Although not intuitively obvious, it follows from eqs. (3) and (4) that the threshold trace is dominated by the "best" stations in the network (i.e., the stations with the highest sensitivity for events in the target area). Thus, the resulting value of the computed threshold trace remains essentially unchanged if a station with poor detectability is added to the network. In practice, we have found that a cost-effective approach is to select the 5 - 10 most sensitive stations, preferably with good azimuthal distribution, to monitor a given target area.

An example might serve to illustrate the threshold monitoring principle. Suppose that we are monitoring the NZ test site, and thereby aligning the threshold traces of the network stations in accordance with the expected travel-times of the considered phases. If an interfering event occurs in Scandinavia, the signals will cause significant increase on the Scandinavian stations. But due to travel-time differences the threshold traces will not line up as expected for an event at the target site (NZ), and consequently there will at any time be stations in the network that are little affected by the interfering event. If these stations have normal background conditions, they can be used to show that any hypothetical event at the NZ test site is likely to have been very small.

2.2.2 Tuning the Threshold Trace.

Let us consider threshold monitoring of a specific target area of limited geographical extent. The size of the target area may vary depending upon the application, but typically such an area might be a few tens of kilometers in diameter.

A basic assumption is that the target area is defined such that all seismic events within the area show similar wave propagation characteristics.

Parameters such as travel-times of the different phases and steering delays for array beamforming are typically obtained by processing previous events located in the target area. However, our experience has shown that these parameters can be well estimated on the basis of standard earth models. The most critical parameters for threshold monitoring are the filter frequency bands, the STA window lengths and the magnitude calibration, which are discussed below.

Filter bands and STA lengths

The optimum frequency filters and STA window lengths for signal level estimation are derived from analysis of previous events located in the region. Several different filters and STA window lengths are tested by comparing the maximum STA value of the signal to the mean and variance of the background noise. The analysis procedure is as follows:

- Select a number of representative time intervals with background noise, bandpass filter and create STA traces. We assume a lognormal distribution of the STA data, and convert to a normal distribution by taking the logarithm of each sample STA value.
- Determine the mean ($\log(STA)_{mean}$) and standard deviation (σ_{noise}) of the noise observations.
- Determine how many standard deviations the calibration signals are above the noise level by calculating the quantity
  $nstdev = (\log(STA)_{max} - \log(STA)_{mean})/\sigma_{noise}$, where $\log(STA)_{max}$ is measured at the maximum of the signal. A high *nstdev* value indicates a low probability of having noise peaks approaching the level of the signals.
- Compare the *nstdev* measurements for different bandpass filters and STA lengths and use this number as an indicator for selecting the optimum STA length and filter band.

In general, there is a trade-off between the STA window length and the sharpness of the focusing on the target site. A long STA window will make it more likely that off-site events will produce significant peaks on the threshold trace. This trade-off must be seen in conjunction with the desire to maximize the variable *nstdev* defined above.

Magnitude calibration

The distance-depth correction factors $b_j(\Delta, h)$ in (1) and (2) can either be determined by using globally averaged values (e.g., Veith and Clawson, 1972), by applying a regional model, or by calibration for path effects to the specific target area. The latter method is the most accurate and is preferable, assuming that data from previous calibration events are available. We then obtain the necessary magnitude calibration factors from processing previous events with known magnitudes, using the relation

$$\hat{b}_{ij} = \hat{m}_j - \log(\hat{STA}_{ij}) \qquad (i = 1, \ldots, K; j = 1, \ldots, L) \tag{5}$$

where $\hat{b}_{i,\,j}$ is our estimate of the magnitude correction factor for phase i and event j,

$\hat{m}_j$ is the estimate of the magnitude for event j (based on independent network observations), and $\hat{STA}_{ij}$ is our estimate of the signal level at the predicted arrival time of phase i for event j. K is the number of phases considered (there might be several stations and several phases per station), and L is the number of events.

The magnitude correction factor to be used for phase i is then given by

$$b_i = \frac{1}{L} \cdot \sum_{j=1}^{L} \hat{b}_{ij} \tag{6}$$

2.3 Calibrating the Network for Monitoring Novaya Zemlya.

We have implemented a site-specific monitoring capability for the Novaya Zemlya (NZ) test site by deriving optimized processing parameters for the four arrays ARCES, SPITS, FINES and NORES (see **Figure 1**).

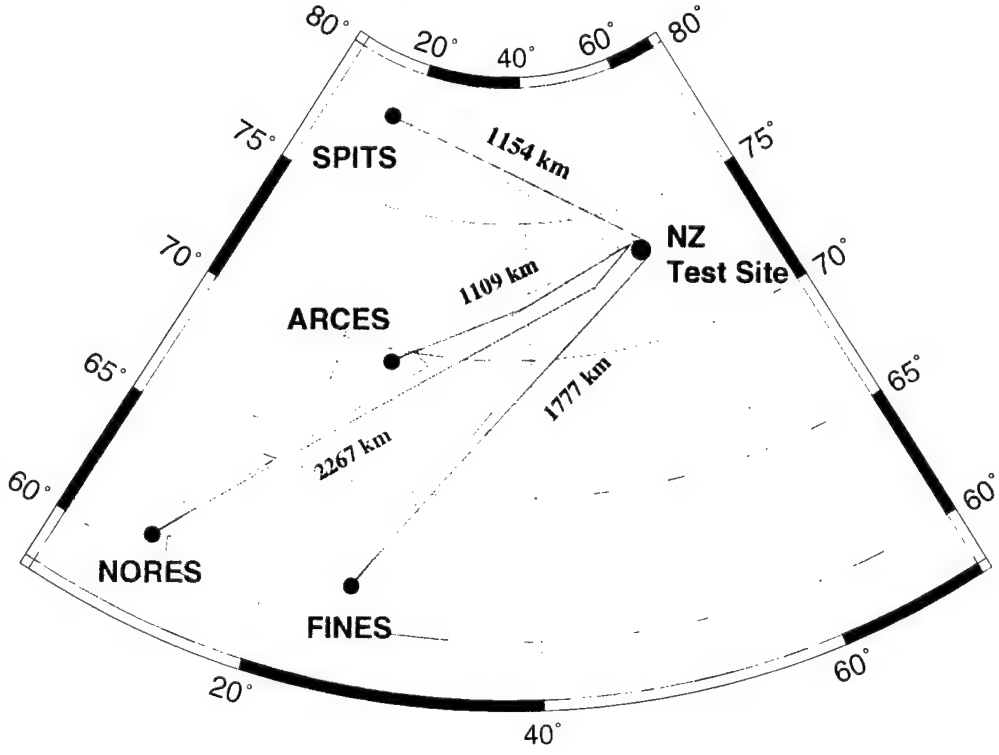

Figure 1. *Map of Novaya Zemlya and the locations of the four arrays (SPITS, ARCES, FINES, and NORES) used to monitor the region around the former underground nuclear test site.*

For all arrays except SPITS, the processing parameters could be derived from previous recordings of underground nuclear explosions at the test site. In particular, the m_b 5.7 nuclear test of October 24, 1990 was well recorded by these three arrays, and the data from this event will be used to derive the optimum parameters for threshold monitoring. For SPITS no recordings of NZ nuclear tests are available, and we have to use

recordings of other events in the region to derive the optimum processing parameters. A detailed map of the Novaya Zemlya target area and selected seismic events in the region is shown in **Figure 2**.

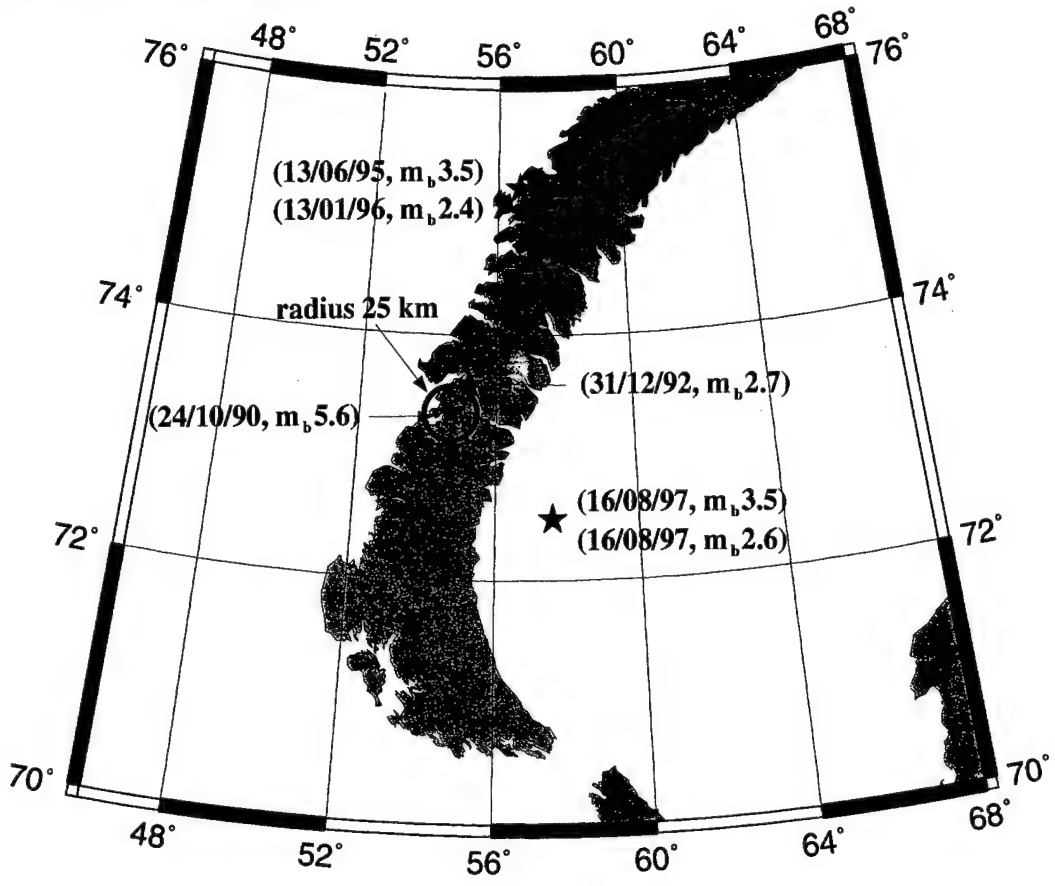

Figure 2. *Map of Novaya Zemlya and the monitoring region around the former underground nuclear test site. The radius of the circle is 25 km. Also shown are the locations of selected events in the region.*

In the following we describe the calibration data used for each of the four arrays, with a summary of the processing parameters **Table 1**.

Table 1. TM processing parameters for the NZ test site.

Station	Distance (km)	Phase	Obs. slowness (s/deg)	Obs. back azimuth (deg)	Frequency band (Hz)	STA length (s)	Travel time (s)	Travel time tolerance (s)	Mag. calib.	St. dev of calib.
NORES	2267.3	P	10.9	33.6	1.5 - 3.5	1.0	281.4	±4*s*	2.68	0.3
ARCES	1108.6	P	11.2	62.2	3.0 - 5.0	5.0	147.5	±4*s*	2.84	0.3
-	-	S	23.2	64.3	3.0 - 5.0	3.0	254.2	±6*s*	2.99	0.3
FINES	1776.9	P	11.6	29.6	2.0 - 4.0	1.0	224.2	±4*s*	2.78	0.3
SPITS	1154.2	P	14.8	109.6	3.0 - 5.0	5.0	152.6	±6*s*	2.95	0.3
-	-	S	23.0	97.6	3.0 - 5.0	3.0	263.0	±8*s*	3.11	0.4

2.3.1 Processing Parameters for NORES.

The ISC event information for the October 24, 1990 explosion is the following:

Date	Time	Latitude	Longitude	Depth	m_b	M_S
24/10/90	14:57:58.3	73.360	54.674	0.0	5.7	4.3

At NORES, only the P-phase is clearly observed from explosions at the NZ test site (see **Figure 3**), and the theoretical travel-times and slownesses of the Fennoscandian crustal and upper mantle model (Mykkeltveit and Ringdal, 1981) are given in **Table 2**.

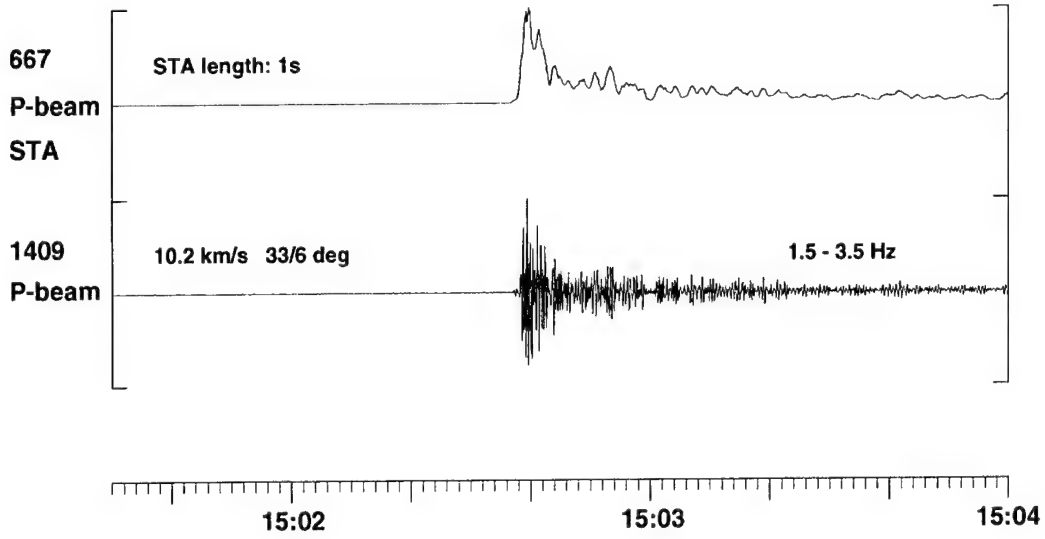

NORES October 24, 1990

Figure 3. *The lower trace is a NORES P- beam of data from the Oct. 24, 1990 event, filtered in the optimum frequency band 1.5-3.5 Hz. The upper trace is the short-term-average (STA) functions of the filtered beams. The maximum amplitudes given together with the trace labels are the original digital counts multiplied by the NORES calibration constant (0.006838 nm/counts) at 1 Hz.*

Table 2. Theoretical back-azimuth, travel-time and slowness of NORES P-phases from events at the NZ test site.

Distance	Back-azimuth	P travel-time	P slowness
2267.3 km	34.4 deg	279.4 s	13.06 s/deg

The actual processing parameters found from analysis of the event are given in the first row of **Table 1**, and we will in the following discuss the derivation of these parameters.

The target region for monitoring is a circular region with a radius of 25 km centered around the northern Novaya Zemlya test site, see **Figure 2**. Optimum processing will be achieved in this target area. At distances greater that 25 km from the central target point, the monitoring capability will gradually decrease, but will still be significant.

Back-azimuth and slowness

The back-azimuth and slowness used for beamforming are taken from f-k analysis of the P-phase. As seen in **Table 1**, these values (33.6 deg, 10.9 s/deg) differ somewhat from the theoretical values given in **Table 2**. Structural inhomogeneities along the propagation path and estimation uncertainties at arrays are the causes for this difference. The time window used for f-k analysis is centered around the peak amplitudes of the phase.

Filter band

For optimum monitoring capability we would like to filter the data in the frequency band where we expect to have the highest signal-to-noise ratio (SNR) for small events. In **Figure 4** we show for the Oct. 24, 1990, event the NORES P-spectrum (of the P-beam) together with a beam spectrum of the noise preceding the phase. For this event, the best SNR was found in the 1.5 - 3.5 Hz frequency band.

In order to determine if the best SNR is expected to occur at higher frequencies for smaller explosions at the Novaya Zemlya test site, we have calculated P-wave spectra of NORSAR recordings (seismometer 01A01) of six Novaya Zemlya explosions of varying magnitudes. These events were also used by Ringdal (1997) for investigation of the P/S ratios.

The spectra are shown in **Figure 5**, together with an average background noise spectrum. The SNRs of the different P-arrivals relative to the background noise are shown in **Figure 6.** Although we can not interpret the spectra above the cutoff frequency of the anti-aliasing filter (4.75 Hz), it seems that for the smallest event there is a slight increase in the frequencies providing the best SNR.

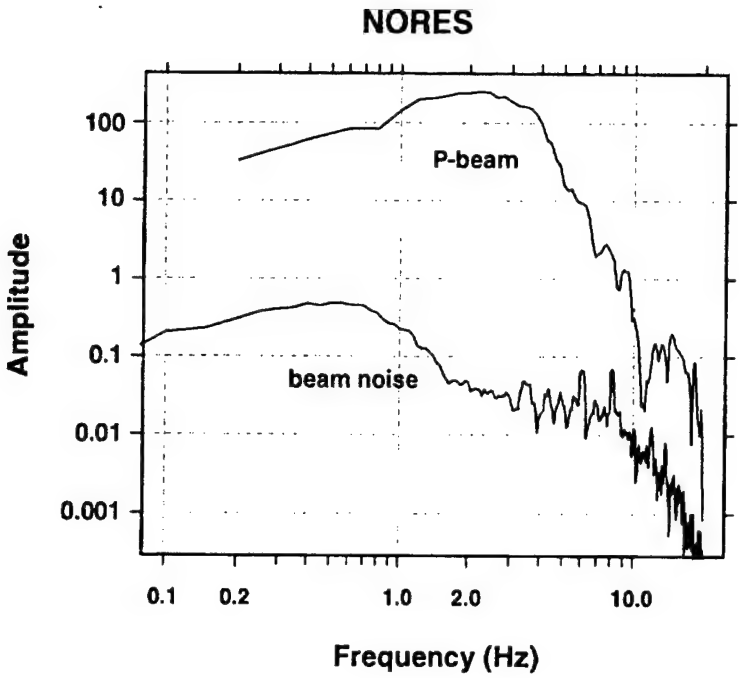

Figure 4. *This figure shows the spectrum of the P-phase beam of the 24 Oct. 1990 event recorded at NORES, together with a spectrum of the background noise preceding the P-phase for the same beam.*

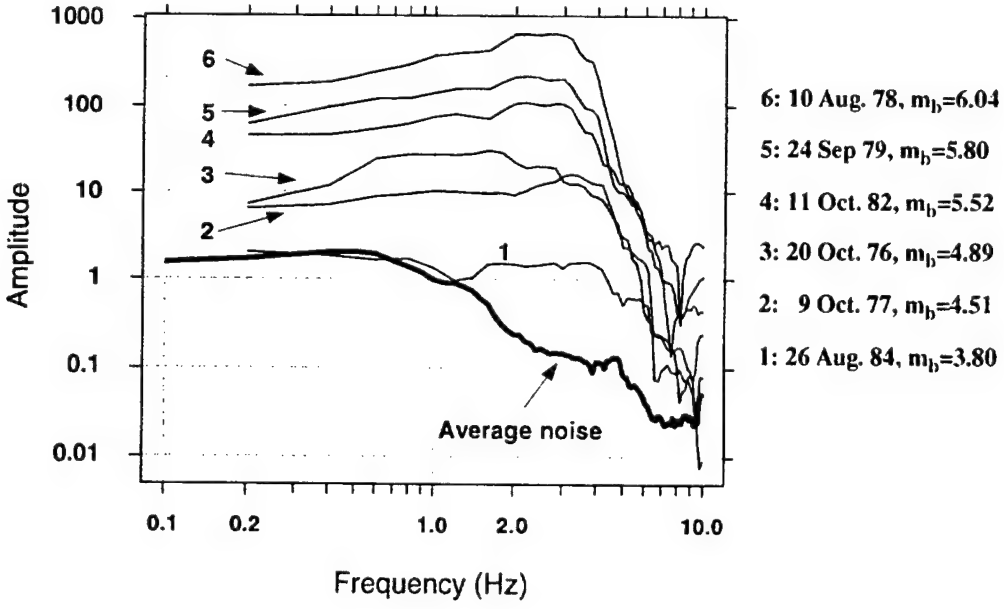

Figure 5. *P-spectra of NORSAR recordings (seismometer 01A01) of six Novaya Zemlya explosions of varying magnitudes. An average background noise spectrum from seismometer 01A01 is also plotted. Notice the strong anti-aliasing filter at NORSAR with a cutoff at 4.75 Hz.*

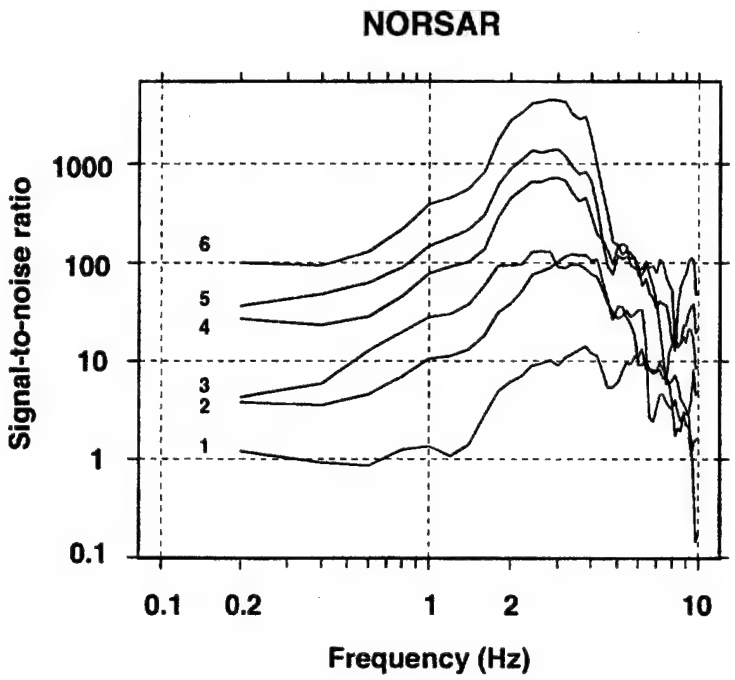

Figure 6. *Signal-to-noise ratio (SNR) calculated from the NORSAR signal and noise spectra shown in* ***Figure 5****.*

Traditionally, the site-specific TM algorithm has made use of only one frequency band for each station-phase combination. If an event occurs for which the "best" frequency band (i.e. the band with best SNR) happens to be outside of the chosen band, it will result in a situation where the signal for the event may not be seen as a clear peak on the resulting threshold trace.

For example, in earlier site-specific monitoring studies of the NZ test site, we have for NORES used the frequency band 1.5-3.5 Hz. However, for the "new year's eve" event on 31 Dec. 1992, located about 35 km north-east of the test site, the NORES beam had a detectable signal only above 4 Hz. As a result, the NORES TM trace did not show a clear peak for this event. Nevertheless, the calculated threshold (upper 90% limit) was quite accurate, since the signal energy in this band (comparable to nuclear explosions) was definitely below the calculated upper threshold.

A clear peak in the TM trace would, in this case, have occurred if we had used, e.g., a 4-8 Hz filter for the site-specific monitoring. The trade-off would have been that optimum performance would not have been achieved for any nuclear explosion with "standard" frequency characteristics.

Travel-times, travel-time tolerances, and STA lengths

For traditional detection and location processing, the onsets of the different phases are the important parameters. On the other hand, for threshold monitoring we focus on the maximum amplitude of the different phases, and the travel-times to the phase maxima are the parameters used.

For the Oct. 24, 1990 event, the travel-time to the peak STA of the P-phase was mea-

sured at 281.4 s (see **Table 1**). Along with the travel-time, we also introduce a time tolerance to accommodate for differences in travel-time for events within the source region. From the theoretical ray-parameter (see **Table 2**), we find that for NZ events at NORES the change in travel-time is 13.06 seconds per degree, such that for events within a circular radius of 25 km, the corresponding tolerance is about $\pm 3s$. To accommodate a possible change in the position of the peak signal energy we have increased the travel-time tolerance to $\pm 4s$.

As seen from **Figure 3,** the main signal energy has a rather short duration at NORES (distance 2267 km), and we believe that an STA length of 1 second will be close to optimum.

Magnitude calibration and uncertainty

In earlier studies (e.g., Kværna, 1996) we have shown that the STA measurement can be used as a very good approximation of A/T (amplitude/period) commonly used for estimating the body-wave magnitude m_b. The magnitude relation then becomes $m_b \approx \log(\pi/2 \cdot STA \cdot calib) + b$, where *calib* is the calibration constant at the reference period and b is a correction factor. The global average magnitude of the 24 Oct. 1990 event was reported by ISC as 5.7. By substituting this into the magnitude relation given above, we find a b correction factor of 2.68 m_b units for NORES P-phases.

Along with the correction factor b, the calculation of the 90% magnitude thresholds requires an estimate of the uncertainty (standard deviation) of the magnitude measurements. According to Ringdal (1977) the standard deviation of the logarithm of signal amplitudes is found to be slightly below 0.2 m_b units among NORSAR sensors covering a circular area with a radius of approximately 25 km. By using the reciprocity principle, a similar standard deviation can be assumed for events originating within the Novaya Zemlya target area, as shown in **Figure 2**. In addition to the inherent σ of about 0.2 for events in the target region, the log amplitude observation of the Oct. 24, 1990 event is associated with the same uncertainty. By adding these variances together, we get a σ close to 0.3 which will be used in the calculation of the 90% magnitude thresholds.

2.3.2 Processing Parameters for ARCES.

At ARCES, both P-and S-phases are clearly observable from explosions at the Novaya Zemlya test site (see **Figure 7**), and the corresponding theoretical travel-times and slownesses are given in **Table 3**. The TM processing parameters for ARCES have been derived along the same lines as for NORES, and the results are summarized in **Table 1,** rows 2 and 3.

As seen by comparing **Figure 7** with **Figure 3**, the main P-wave energy at ARCES has a longer duration than at NORES, and a 5 second STA length was chosen for TM processing. For the S-phase, the main energy had a duration of about 3 seconds in the 3 - 5 Hz filter band.

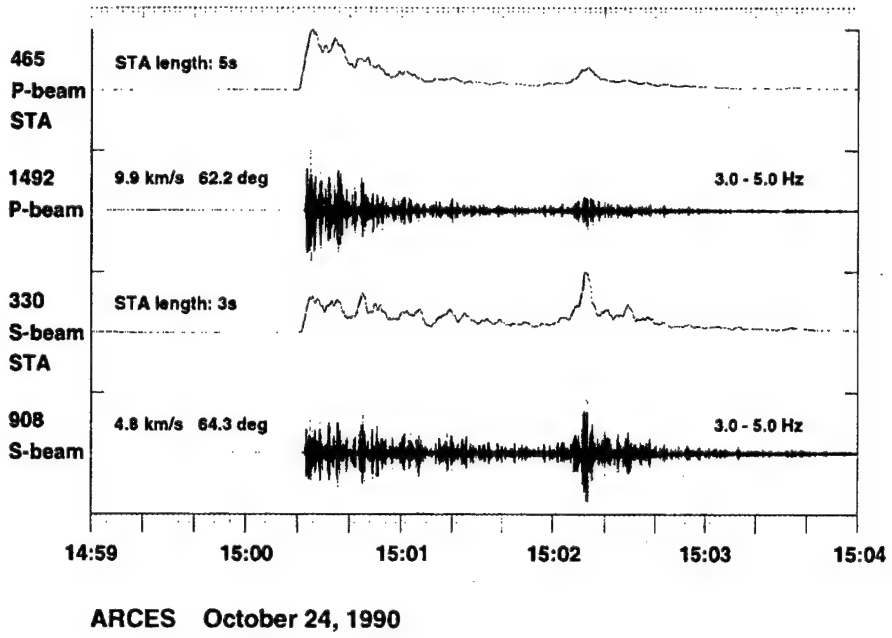

Figure 7. *Traces no. 2 and 4 from the top of the figure are ARCES P- and S-beams from the Oct. 24, 1990 event, filtered in the optimum frequency band 3.0 - 5.0 Hz. Traces no. 1 and no. 3 are short-term-averages (STAs) of the filtered beams.*

Table 3. Theoretical back-azimuth, travel-times and slownesses of ARCES P- and S-phases from events at the NZ test site.

Distance	Back-azimuth	P travel-time	P slowness	S travel-time	S slowness
1108.6 km	54.2 deg	142.2 s	13.52 s/deg	246.4 s	22.97 s/deg

Concerning the optimum filter bands, we show in **Figure 8** the ARCES P- and S-spectra (measured on the P- and S-beams) together with an average noise spectrum of the beams for the Oct. 24, 1990 event. The highest SNR for both phases is found in the passband 3 - 5 Hz, which is the filter to be used for TM processing.

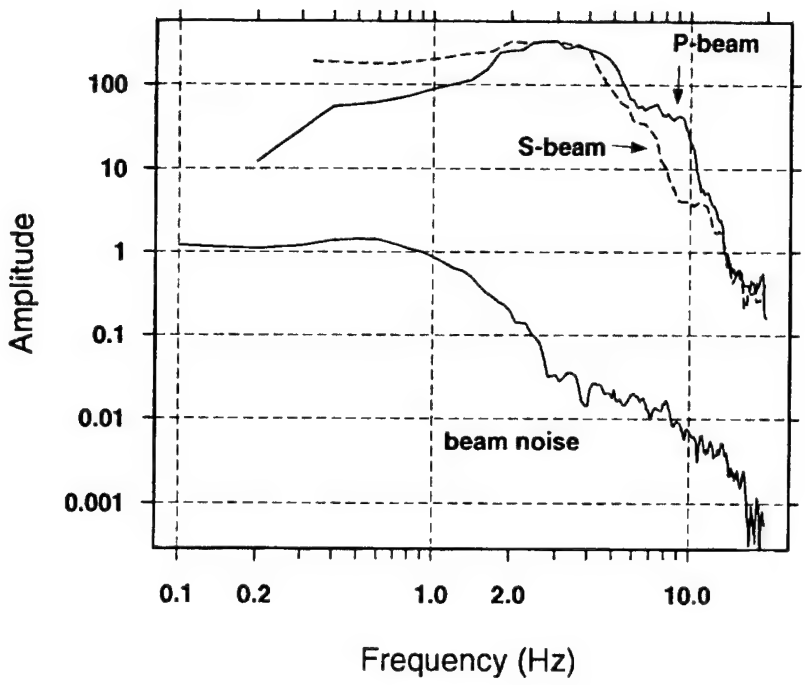

Figure 8. *This figure shows beam spectra of the P- and the S-phase of the Oct. 24., 1990 event recorded at ARCES, together with an average beam spectrum of background noise preceding the P-phase.*

2.3.3 Processing Parameters for FINES.

At FINES, the signals from the Oct. 24, 1990 explosion were clipped, but there were unclipped data available on the low-gain channel FIA0_sl, which was damped 30 dB relative to the regular channel FIA0_sz. A plot of the P-wavetrain at FINES is shown in **Figure 9**.

At this distance around 16 degrees, the first P-waves have their turning points in the depth range of 150 to 400 km. Further P-onsets arrive from other discontinuities in the upper mantle (e.g., 400 km, 670 km). The strongest signal arriving about 10 seconds after the first P, is most likely associated with the critical point of the 400 km triplication. A higher apparent velocity from f-k analysis supports this interpretation. The theoretical travel-time and slowness according to the model of Mykkeltveit and Ringdal (1981) are given in **Table 4**

Table 4. Theoretical back-azimuth, travel-time and slowness of FINES P-phases from events at the NZ test site.

Distance	Back-azimuth	P travel-time	P slowness
1776.9 km	30.1 deg	221.6 s	13.18 s/deg

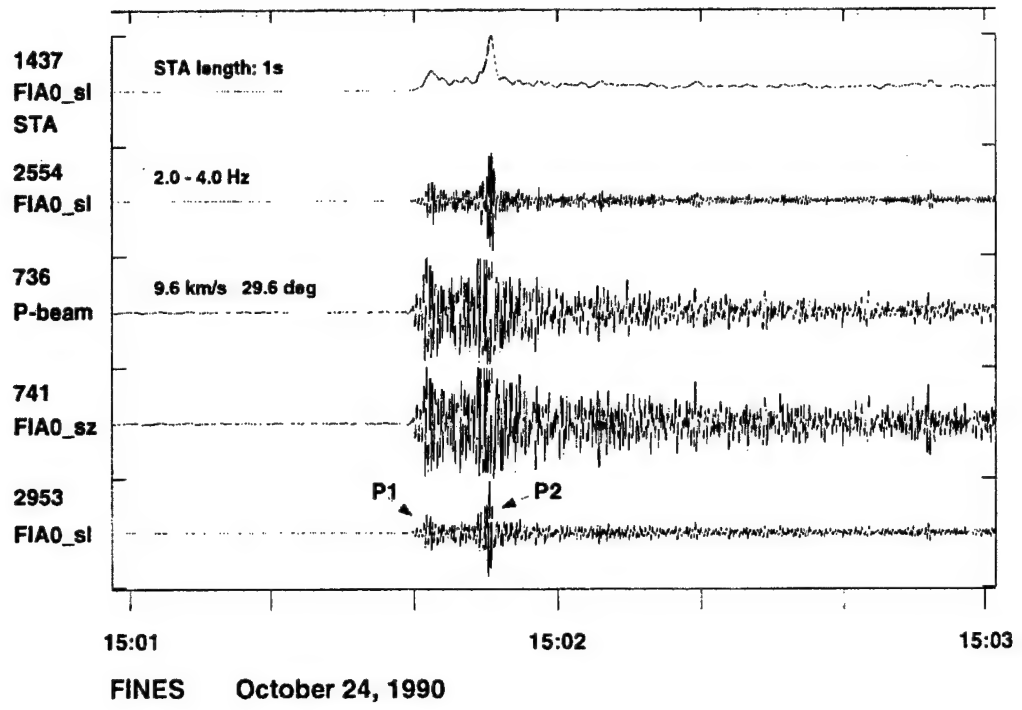

Figure 9. *FINES data from the Oct. 24, 1990 event. Phases P1 and P2 are clipped on the regular channel (FIA0_sz) and array beam (P-beam) traces. Trace no. 2 is the low-gain (FIA0_sl) data filtered between 2.0 and 4.0 Hz, which is the frequency band providing the highest SNR. The upper trace is the corresponding STA trace.*

Back-azimuth and slowness

A detailed picture of the P-wavetrain at FINES is shown in **Figure 10**. For the array data we have estimated by f-k analysis the back-azimuth and slowness of both the clipped **P1** and **P2** arrivals, as well as the unclipped arrival preceding **P1**, called **P0**. The clipping does, of course, influence the f-k results to some degree, but our general experience is that even for clipped data quite accurate back-azimuth and slowness estimates can be obtained. For **P0** and **P1**, the estimated apparent velocities are close to 8.5 km/s, whereas for **P2** the estimate is 9.6 km/s. Because of the relatively small diameter of the FINES array (about 2 km), the effect of a slight mis-steering of the beams has little effect on the resulting beam amplitude. When comparing the **P0** amplitude on the beam (using the steering parameters of **P2**) with the **P0** amplitude of the center array element FIA0_sz, we find an amplitude reduction of less than 0.1 dB. We will therefore use a single beam in the TM analysis, with steering parameters derived from **P2**, for representing the signal amplitudes of both **P1** and **P2**.

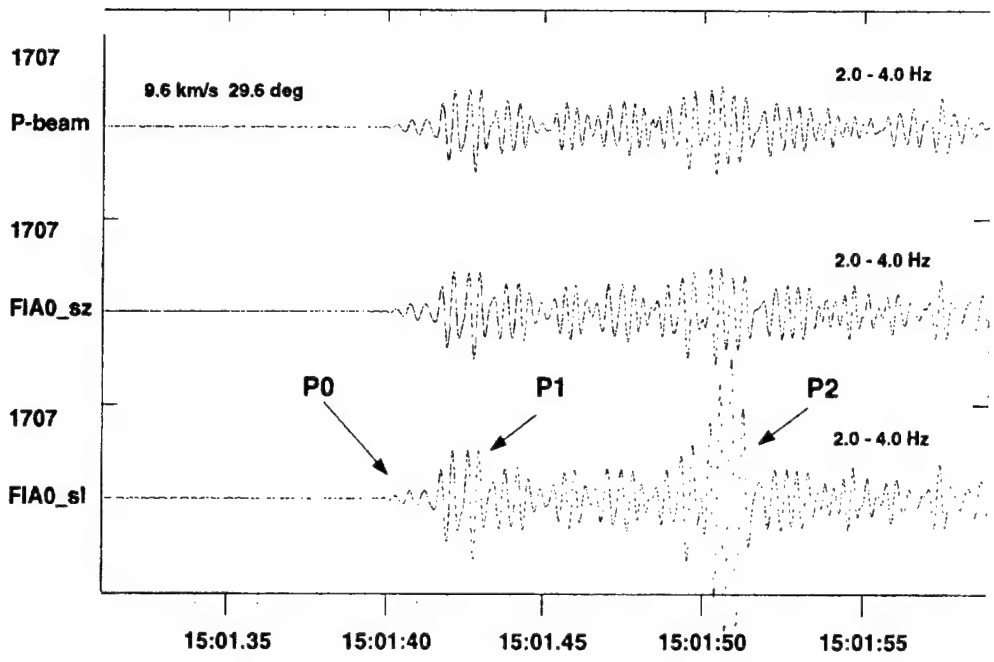

Figure 10. *FINES data from the Oct. 24, 1990 event, filtered between 2.0 and 4.0 Hz. The traces are scaled with the calibration constants at 1 Hz. Notice that the amplitudes of P0 are approximately equal on all three traces, validating our strategy of deriving TM processing parameters like magnitude calibration, STA lengths and travel-times from the single low-gain channel FIA0_sl.*

Filter band

In **Figure 11** we show the FINES (FIA0_sl) spectra of the main P arrivals **P1** and **P2** for the Oct. 24, 1990 event. When comparing the signal spectra with the spectrum of the preceding noise, we find the highest SNR between 2 and 4 Hz. Although the noise spectrum is somewhat lowered on the beam, the SNR still attains its highest value in the 2 - 4 Hz band.

Travel-times, travel-time tolerances, and STA lengths

The travel-times and travel-time tolerances have been set along the same lines as for NORES. From **Figure 10** we find that the main energy of the signals **P1** and **P2** has a duration between 1 and 2 seconds. An STA length of 1 second will be used for threshold monitoring purposes.

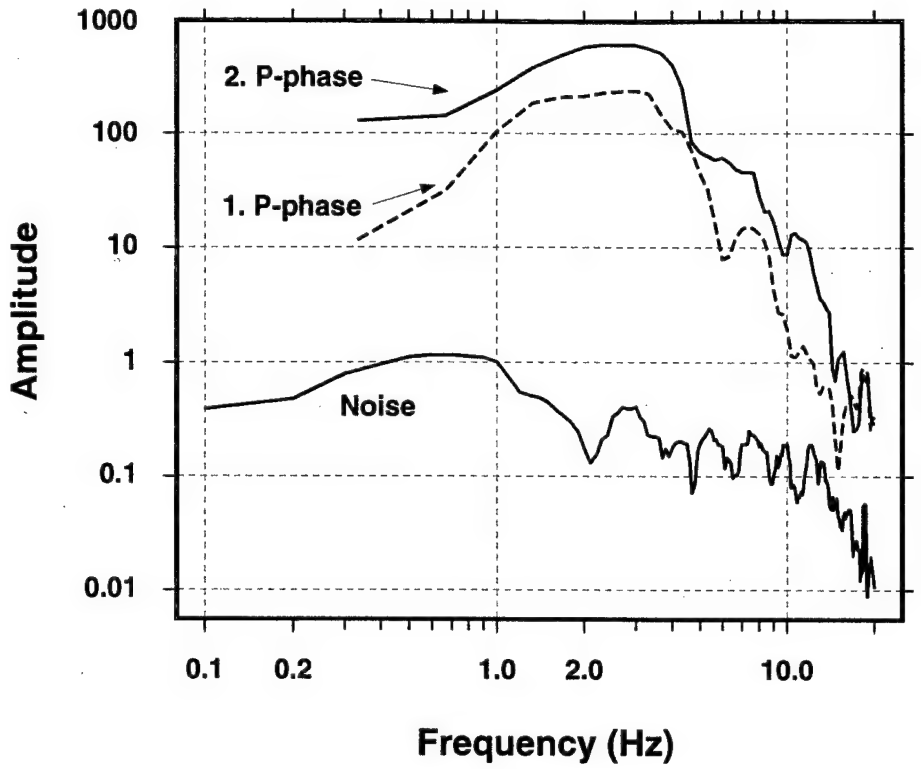

Figure 11. *This figure shows spectra of the two main P-arrivals from the Oct. 24, 1990 event recorded at FINES channel FIA0_sl, together with a spectrum of the preceding noise.*

Magnitude calibration and uncertainty

During the fall of 1993, the FINES array was upgraded with a new system, such that the system currently running is different from the one which recorded the 24 Oct., 1990 event. But as seen from **Figure 12**, the velocity response curves have similar shapes above 1 Hz. This should enable us to still use the magnitude-amplitude relation $m_b \approx \log(\pi/2 \cdot STA \cdot calib) + b$, but now with a *calib* of 0.01 nm/count instead of 0.0226 nm/count as for the old system.

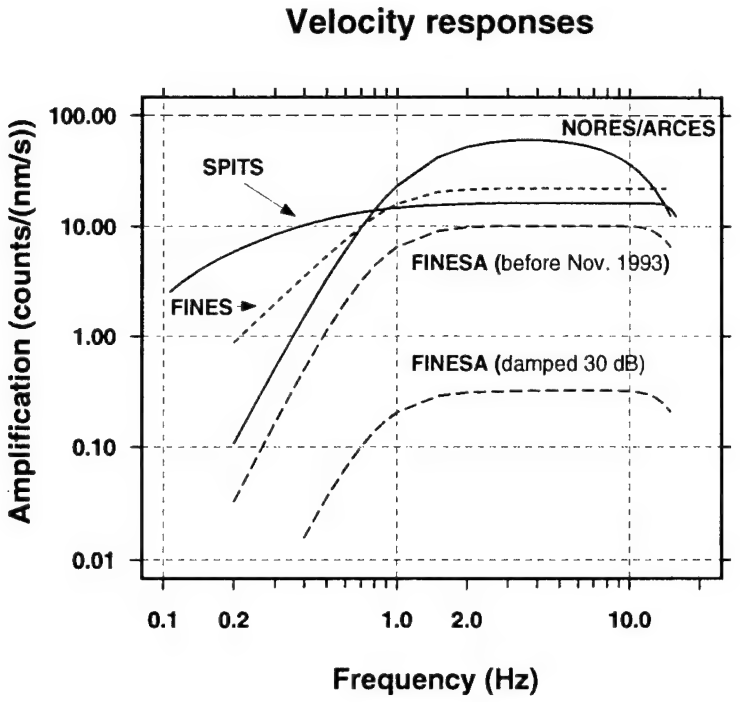

Figure 12. *Velocity responses of the systems used for monitoring of the Novaya Zemlya test site. FINESA was the name of the FINES system prior to Nov. 1993. Notice that the velocity responses of both FINES and SPITS are almost flat in the passband above 1 Hz, whereas the NORES and ARCES systems are slightly curved with a peak between 3 and 5 Hz.*

With the lack of additional Novaya Zemlya explosions recorded at FINES, we can not rule out the possibility that the large amplitude of the secondary P-arrival **P2** may be caused by a local source focusing effect. E.g., the 31 December 1992 event ($m_b \approx 2.7$) located about 25 km north of the test site provided a FINES P magnitude of only 2.2 when using the **P2** magnitude calibration (see **Table 5**) derived from the 24 October 1990 explosion. This observation indicates that the monitoring levels based on the **P2** magnitude calibration may be somewhat low when considering an area with a radius of 25 km around the test site. In order to be conservative with respect to the estimated magnitude thresholds, we will only consider the **P1** phase and its associated magnitude calibration (see **Table 5** and **Table 1**).

Table 5. TM processing parameters for FINES.

	Back-azimuth	Slowness	Filter band	STA length	Travel time to peak STA	Travel-time tolerance	Magnitude calibration	St.dev of magnitude calibration
P1	29.6 deg	11.6 s/deg (9.6 km/s)	2.0-4.0 Hz	1 s	224.2 s	±4s	2.78	0.3
P2	29.6 deg	11.6 s/deg (9.6 km/s)	2.0-4.0 Hz	1 s	232.6 s	±4s	2.35	0.3

2.3.4 Processing Parameters for SPITS

The Spitsbergen array (SPITS) became operational for the first time during the fall of 1992, and thus has no recordings of nuclear explosions from the Novaya Zemlya test site. The SPITS array is located at approximately the same distance from the Novaya Zemlya test site as the ARCES array (see **Figure 1**), and analysis of other events in the Novaya Zemlya region has revealed remarkably similar waveforms both with respect to observable phases (P and S) and frequency content of the signals. As an example, in **Figure 13** we show the SPITS and ARCES recording of the m_b 3.5 event of 13 June 1995, located about 200 km north of the test site. In order to make the waveforms more directly comparable, the ARCES recording has been has adjusted to the SPITS response function (see **Figure 12**). The distances to SPITS and ARCES are 1065 km and 1290 km, respectively. When comparing the single channel observations SPA0_sz with ARA0_sz (traces no. 3 and 6 from the top, respectively), we find slightly higher amplitudes at SPITS, but the general seismogram characteristics with distinct P- and S-phases remain the same. Also notice that the reduction of the beam amplitudes at ARCES is larger that at SPITS, which is due to the larger aperture of the ARCES array.

The theoretical travel-times and slownesses from the Novaya Zemlya test site to SPITS according to the model of Mykkeltveit and Ringdal (1981) are given in **Table 6** below.

Table 6. Theoretical back-azimuth, travel-times and slownesses of SPITS P- and S-phases from events at the NZ test site.

Distance	Back-azimuth	P travel-time	P slowness	S travel-time	S slowness
1154.2 km	97.6 deg	147.3 s	13.26 s/deg	255.2 s	22.97 s/deg

Our strategy for deriving the SPITS processing parameters for monitoring of the Novaya Zemlya test site is to analyze the recordings of the two m_b 3.5 events located north and south-east of the test site. The locations of these events are shown in **Figure 2**. For discussion of the magnitude estimates of the reference events, see Ringdal (1996, 1997).

For the 13 June 1995 event, shown in **Figure 13**, the SPITS recording contains clear P- and S-phases, where the S amplitude slightly exceeds the P-amplitude. For the other reference event of 16 August 1997, shown in **Figure 14**, the S amplitude is significantly smaller than the P amplitude, and the P amplitude is about half the amplitude of the 13 June 1995 event.

In order to explain the differences in SPITS amplitudes for the two reference events, there are several factors involved. First, there is a difference in distance for the two events, 1065 km versus 1290 km. Second, the propagation path from the 16 August 1997 event crosses the structure of the Novaya Zemlya island, which may lead to a significant attenuation of the phase amplitudes. In addition, there are also differences in P- and S- excitation of the two sources as well as local structural effects.

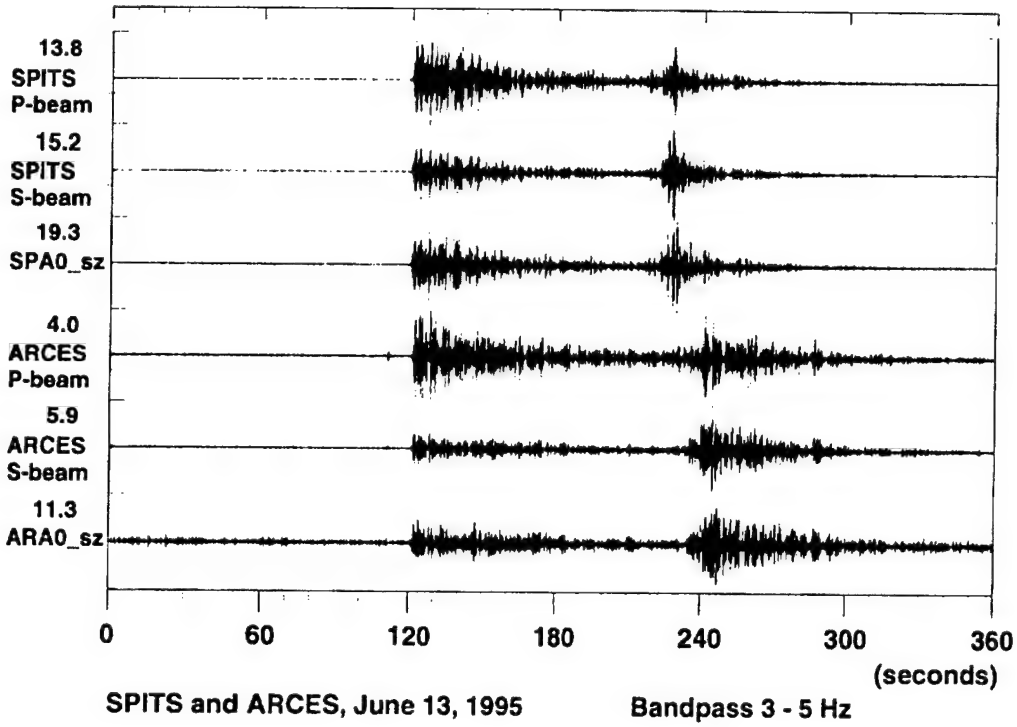

Figure 13. *SPITS and ARCES recordings of the 13 June 1995 event (m_b 3.5) located about 200 km north of the Novaya Zemlya test site. To make the data directly comparable, the ARCES recording has been converted to the SPITS response. The maximum amplitudes given together with the trace labels are the original digital counts multiplied by the calibration constant at 1 Hz. The distances to SPITS and ARCES are 1065 km and 1290 km, respectively.*

The propagation path from the Novaya Zemlya test site to the SPITS array is quite similar to the propagation path from the 13 June 1995 event. Both are located on the western side of Novaya Zemlya and the propagation paths to SPITS do not include the crossing of any major geological structures. The 13 June 1995 event is, however, located about 90 km closer to SPITS than the Novaya Zemlya test site.

As mentioned earlier, the propagation path from the 16 August 1997 event includes the crossing of the structure of the Novaya Zemlya island, and the distance to SPITS is about 135 km longer than for events at the test site.

In order to be conservative with respect to the estimation of the magnitude thresholds at the Novaya Zemlya test site, we will for SPITS use the mean calibration factors derived from the two reference events. To accommodate the uncertainty in the magnitude estimates of the reference events, we will in addition increase their magnitudes by 0.2 m_b units to 3.7. And finally, the standard deviation associated with the S amplitude-magnitude relation is increased from 0.3 to 0.4 m_b units.

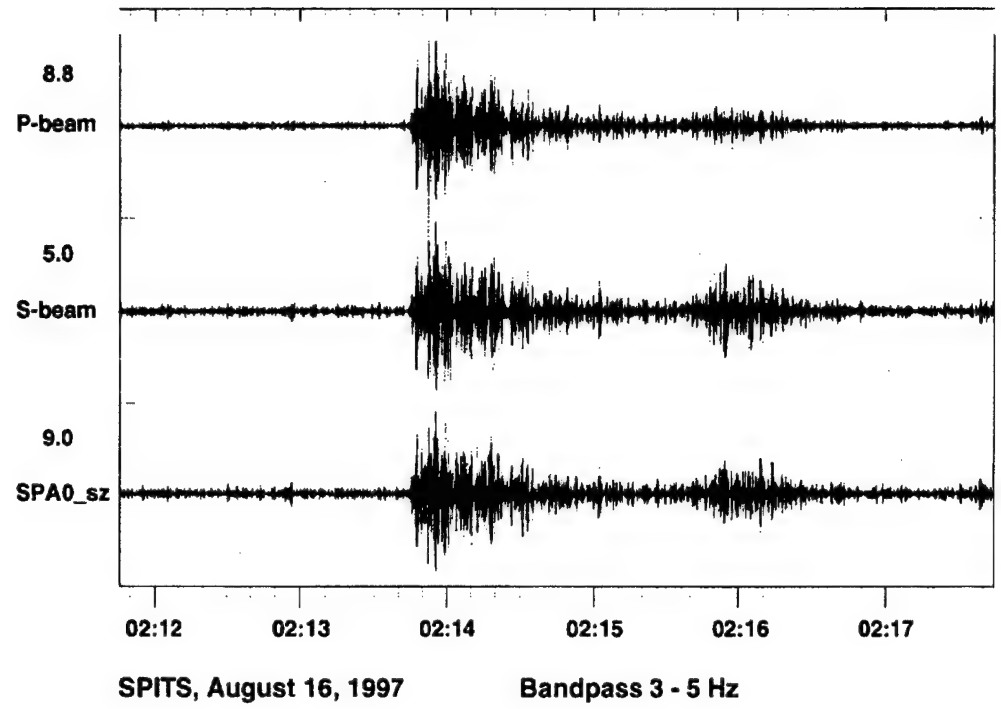

Figure 14. *SPITS recording of the 16 August 1997 event (mb 3.5) located in the Kara Sea, south-east of the Novaya Zemlya test site. The maximum amplitudes given together with the trace labels are the original digital counts multiplied by the calibration constant at 1 Hz. The distance to SPITS is 1290 km.*

Back-azimuth and slowness

For estimation of the expected back-azimuths of phases from events at the NZ test site, we have analyzed P-phases from four events located in the vicinity of the test site. These are given in **Table 7**, together with the P-phase azimuth and slowness estimates from the automatic f-k analysis.

Table 7. Events in the NZ region recorded at SPITS.

Date	*Time (GMT)*	*Lat*	*Lon*	*Delta (km)*	*Azi Theo*	*Slow Theo*	*Azi Obs*	*Slow Obs*	*Azi Diff*	*Slow Diff*
95/06/13	*19.22.37.9*	*75.2*	*56.7*	*1065*	*87.4*	*13.52*	*98.7*	*15.03*	*11.3*	*1.51*
96/01/13	*17.17.23.0*	*75.2*	*56.7*	*1065*	*87.4*	*13.52*	*98.9*	*15.23*	*11.5*	*1.71*
97/08/16	*02.11.00.0*	*72.5*	*57.6*	*1290*	*97.5*	*13.25*	*112.1*	*15.03*	*14.6*	*1.78*
97/08/16	*06.19.10.0*	*72.5*	*57.6*	*1290*	*97.5*	*13.25*	*109.0*	*14.26*	*11.5*	*1.01*
Avg.									*12.22*	*1.50*

Also given are the azimuths and slownesses predicted from the local model used for locating events in the Barents region (Mykkeltveit and Ringdal (1981)). As seen from

Table 7, the differences between the observed and predicted values are consistent for the four events. A plot of the mislocation vectors is shown in **Figure 15**, which illustrates this very consistent behavior. In addition, the events given in **Table 7** are located on both the east and west sides of the island of Novaya Zemlya (see **Figure 2**) such that the average mislocation vector derived from these events should also be representative for the NZ test site. The distance from SPITS to the NZ test site is 1154 km, and as seen from **Figure 15**, the theoretical azimuth and slowness for the NZ test site equals the values for the Kara Sea events.

By applying the mean mislocation vector to the theoretical azimuth and slowness of NZ P-phases (97.4 deg, 13.26 s/deg), we end up with values of 109.6 deg for the back-azimuth and 14.76 s/deg for the slowness of P-phases. For S-phases, no such studies have been conducted, and the theoretical steering parameters, given in **Table 6**, will be applied for beamforming.

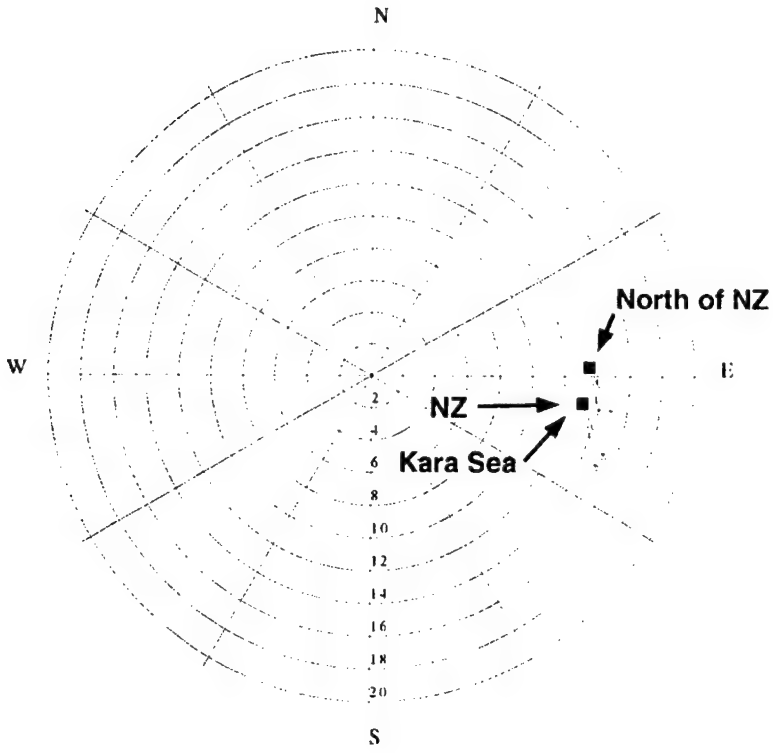

Figure 15. *SPITS mislocation vectors for the four events given in* ***Table 1****. The theoretical azimuths and slownesses of P-phases from the events are given by the filled squares and the observed values from fk-analysis are given by the open circles. The theoretical azimuths and slownesses of P-phases from the NZ test site equal the theoretical values from the Kara Sea events. The distance from SPITS to the NZ test site is 1154 km, 1065 km to the two events located to the north of the test site, and 1290 km to the events in the Kara Sea.*

Filter band

In **Figure 16** we have plotted the P spectra and the spectra of the preceding noise for the two reference events recorded at channel SPA0_sz. For the 13 June 1995 event the best SNR is found for frequencies above 3 Hz. For the 16 August 1997 event the noise level is higher and the best SNR is found above 6 Hz. In order to retain compatibility with the ARCES processing parameters, we will also use the 3 - 5 Hz filter band for SPITS. For intervals with high noise levels, this may not be optimum with respect to threshold monitoring, but as explained by Ringdal (1996) it ensures a more correct magnitude scaling when moving from large to small events

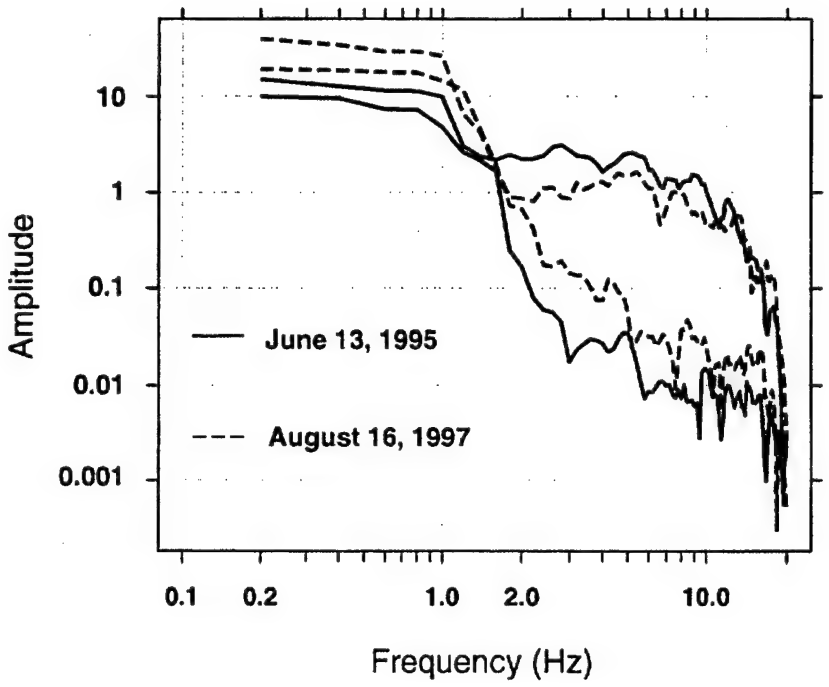

Figure 16. *P spectra and the spectra of the preceding noise for the two reference events recorded at channel SPA0_sz.*

STA lengths

From analysis of the waveforms of the two reference events we find it reasonable to use the same STA lengths as used at ARCES. The durations of the main P and S energy of the reference events recorded at SPITS are quite similar to the durations of P and S signals of the October 24, 1990 explosion recorded at ARCES (see **Figure 7**, **13**, and **14**).

Travel-times and travel-time tolerances

We have shown that recordings at SPITS and ARCES from events near in the Novaya Zemlya region exhibit the same wavetrain characteristics. In addition, the distance from the Novaya Zemlya test site to SPITS and ARCES differ by only 46 km. It is therefore reasonable to assume that the main signal amplitudes at SPITS from potential events at the Novaya Zemlya test site will have the same delay relative to the predicted arrival times as observed at ARCES for the October 24, 1990 event.

To accommodate the additional uncertainty for the travel-time to the signal maxima, the search interval for both P and S is increased with $\pm 2s$ compared to the numbers for ARCES (see **Table 1**).

Magnitude calibration and uncertainty

Under the assumption that the magnitudes of the reference events are both 3.7, we have derived the magnitude calibration factors shown in **Table 8**. For each event the P- and S-beams were steered with back-azimuths and apparent velocities from f-k analysis of the phases. The data were bandpass filtered between 3 and 5 Hz, and the STA lengths were 5 seconds for P and 3 seconds for S.

Table 8. Magnitude calibration factors at SPITS.

Event	P amplitude	P magnitude calibration	S amplitude	S magnitude calibration
June 13, 1995	4.45	2.86	5.90	2.73
August 16, 1997	2.95	3.03	1.04	3.49
Mean calibration	-	2.95	-	3.11

2.3.5 Remarks on the Derivation of Processing Parameters.

During the derivation of optimum processing parameters for threshold monitoring of the Novaya Zemlya test site we have also tried to be conservative with respect to the estimation of the magnitude thresholds. Even though the uncertainties in the amplitude-magnitude relation are included in the calculations, we have in particular avoided taking advantage of the strong secondary P arrival at FINES under the assumption that this may be due to a very local source focusing effect. In addition, for the events used for tuning of the SPITS parameters, we have increased the magnitude estimates from 3.5 to 3.7.

It should also be emphasized that the target region for monitoring is a circular area with a radius of 25 km centered around the Novaya Zemlya test site. For monitoring outside this area, the current parameter setting derived in this paper is not directly applicable.

Further precision in the parameter setting for ARCES and NORES can possibly be obtained by analyzing all nuclear explosions recorded at these arrays.

2.4 Monitoring Examples for the Novaya Zemlya Test Site.

In order to investigate the utility of the TM method in an operational environment, we have implemented continuous calculation of the threshold level for the NZ test site using the four arrays shown in **Figure 1**. Plots have been generated for each day processed, beginning 1 November 1997. **Figure 17** shows as an example results for 9 February 1998.

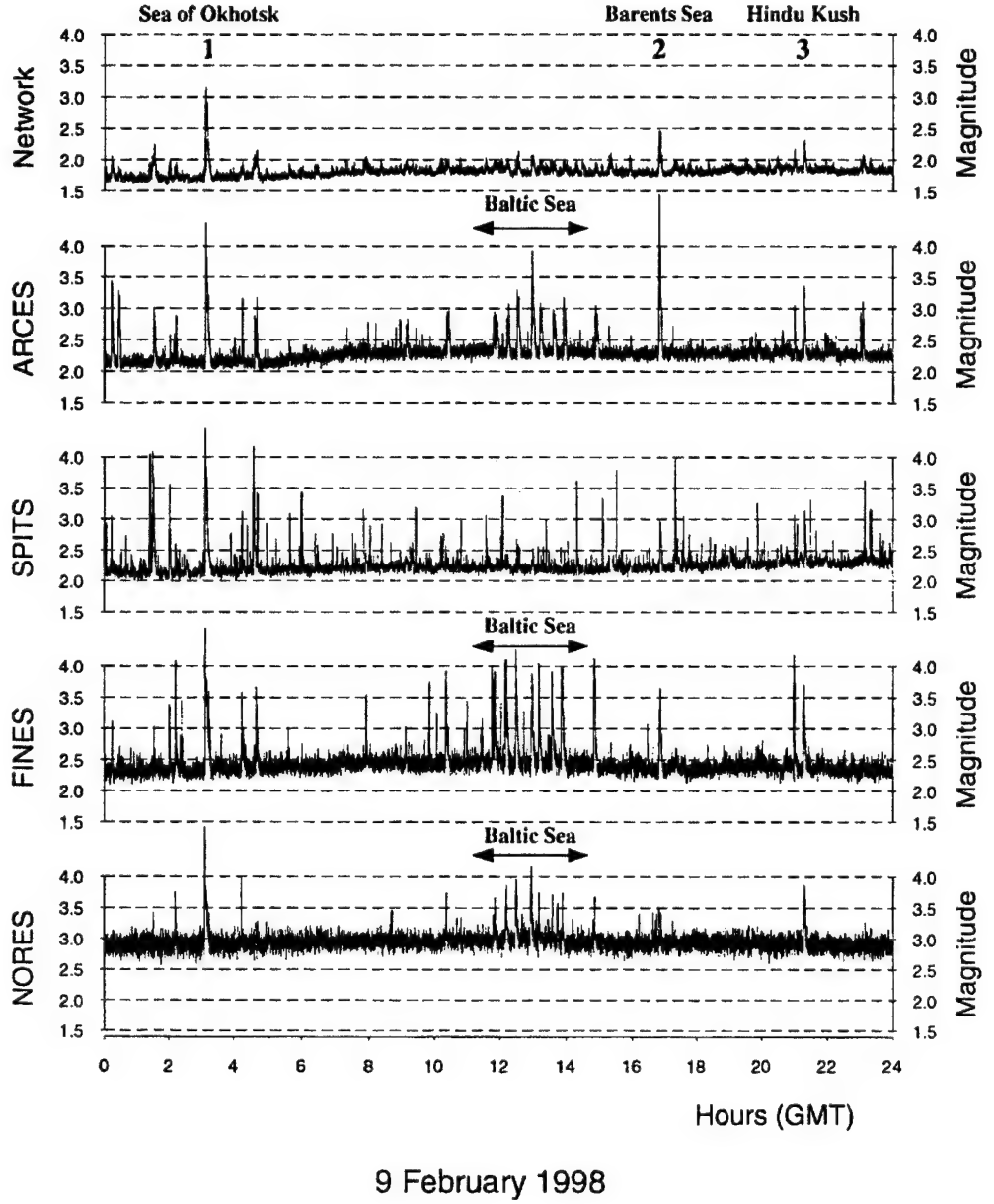

Figure 17. *Example of site-specific threshold monitoring of the Novaya Zemlya test site for 9 February 1998. See text for detailed explanation.*

The plot shows the magnitude thresholds for P-phases at each of the four arrays, with the combined network threshold monitoring trace on top. We have also included S-phases for the two closest arrays (SPITS and ARCES) in the threshold monitoring calculations for Novaya Zemlya, but these traces are not shown on the plot. The network trace is a composite trace taking into account the individual traces for P and S on SPITS and ARCES, P for FINES and P for NORES.

We note that the individual arrays have a number of peaks corresponding to both regional and teleseismic events. For example, a sequence of peaks during the middle of the day (marked on the figure) is especially pronounced on FINES, ARCES, and NORES. These peaks are caused by a sequence of presumed underwater explosions in the Baltic Sea. We note that this sequence of peaks is effectively suppressed on the combined network threshold trace, since the phase arrival times do not correspond to the predicted time pattern for the target area. In fact, the network threshold trace has only three significant peaks, which can all be associated with seismic events detected and located by conventional processing. The peaks numbered 1 and 3 result from earthquakes at teleseismic distances (Sea of Okhotsk and Hindu Kush, respectively). Peak number 2 corresponds to a presumed underwater explosion in the Barents Sea, near the northern coast of the Kola Peninsula. Otherwise, the threshold trace is well below m_b 2.5, thus showing that the monitoring capability is below this level for essentially the entire time period. Within the uncertainties inherent in the statistical formulation, and taking a reservation for the short time instance surrounding the interfering event, we can therefore conclude that no seismic event of m_b 2.5 or larger occurred at the test site for this day.

Figure 18 shows a second example, which covers 16 December 1997. Two important features are illustrated in this figure. First, the key array SPITS happened to be out of operation, resulting in a general deterioration of the combined network capability. Second, there was an unusually large increase in the background noise level at the other key array, ARCES. This increase was caused by a very strong storm system moving through northern Norway at that time, producing increased microseismic noise at ARCES over the entire frequency spectrum. In spite of the coincidence of these two unfavorable factors, we note that the network threshold trace still, in general, remains below magnitude 2.5. There are about 10 peaks slightly exceeding 2.5 on this day, but they can all be "explained" as resulting from interfering events.

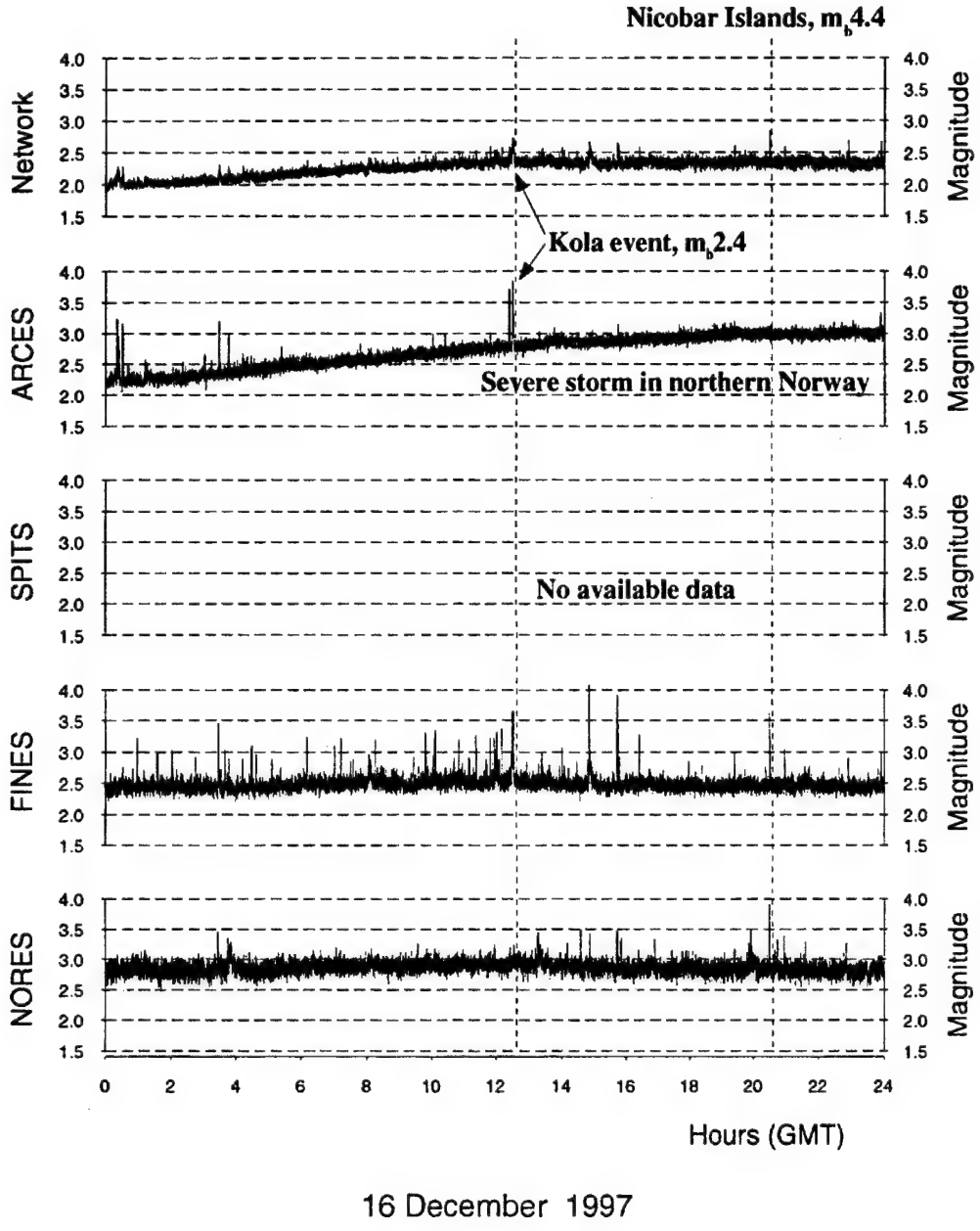

Figure 18. *Example of site-specific threshold monitoring of the Novaya Zemlya test site for 16 December 1997. See text for detailed explanation.*

During a two-month period (November and December, 1997), we analyzed the results in detail, and found 90 peaks on the network threshold trace that exceeded m_b 2.5. Of these, 73 were caused by teleseismic earthquakes, and in particular by a large aftershock sequence near Kamchatka. The remaining 17 peaks were correlated with small earthquakes close to SPITS and some local events in Fennoscandia (mostly mining explosions).

During these two months, the continuous TM method was able to provide results that enabled monitoring of the NZ test site down to m_b 2.0 for most of the time period. All peaks exceeding mb 2.5 were correlated to events outside the target region, so we can therefore conclude at the confidence level inherent in the method that no seismic event of magnitude exceeding 2.5 occurred at the NZ test site during this time period. Although we have not continued to analyze subsequent months in the same detail, we have been able to confirm, within the uncertainty previously discussed, that no seismic event significantly above m_b 2.5 occurred near the test site during all of 1998.

The site-specific threshold monitoring technique can be successfully applied even when using only a single station. This is of particular interest in cases where one station has a much higher capability than other network stations. As an example, in **Figure 19** we show the results of optimized threshold monitoring, using the SPITS array, of the region around the location of the Kara Sea event on 16 August 1997 (Hartse, 1998; Richards and Kim, 1997). Our main reason for using SPITS only is that the other key array, ARCES, was out of operation at the time. Furthermore, we have calibrated the SPITS array to the main event (m_b 3.5) at 02.11 GMT, which was detected and located by the prototype International Data Center in Arlington, Virginia.

The traces in the figure show the magnitude thresholds for the first 12 hours of 16 August 1997. Four peaks stand out on the trace, and the causes of these peaks are the following:

1) The main Kara Sea event (the strongest peak)
2) A series of small disturbances very close to the SPITS array
3) A local/regional event at a distance of about 250 km from SPITS
4) A second, smaller event from the same location as the main Kara Sea event

Thus, in this case we are able, by carefully analyzing the peaks on the threshold trace, to detect and locate the second, smaller Kara Sea event (m_b 2.6), which was not automatically associated and located by either the prototype IDC (Bache et al., 1990) or by the regional detection processing routinely carried out at NORSAR (Mykkeltveit at al., 1990). The reason that this event was not in the NORSAR list of located events is that only the SPITS P-onset was automatically detected, while the S-phase did not exceed the detection threshold. Thus the event did not satisfy the event definition criteria used at NORSAR, which requires at least two matching phases (1 P and 1 S) from the same array or detections at two different arrays.

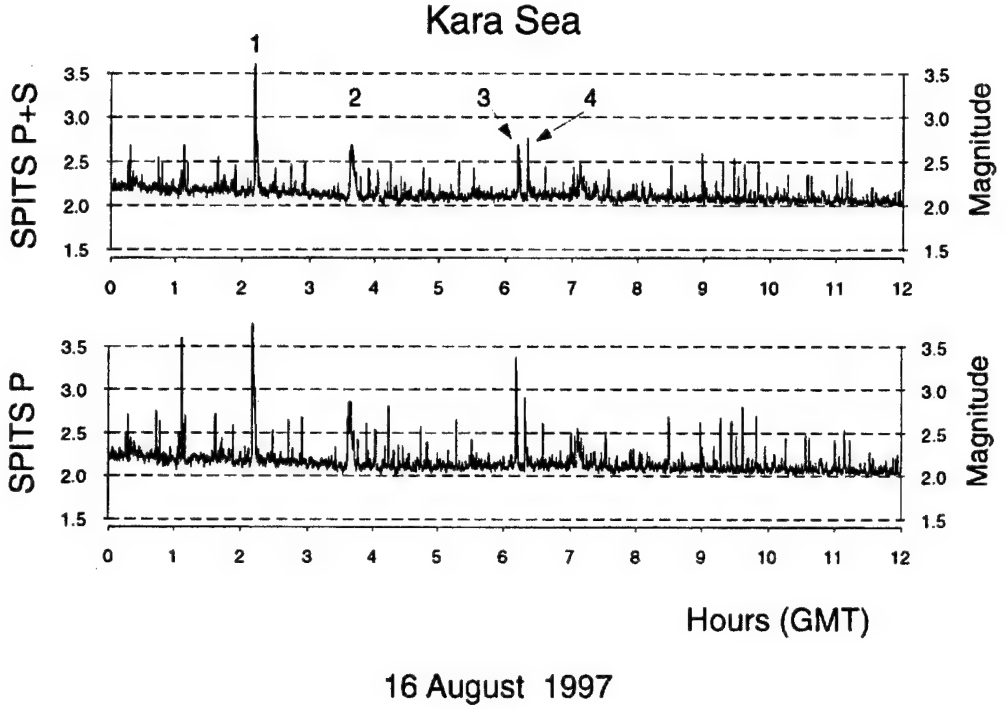

Figure 19. *An example of optimized threshold monitoring of the region around the location of the Kara Sea event, using data from SPITS alone for the first 12 hours of 16 August 1997, calculated when using parameters derived from the event on 02:11 GMT.*

Figure 20 shows waveforms of the two Kara Sea events, as recorded by SPITS. With the appropriate filters and beamsteering, it is quite clear that these two events are from very nearly the same location. This conclusion was further confirmed after analyzing data from the Amderma station in northern Russia (Ringdal et al., 1997). Both the P and S phases at SPITS can be identified visually, and with the aid of additional f-k analysis the coinciding locations of these two events can be further confirmed. We might note that such additional f-k analysis is a useful supplement in the threshold monitoring procedure, and such analysis has indeed confirmed that the additional peaks in **Figure 19** are not consistent with a Kara Sea location.

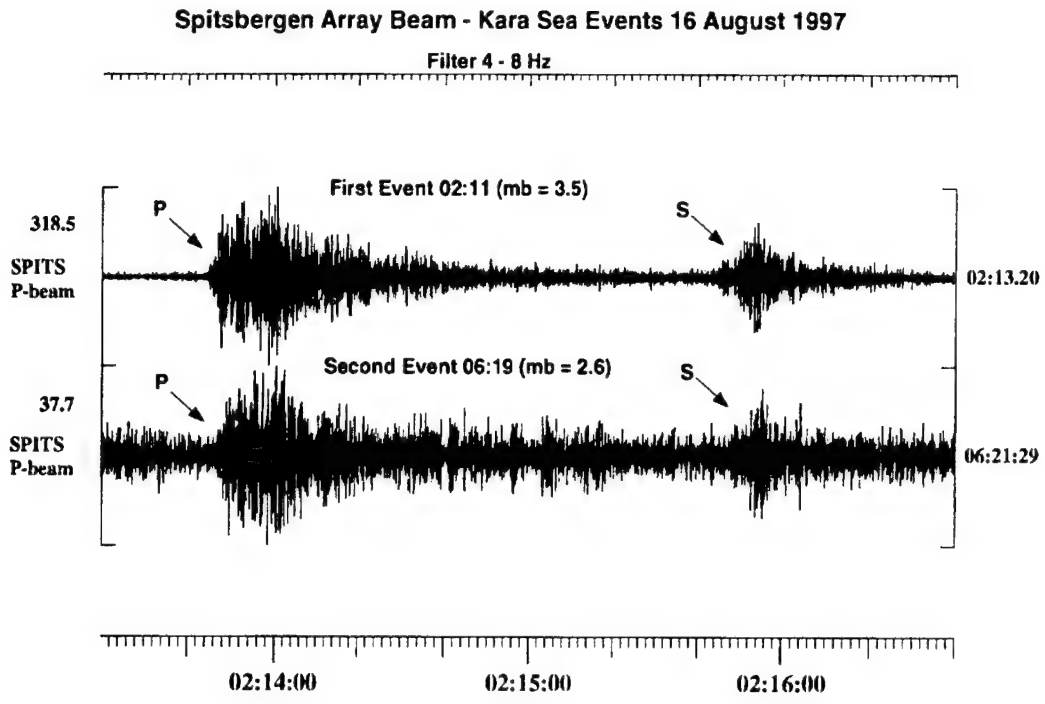

Figure 20. *SPITS array beams filtered in the band 4-16 Hz for the two seismic events in the Kara Sea on 16 August 1997. In order to enhance the S-phase, both traces have been steered using an S-type velocity (4.5 km/s) together with the appropriate azimuth.*

2.4.1 Discussion.

As stated by Kværna and Ringdal (1999) it is important to be aware that the main purpose of the threshold monitoring method is to call attention to any time instance when a given threshold is exceeded. This will enable analysts to focus their efforts on those events that are truly of interest in a monitoring situation. The analyst will then apply other, traditional analysis tools in detecting, locating and characterizing the source of the disturbance. Thus, the threshold monitoring method is a supplement to, and not a replacement of, traditional methods.

In principle, site-specific threshold monitoring, given enough calibration data and computer resources, could be expanded to be applied on a global level. However, in practice, there will be a need to apply both the site-specific and the regional or global approaches in day-to-day monitoring. Nevertheless, the site-specific method could be further optimized, *e.g.*, by considering different filter bands in parallel and applying specially generated digital filters to search for signals conforming to predetermined characteristics. We are currently investigating the feasibility and benefits of this type of optimization.

In studies of network detection capability, the question of "false alarms" is an important consideration, and in general there is a trade-off between detectability and false

alarm rate. In the threshold monitoring application, no "detection threshold" is set, and the question of "false alarms" therefore has a different meaning. The "peaks" seen on the threshold plots could be defined as false alarms if they correspond to seismic events outside the target area. However, it is important to remember that these peaks correspond to time intervals of high "noise" values due to signals from interfering events, and therefore are an integral part of the overall background threshold level. The possibility that on-site events could be "hidden" during such times of interference must be considered, and it is a question of judgement whether realistic "evasion scenarios" could be provided in practice in this connection.

The excellent capability of the site-specific threshold monitoring technique as demonstrated in this paper is due, to a large part, to our emphasis on high-frequency passbands in the regionally based site-specific monitoring. High-frequency arrays as used in our example from Novaya Zemlya have the advantage of suppressing the noise (or signal coda) from interfering events, and retain signal coherency even at high frequencies. This adds to the capability of detecting small events in the background of interfering events.

The optimized site-specific threshold monitoring technique is especially suited to monitor earthquake activity at low magnitudes for sites of special interest, and could also be useful for monitoring earthquake aftershock sequences. This paper has focused on the application of the method to a regional seismic network. As will be discussed in **Section 3**, the method is equally applicable to a teleseismic network, or a combination of the two. We will be continuing these studies in order to expand the scope and characterize the long-term capabilities of the threshold monitoring method. At the same time, we are working on streamlining and optimizing the technique, in order to further improve performance.

To obtain a fully automatic monitoring procedure, we have also investigated the possibility of utilizing detector information for labelling the threshold peaks. The results, provided in **Section 4**, indicate that the azimuth and slowness estimates of the detected phases at the individual arrays can be effectively used for such labelling. It is, however, important to quantify the quality of these azimuth and slowness estimates, to take into account the possibility of incorrect estimates.

Section 3
Optimized Threshold Monitoring of the Indian and Pakistani Test Sites

3.1 Introduction.

In **Section 2** we gave a general description of the continuous seismic threshold monitoring technique that has been developed at NORSAR over the past several years to monitor a geographical area continuously in time. Data from a network of arrays and single stations are combined and "steered" toward a specific area to provide an ongoing assessment of the upper magnitude limit of seismic events that might have occurred in that area.

While the case of optimized seismic threshold monitoring using a regional network was discussed in **Section 2**, we will in this section present results from applying the method to a teleseismic network or a combined regional-teleseismic network. In particular, we apply the method to selected time intervals during India's and Pakistan's nuclear tests in May 1998 (Barker et al., 1998; Schweitzer et al, 1998; Wallace, 1998) using data from the GSETT-3 network (Ringdal, 1994) transmitting data to the Prototype International Data Center in Arlington, VA for joint processing. We carefully select a subset of the stations in the GSETT-3 global network which have the highest detection capabilities for these regions, and calibrate these stations with regard to the basic processing parameters. We show that the network can be used to achieve a high capability for continuous monitoring of the test sites, and we include a brief discussion of the relationship between the traditional detection capability estimates and the threshold monitoring levels.

3.2 Method Description.

3.2.1 Selecting the Network.

The basic principles for the site-specific threshold monitoring method were given in **Section 2**, and are equally applicable to the regional case and to the teleseismic or combined approach discussed here. There are, however, some differences in selecting the network to be used. In either case, it is naturally important to select a network composed of stations with high detection capability for the site to be monitored, and with a good azimuthal distribution around the site. In the teleseismic case, there is, nevertheless, a need to limit the number of stations to be included in the threshold computations. This is for three main reasons:

- The main contribution to lowering the threshold trace will come from the stations with the highest sensitivity to the target area. There is no need to include stations that will contribute essentially nothing.
- The optimization of the processing parameters is a very time-consuming task, and even small mistakes can cause erroneous results when combining date from several stations.

- The projected International Monitoring System will comprise 170 primary and auxiliary stations worldwide. Making probability calculations based upon such a large number of stations could easily lead to calculations at the tail of the magnitude distribution, where the basic normality assumptions may not be valid.

For these reasons, we recommend limiting the number of stations to around 10, and we will stay with approximately this number of stations in the examples shown.

3.2.2 Tuning the Threshold Trace.

As in the regional case discussed in **Section 2**, we consider a specific target area of limited geographical extent. The size of the target area may vary, but typically such an area might be a few tens of kilometers in diameter. A basic assumption is that the target area is defined such that all seismic events within the area show similar wave propagation characteristics. When using a teleseismic network, a typical target area may usually be somewhat larger than in the regional case, because small shifts in travel time patterns or azimuths may correspond to a relatively larger shift of the geographical aiming point.

As in the regional case, parameters such as travel-times of the different phases, steering delays for array beamforming, filter frequency bands, the STA window length and the magnitude calibration values are obtained on the basis of processing results for a set of calibration events. The procedure for developing such optimized parameters is similar to the regional case, and will not be repeated here.

3.3 Data.

In May 1998, India and Pakistan conducted several underground nuclear tests. **Figure 21** shows the station network used in this study, the locations of the Pakistani and Indian nuclear tests, and the location of the Afghanistani earthquake (main shock) occurring about 30 minutes ahead of the second Pakistani test. The corresponding event information from the Reviewed Event Bulletin (REB) of the Prototype International Data Center is given in **Table 9.**

Table 9. Event information from the Reviewed Event Bulletin (REB).

Origin time	Lat	Lon	Depth	m_b	Nsta	Flinn-Engdahl Region
1998/05/11 10:13:44.2	27.0716	71.7612	0.0	5.0	50	India-Pakistan Border Reg.
1998/05/28 10:16:17.6	28.9032	64.8933	0.0	4.9	60	Southwestern Pakistan
1998/05/30 06:22:25.7	37.1570	70.0682	0.0	5.5	33	Afghanistan-Tadjikistan Bord. Reg.
1998/05/30 06:54:57.1	28.4948	63.7814	0.0	4.6	51	Southwestern Pakistan

We have used available data from these nuclear explosions to test the performance of the threshold monitoring technique for selected time intervals. Both the Indian and Pakistani explosions provide interesting case studies, for a number of reasons:

- The Indian explosions on 11 May 1998 occurred at the same site as the nuclear explosion on 18 May 1974. This provides for a very detailed and instructive comparison between the recorded waveforms for the 1974 and 1998 events.

- The second set of Indian nuclear explosions, on 13 May 1998, were not detected seismically by any station available to us. The threshold monitoring technique can therefore be used to provide an estimate of the upper magnitude limit of these explosions.

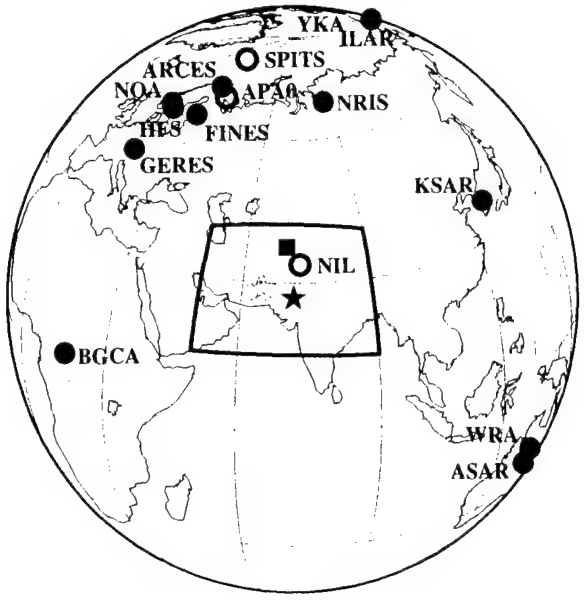

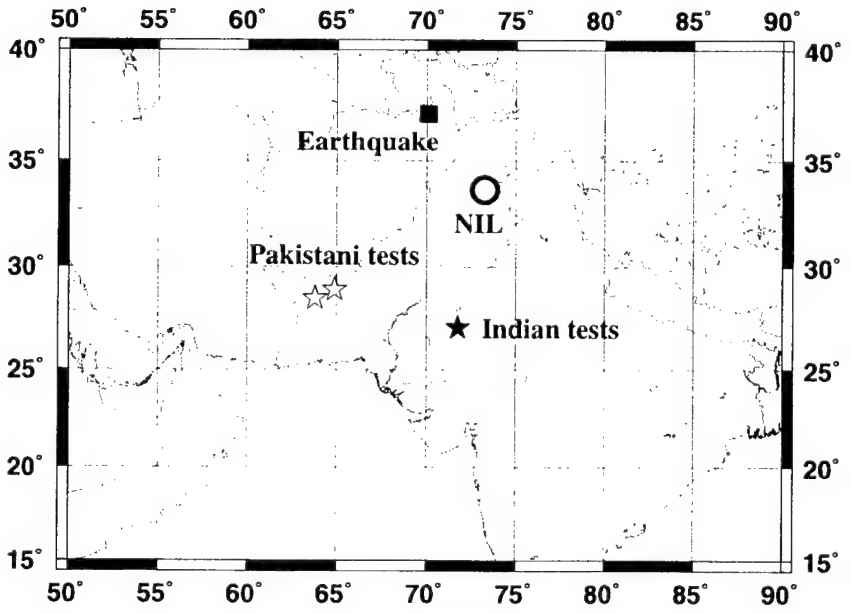

Figure 21. *Locations of the seismic stations and events used in this study. The filled circles show GSETT-3 stations which provide continuous data to the Prototype International Data Center (PIDC) in Arlington, Virginia. The stations NIL, HFS, SPITS and APA0 (open circles) do not provide continuous data to the PIDC. The filled and open stars indicate the locations of the Indian and Pakistani explosions respectively, and the filled square shows the location of the main shock of the earthquake sequence in northern Afghanistan.*

- The two sets of Pakistani explosions, on May 28 1998 (Explosion P1) and May 30 1998 (Explosion P2) were located about one degree apart, and it is interesting to investigate how the TM method performs for Explosion P2 when the tuning parameters from Explosion P1 are used.
- The origin time of Explosion P2 was about 38 minutes after the origin time of an m_b 5.5 earthquake in Afghanistan, followed by numerous large aftershocks, and this gives us an opportunity to study the performance of the TM method during a strong interfering earthquake sequence. The earthquakes were located 9-10 degrees away from the explosion sites.

Very limited data at local and regional distances were available for these explosions. In fact, for the Indian explosions, only one such station (NIL in Pakistan) was in operation, whereas for the Pakistani explosions, only teleseismic data were available. The available station geometry should provide us with important information on the characteristics of site-specific monitoring at teleseismic distances.

3.4 Monitoring India's Nuclear Test Site.

During the Indian nuclear tests on 11 and 13 May 1998, the GSETT-3 monitoring network had in operation a number of sensitive stations at teleseismic distances. However, only one station was available within the local or regional distance range. This station, a GSETT-3 auxiliary station in Nilore, Pakistan (NIL), is located 6.7 degrees away from the Indian test site and provided the P-phase with the highest SNR (937.4) of any station in the global network for this event. The NIL vertical-component recording of the Indian test is shown in **Figure 22**. The highest SNR relative to the background noise level was found between 1 and 2 Hz for both the P and the Lg phase, and this filter was used prior to the calculation of STA traces. A 1.5 second STA length was used for P, and for the longer duration Lg phase an STA length of 8 seconds was used.

The remaining 12 stations used for monitoring were all located at teleseismic distances, and only P-phases were considered for calculation of the magnitude thresholds. A typical example of teleseismic recording is the observations at the large-aperture NORSAR array (NOA). The recordings of the 11 May 1998 test and the test conducted at the same site on 18 May 1974 are illustrated in **Figure 23**, which shows a pairwise comparison of NOA P-wave recordings for both events. The data were band-pass filtered between 1 and 3 Hz, the traces were aligned visually, and sorted by the NOA sites, with the upper bold trace for each site corresponding to the 1998 event and the lower trace corresponding to the 1974 event.

The 1974 event was a single explosion, whereas the 1998 event comprised three separate explosions, apparently detonated simultaneously. It is interesting to note the remarkable similarity of the two event recordings at each NOA site. In contrast, the variability of the waveform shape across the NOA array is rather large, and we attribute this variation to near receiver scattering/focusing effects. Another interesting observation from the NOA recordings is that the amplitudes of the two events are not very different, with the 1998 event having true amplitudes 1.5-2 times larger than the 1974 event.

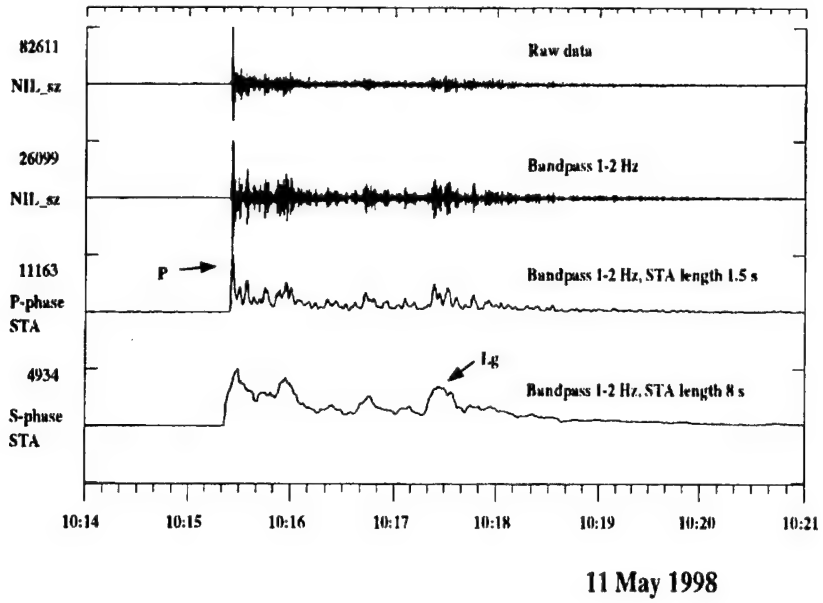

Figure 22. *Panel showing NIL recording of the Indian nuclear test of 11 May 1998. The two lower traces show the STA traces used for representing the amplitudes of the P and Lg phases. Notice that different STA lengths were used for P and Lg.*

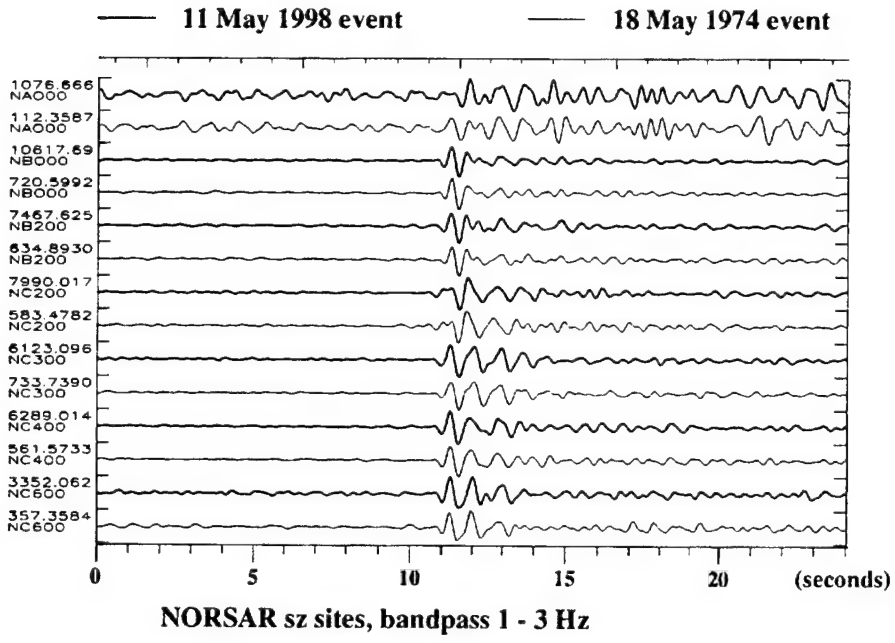

Figure 23. *Observations of the 18 May 1974 and of the 11 May 1998 explosions at the Indian nuclear test site. Pairwise seismograms at single sites of NORSAR are shown. All traces were 1 - 3 Hz band-pass filtered, normalized, and aligned visually to a common onset time.*

The list of stations and the TM processing parameters derived from the recordings of the 11 May 1998 explosion are given in **Table 10**. **Figure 24** shows the results from site-specific threshold monitoring of a five-hour time interval around the 11 May 1998 Indian nuclear test, using the processing parameters derived from the nuclear test itself. The top trace shows the combined network thresholds, and the following eight traces show the thresholds derived from each of eight station selected (P-phase only).

Table 10. TM Processing Parameters Derived from Recordings of the 11 May 1998 Indian Nuclear Test.

Station	Distance (deg)	Phase	SNR in REB	Theo. ray parameter (s/deg)	Obs. slowness (s/deg)	Obs. back azimuth (deg)	Frequency band (Hz)	STA length (s)	Travel time (s)	Mag. calib.	St. dev of calib.
NIL	6.68	P	937.4	13.73	-	-	1.0 - 2.0	1.0	102.0	1.55	0.15
-	-	Lg	(3.8)	33.04	-	-	1.0 - 2.0	8.0	223.5	2.18	0.15
NRIS	43.05	P	191.1	8.10	-	-	2.0 - 4.0	1.0	481.6	3.16	0.15
FINES	45.87	P	80.3	7.90	7.34	120.37	2.0 - 4.0	1.0	504.5	3.48	0.15
KSAR	47.96	P	51.4	7.75	7.66	269.29	1.5 - 3.0	1.0	521.3	3.93	0.15
GERES	49.39	P	43.3	7.65	6.95	95.05	1.0 - 2.0	1.0	532.3	4.08	0.15
ARCES	50.16	P	182.6	7.59	7.53	125.88	2.0 - 4.0	1.0	538.3	3.29	0.15
NOA	52.49	P	48.0	7.41	7.52	101.84	1.2 - 3.2	1.0	554.3	3.63	0.15
BGCA	55.19	P	174.0	7.23	-	-	1.5 - 3.5	1.0	575.6	3.59	0.15
WRA	76.54	P	314.1	5.66	5.35	318.10	1.0 - 3.0	1.0	713.8	3.59	0.15
ASAR	78.39	P	199.3	5.53	5.67	307.30	1.0 - 3.0	1.0	724.1	3.52	0.15
ILAR	83.65	P	157.0	5.12	3.93	323.11	1.5 - 3.5	1.0	750.3	4.19	0.15
YKA	90.60	P	238.0	4.65	5.02	349.59	1.5 - 3.0	1.0	785.6	3.89	0.15

The time tolerances were set to accommodate a target area with a radius of 25 km around the explosion site. Several distinct peaks are seen on the threshold traces for the individual arrays, but for the network trace the only significant peak corresponds to the nuclear test. The 90% magnitude thresholds during noise conditions vary around m_b 2.7-2.8. We would also like to emphasize that the peak on the network threshold trace caused by the nuclear test has a value that is slightly lower than the actual event magnitude. In cases when an event occurs in the target region, the threshold calculations should be replaced by the maximum likelihood estimate of the event magnitude (Ringdal and Kværna, 1992; Kværna and Ringdal, 1999).

According to the Indian authorities, two explosions of 0.5 and 0.3 kt took place on 13 May 1998, with origin time 06:51 GMT, however, no signals were detected by the GSETT-3 stations, and we have calculated the magnitude threshold (90% upper magnitude limit) of the reported event, using the processing parameters derived from the Indian test of 11 May 1998. Our estimated upper magnitude limit of the reported explosions is m_b 2.4, which is consistent with the value (m_b 2.5) obtained by Schweitzer et al. (1998), calculated from NIL data alone. Using the same NIL data, Wallace (1998) estimated a slightly smaller value of m_b 2.2.

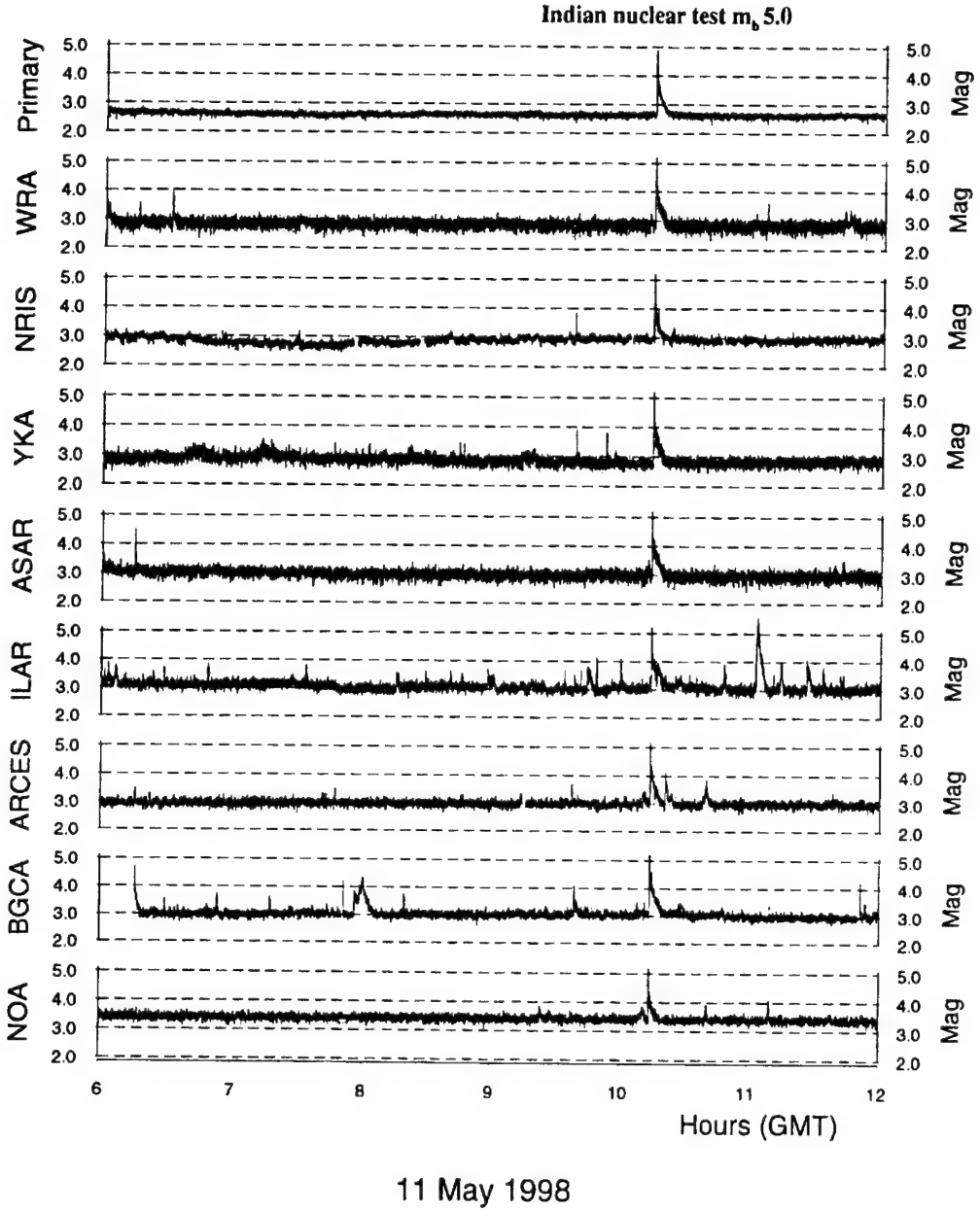

Figure 24. *Site-specific threshold monitoring of a 6-hour time interval around the Indian nuclear test, using the processing parameters given in* ***Table 10****. The plot shows the individual P-phases (STA traces) for 8 selected stations, with the combined network threshold trace on top (Primary). The time tolerances were set to accommodate a target area with a radius of 25 km around the explosion site. The only significant peak on the network threshold trace corresponds to the nuclear test.*

Figure 25 shows results from analysis of a four-hour time interval around the announced nuclear test, and it is instructive to compare the two traces on the figure. The upper trace corresponds to the GSETT-3 90% network detection capability, requiring at least 3 P-detections (Kværna and Ringdal, 1999). The lower trace is the TM result for the same 11 stations (i.e. the 90% upper limit of any event that could have occurred at the site). For the purpose of this comparison, we included the NIL station in the detection capability estimation during the two hours of available data. It is clear that the inclusion of one excellent station does not significantly improve the three-station network detection capability, which is in effect governed not by the best station, but by the "third-best" station in the network. In contrast, the TM approach takes full advantage of NIL capabilities, which cause the monitoring threshold to be lowered by about 0.4 magnitude units when data from this station is available.

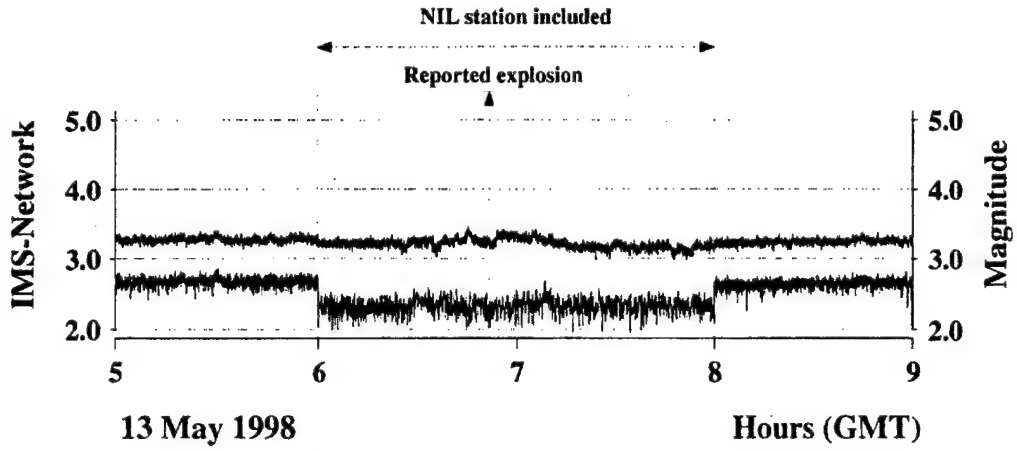

Upper trace - Three-station detection threshold of IMS network

Lower trace - Threshold monitoring limit of IMS network (largest possible event)

Figure 25. *The plot shows magnitude thresholds for a four-hour time interval around the announced Indian nuclear test of 13 May 1998. The upper trace corresponds to the GSETT-3 90% network detection capability (requiring at least 3 P-detections), whereas the lower trace is the TM result (i.e. the 90% upper limit of any event that could have occurred at this site). For the time interval 06:00 to 08:00 data from the Pakistani station NIL are included in both calculations. The largest TM peak around 07:10 is caused by the P-phase from an m_b 4.5 event located in Java, Indonesia.*

3.5 Monitoring Pakistan's Nuclear Test Sites.

According to the official Pakistani reports, their first nuclear test consisted of one large explosion and four detonations of small tactical weapons. The seismic observations do not reveal any separate signals, so we assume in the following discussion that Explosion P1 is a single event with a network m_b of 4.9. Except for the Australian station ASAR, we only used stations with continuous data available at NORSAR in this threshold monitoring study.

The parameters derived from analysis of this event are listed in **Table 11**.

Table 11. TM processing parameters derived from recordings of the 28 May 1998 Pakistani nuclear test.

Station	Distance (deg)	Phase	Theo. ray parameter (s/deg)	Obs. slowness (s/deg)	Obs. back azimuth (deg)	Frequency band (Hz)	STA length (s)	Travel time (s)	Mag. calib.	St. dev of calib.
FINES	41.413	P	8.21	7.91	127.7	1.5 - 3.0	3.0	469.6	3.71	0.3
APA0	43.167	P	8.09	7.73	140.79	2.0 - 4.0	2.0	483.4	4.20	0.3
GERES	43.015	P	8.06	6.84	93.20	1.0 - 2.0	4.0	487.7	4.22	0.3
HFS	46.269	P	7.87	5.54	146.35	1.5 - 3.0	4.0	508.4	3.66	0.3
ARCES	46.492	P	7.85	8.30	130.59	2.0 - 4.0	3.0	507.0	3.82	0.3
NORES	47.472	P	7.79	7.75	99.08	2.5 - 5.0	2.5	516.5	3.54	0.3
SPITS	53.825	P	7.33	8.89	129.44	3.5 - 7.0	4.0	568.6	5.18	0.3
ASAR	84.490	P	5.05	3.13	312.13	1.5 - 3.0	2.0	755.4	3.71	0.3

Figure 26 shows the results from site-specific threshold monitoring of a 7-hour time interval around the first Pakistani nuclear test, using the processing parameters derived from the nuclear test itself. The plot shows the individual P-phases (STA traces) for each of the 8 arrays, with the combined network threshold trace on top. The time tolerances were set to accommodate a target area with a radius of 25 km around the explosion site. Several distinct peaks are seen on the threshold traces for the individual arrays, but for the network trace the only significant peak corresponds to the nuclear test. During noise conditions on this day, the 90% magnitude thresholds varies around m_b 3.0.

The best performance of the threshold monitoring method is obtained by using processing parameters derived from recordings of previous events located in the target region. In our case we will use the processing parameters derived from Explosion P1 to obtain a close to optimum monitoring of the target region surrounding the explosion site. An interesting question that arises in this context is how far away from the location of Explosion P1 can the processing parameters effectively be used?

In **Figure 27** we show the monitoring results of a 2 hour time interval around Explosion P2. In order to investigate how sensitive the network magnitude thresholds are to the definition of the target area, we have calculated several network threshold traces for this two-hour time interval using different parameter settings:

- In the upper panel, the processing parameters derived from Explosion P1 are used and the time tolerances correspond to a region with 25 km radius around the location of Explosion P1. The peak of Explosion P2, located about 100 km from the center of the target region, is clearly visible.
- In the second panel we have again used the processing parameters of Explosion P1, but the time tolerances are now increased to include a region with 100 km radius. To accommodate an expected larger amplitude variation within such a large region, the assumed standard deviation of the magnitude estimates are increased from 0.3 to 0.4. The threshold peaks are marginally higher and broadened relative to the peaks shown in the upper panel.

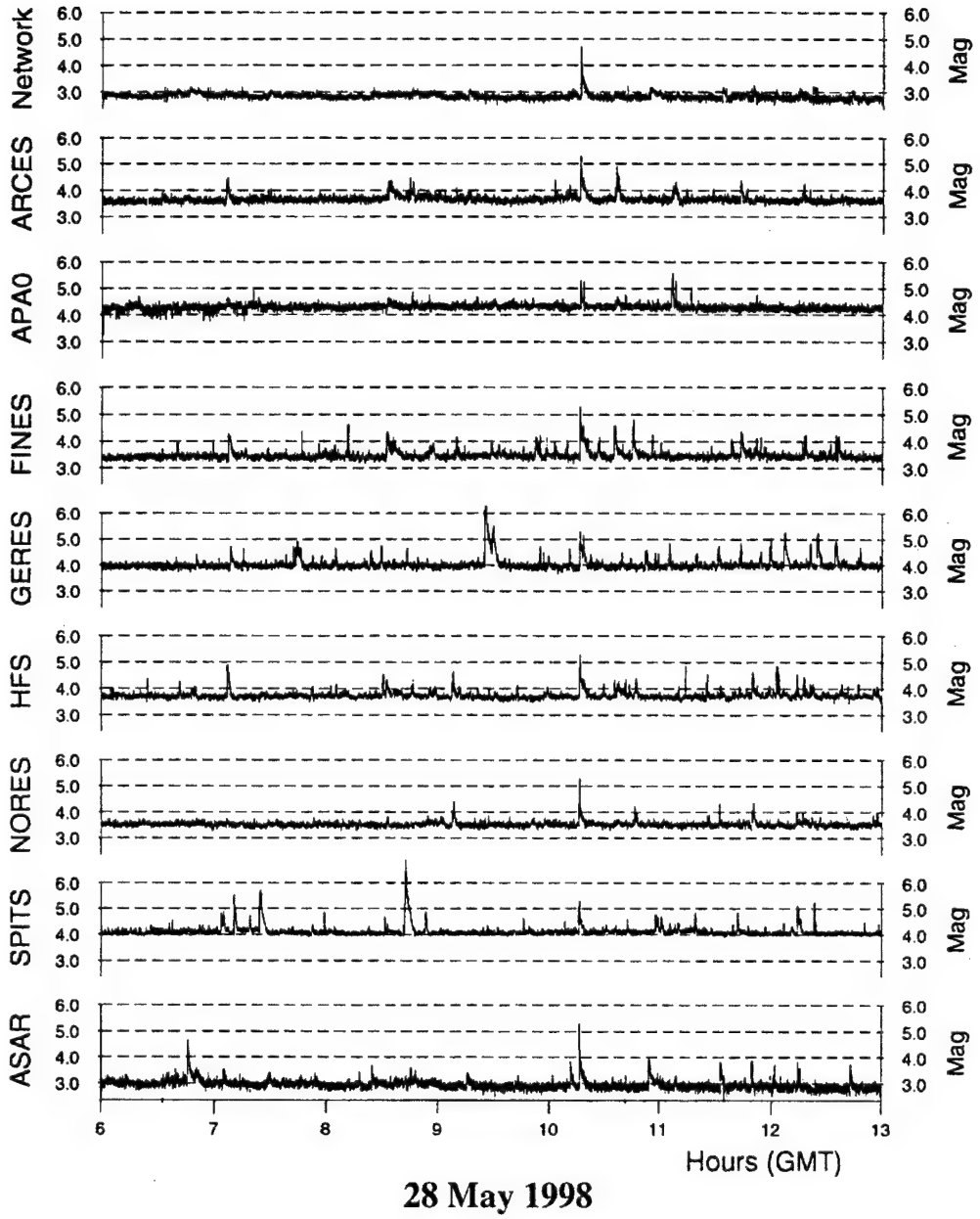

Figure 26. *Site-specific threshold monitoring of a 7-hour time interval around the first Pakistani nuclear test, using the processing parameters given in* ***Table 11****. The plot shows the individual P-phases (STA traces) for each of the 8 arrays, with the combined network threshold trace on top. The time tolerances were set to accommodate a target area with a radius of 25 km around the explosion site. Notice that for the network trace the only significant peak corresponds to the nuclear test.*

- In the third panel, we have used processing parameters derived from Explosion P2 itself. The threshold peak for Explosion P2 is now slightly sharper than in the upper two panels, and the peak value is increased by about 0.3 m_b units.
- In the lower panel we have used the processing parameters derived from the main shock of the Afghanistani earthquake sequence, located about 1100 km away from Explosion P2. A target region with a radius of 25 km is assumed. Through detailed analysis we found 16 distinct peaks that have "sharp" signatures consistent with aftershocks at this location. In this case, the peak caused by Explosion P2 is smeared out and is clearly lower than several of the aftershock peaks.

The results shown in **Figure 27** indicate that for the given teleseismic station geometry, a shift of 100 km relative to the target location has a relatively small influence on the definition on the threshold peaks. The same applies to changing the radius of the target area by increasing the time tolerances. This implies that the processing parameters derived from Explosion 1 can be effectively used to monitor a radius of at least 100 km from the location of Explosion 1. But as seen from the lower panel in **Figure 27**, efficient monitoring can not be conducted when the location difference between the target site and the calibration site is of the order of 1000 km.

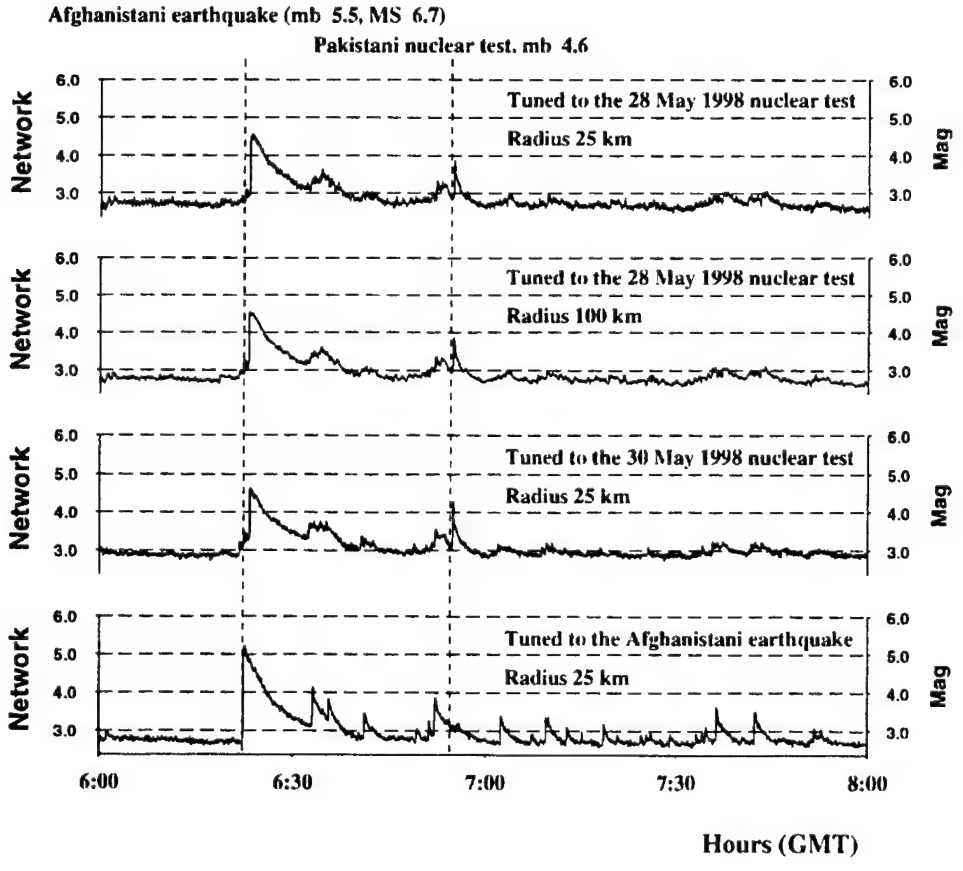

Figure 27. *The panels illustrate the difference in 90% network magnitude thresholds for a 2 hour time interval around the second Pakistani nuclear test when using different processing parameters. See text for details.*

3.6 Monitoring of the Afghanistani Earthquake Sequence.

A large earthquake followed by a large number of aftershocks often causes problems and a lot of work for the automatic processing and the manual data analysis at the PIDC. By focusing the threshold monitoring on the location of the main earthquake, using processing parameters derived form the earthquake itself, we should be able to obtain an efficient monitoring of the aftershock sequence. The results for a two-hour interval around the main Afghanistani event are shown in **Figure 28.** The top panel shows the network threshold trace, whereas the lower panels show the individual P-phase thresholds for the arrays assumed to have the best capability to detect signals from events in the region.

For the aftershocks, the threshold peaks line up nicely across all panels, as indicated by the dashed lines. The line-up indicates that the pattern of observed phases at the different stations fit with the expected travel times from events in the region. In addition, the network threshold peaks exhibit a sharp onset.

Network threshold peaks caused by events outside the target region are indicated by arrows. In these cases, the network threshold peaks are smeared out and the threshold peaks from the different arrays do not fit a straight line.

The aftershocks indicated on **Figure 28** were all identified by a simple visual inspection, where the line-up of the threshold peaks across the panels and the sharpness of the network threshold peaks were used as criteria for declaring an aftershock. When comparing to the aftershocks reported in the REB, we found that all events were found by our method. For the time interval 06:22 - 11:00, we did in addition come up with more that 10 possible aftershocks that were not reported in the REB.

3.7 Discussion.

The results presented show that the site-specific threshold monitoring method can be effectively used at teleseismic distances. From observations of the 11 May 1998 Indian nuclear test we have derived optimum processing parameters for the 11 GSETT-3 stations assumed to have the best detection capability for the Indian test site. Our results can be summarized as follows:

- The TM magnitude threshold of the GSETT-3 primary network for the Indian test site is around m_b 2.8 during normal noise conditions. The stations of this network are located at teleseismic distances from the test site.
- During background noise conditions, regional data from the Nilore (NIL) station alone provides TM magnitude threshold of about m_b 2.4 for the Indian test site (Schweitzer et al., 1998). Supplementing NIL data with data from the other teleseismic GSETT-3 stations does not lower the TM magnitude thresholds during normal noise conditions, but are important if interfering events occur.
- During background noise conditions, the GSETT-3 three-station detection capability varies around m_b 3.3, both with and without the use of NIL data. This illustrates that supplementing a network with one additional good station does not necessarily significantly improve the three-station detection capability of the network.

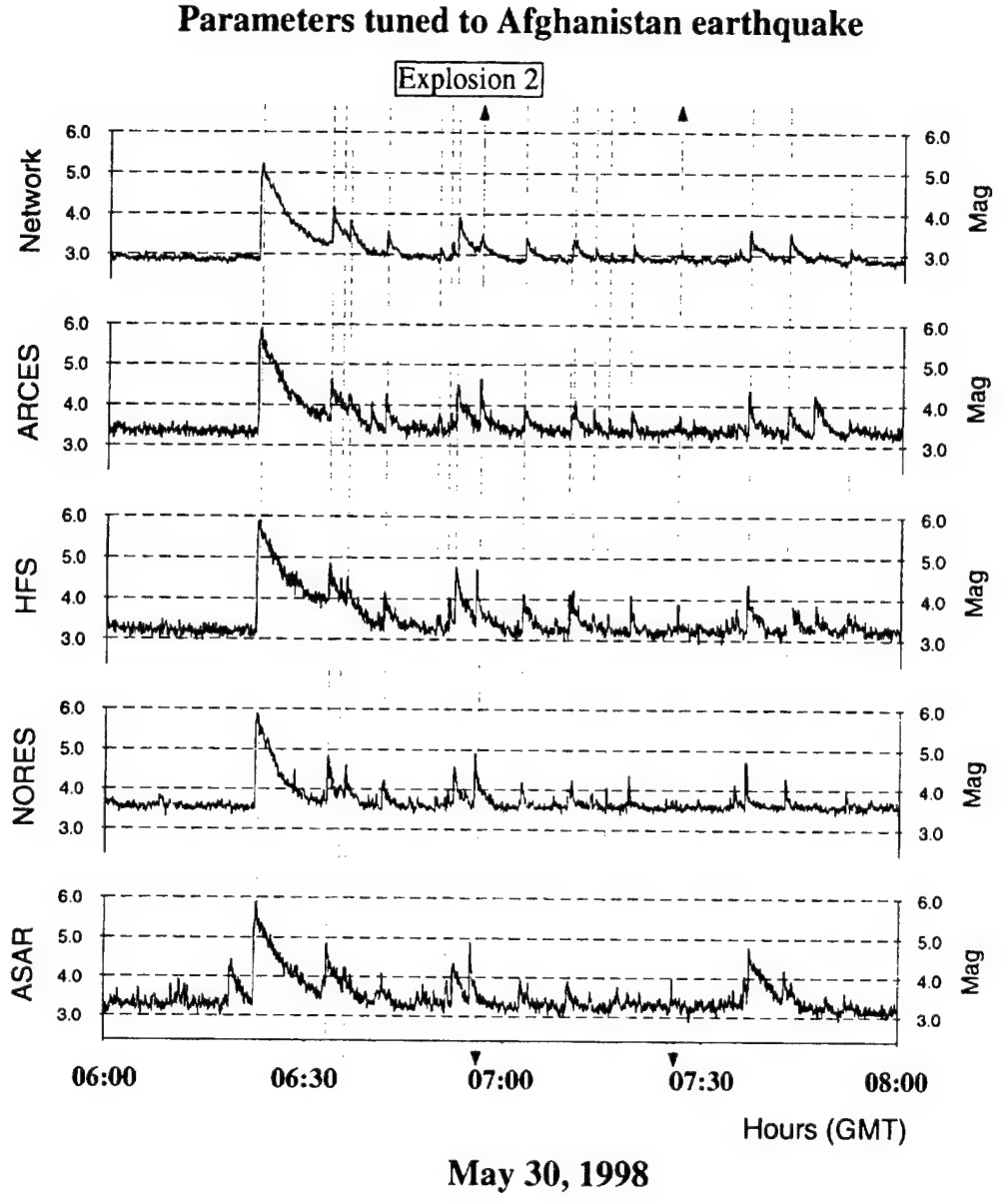

Figure 28. *This figure illustrates how the site-specific threshold monitoring method can be used to identify events in an aftershock sequence. The processing parameters are obtained from the main event, and in this case using time tolerances corresponding to a target region with a radius of 25 km. See text for details.*

Using data from the arrays located in northern Europe supplemented with data from the Australian array ASAR, the Pakistani test area can be monitored down to a magnitude of 3.0 during normal background noise conditions. We have also verified that the monitoring performance is only marginally reduced for a test site located as far as 100 km from the location of the tuning event.

The benefit from using a network for monitoring becomes particularly evident during an earthquake sequence located as close as 10 degrees from the target region. The signals from the aftershocks are suppressed by up to 0.5 m_b units, making the peak of the nuclear test within the aftershock sequence stand out clearly on the network threshold trace.

An interesting application is to provide monitoring of an aftershock sequence. We analyzed a five hour interval of the Afghanistani earthquake sequence, using the sharpness of the network threshold peaks as criteria for declaring an aftershock. When comparing to the aftershocks reported in the REB, we found that all events were found by our method. For the five-hour time interval, we did in addition identify more than 10 possible aftershocks that were not reported in the REB.

Another application of the TM approach would be to determine consistent magnitudes for the aftershocks. After introducing the region-specific magnitude calibrations from the main events, and subsequently using the maximum likelihood method for calculating the network magnitudes, we expect to achieve much more precise estimates than those calculated by traditional averaging.

We conclude that the optimized site-specific threshold monitoring technique is well suited to monitor seismic activity at low magnitudes for sites of special interest, and could also be useful for monitoring earthquake aftershock sequences.

Section 4
Automatic Explanation Facility for Analysis of Threshold Traces

4.1 Introduction

Seismic events occurring at or near the former underground nuclear test site on Novaya Zemlya have been subjected to extensive investigation over the last four decades, as monitoring of the events in this region has been of special interest to the international community. Following the developments of sensitive regional arrays in northern Europe (see **Figure 1**), events with magnitudes as low as 2.5 have been successfully detected and located in this region.

The development of the Threshold Monitoring (TM) method (**Section 2**; Kværna and Ringdal (1999); Ringdal and Kværna (1989, 1992)) has further improved the monitoring capability of this area. By optimizing the processing parameters from recordings of previous events in the region, the joint TM processing of the regional arrays ARCES, SPITS, FINES, and NORES place an upper bound on possible events in this area, which during normal noise conditions fluctuates around magnitude 2.0. A typical example is shown in **Figure 29,** where the upper trace shows the combined magnitude threshold for the four arrays processed. There are, however, often instances when the monitoring threshold is temporarily increased because of signals from events located outside the region of interest. For complete monitoring, we have until recently investigated the cause of these threshold peaks manually. The procedure used has been to compare the time intervals of the short duration threshold peaks to event and signal detection information found in standard event bulletins or signal detection lists (see **Figure 29**). If a threshold peak could confidently be associated with an event located outside the target area, we considered it highly unlikely that another event simultaneously took place within the target area.

This research has focused on the development of a fully automatic peak explanation facility for analysis of the magnitude threshold traces. In this way we intend to minimize the need for manual classification of the threshold peaks such that manual analysis will only be necessary when events within the actual target region occur. Although the focus of this paper is the Novaya Zemlya test site, the method will be directly applicable to any geographical areas like the other underground nuclear test sites.

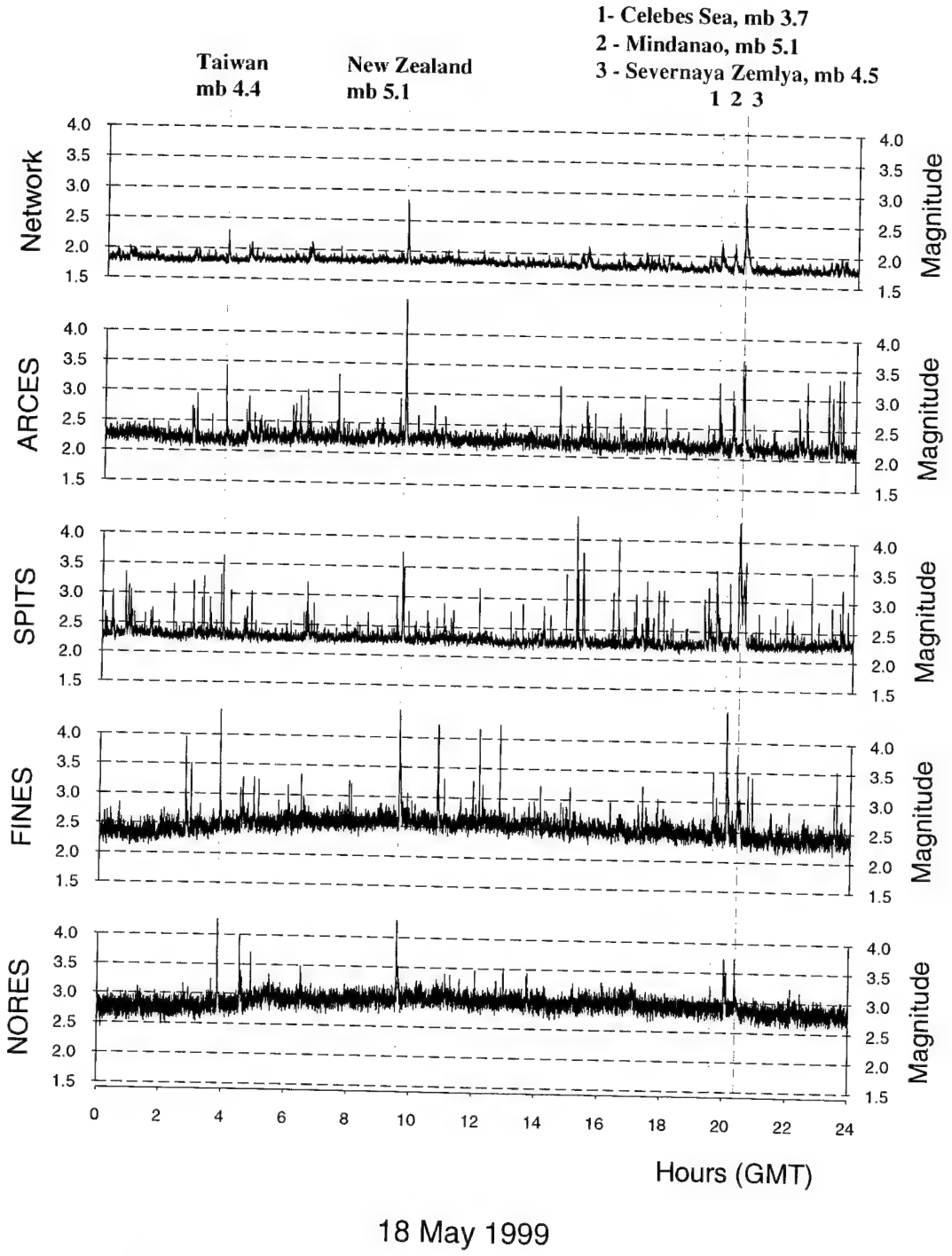

Figure 29. *Results from threshold monitoring of the Novaya Zemlya Test Site for 18 May 1999. The network trace on top is the combined threshold trace, using P phases for all arrays and in addition S phases for ARCES and SPITS. The traces for each of the four stations (P phases only) are shown below the network trace. The results from manual analysis of the threshold peaks are shown. "Blue" events are located at teleseismic distances from the station network, whereas the "red" event is located at Severnaya Zemlya, in the Russian region of the Arctic Ocean.*

4.2 Automatic Detection of Peaks in the Network Threshold Trace.

The first step in the automatic analysis of threshold traces is to identify significant threshold peaks. Our approach has been to develop a peak detection method based on estimates of the noise variance and the long term trend of the threshold trace. From experiments with various data sets, we have developed a method which comprises the following steps:

- Calculate the long-term-median (LTM) of the threshold trace with a typical window length of 30 minutes and a sampling interval of 5 minutes.
- Calculate the overall standard deviation (SIGMA) of the threshold trace around the long-term-median after removing the upper 10% of the data values. The removal of the upper 10% of the data values is done to reduce the influence of the threshold peaks on the estimate of the standard deviation.
- Define the peak detection limit as LTM + 5 * SIGMA
- Alternatively, the peak detection limit is defined separately for each threshold trace using a predefined shift above the LTM. For the Novaya Zemlya network threshold trace we have initially found that LTM + 0.35 provides a reasonable peak detection limit, whereas the individual station/phase threshold traces show a somewhat larger variability, and LTM + 0.4 was consequently used.

Figure 30 shows a panel with threshold traces for 18 May 1999 with predefined peak detection limits superimposed. Notice that several peaks are identified on the network threshold trace which we have to investigate in more detail.

4.3 Association of Network Threshold Peaks with Signals Detected at Each Individual Array.

In order to relate the peaks of the network threshold trace to information obtained by traditional signal processing at each array, we first have to determine the time intervals associated with each network threshold peak. Through experiments, the following procedure has been established:

- Detect peaks on the threshold traces calculated for each individual phase. The procedure is described in the preceding sub-section.
- For each station/phase considered, find the peak detection intervals overlapping the peak detection intervals of the network threshold trace, and use the union as the time interval of interest. See **Figure 31** for details.
- The x-axes of the threshold traces show origin times at the NZ test site. When searching the detection lists for signals associated with the threshold peaks, we have to shift the detection times in accordance with the expected phase travel time from the NZ test site to the actual array.

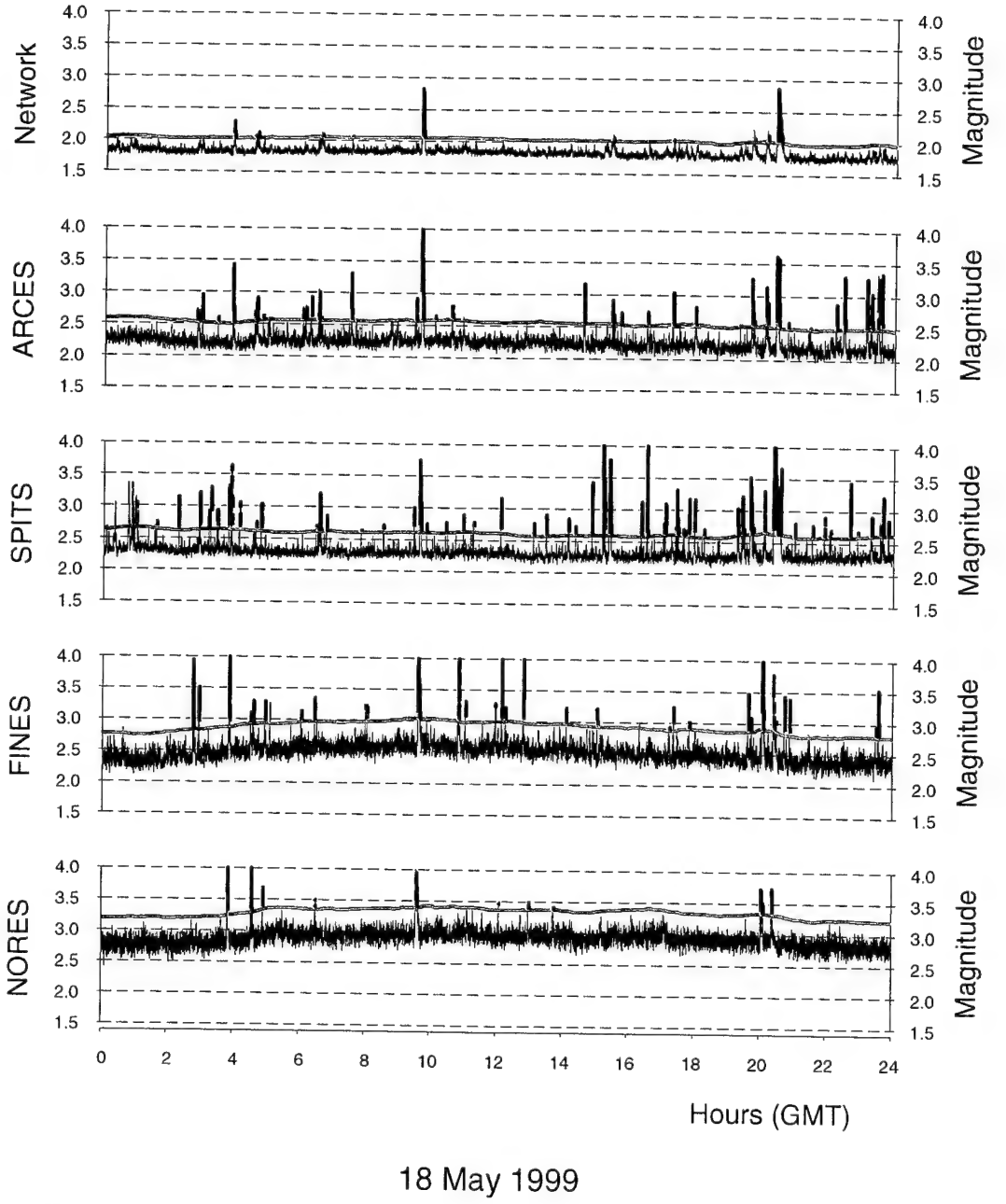

Figure 30. *Site-specific Threshold Monitoring of the NZ test site for 18 May 1999. The plot shows the 4 individual station thresholds (P-phases), with the combined threshold trace on top. Peaks exceeding the running magnitude limit (in blue) are shown in red.*

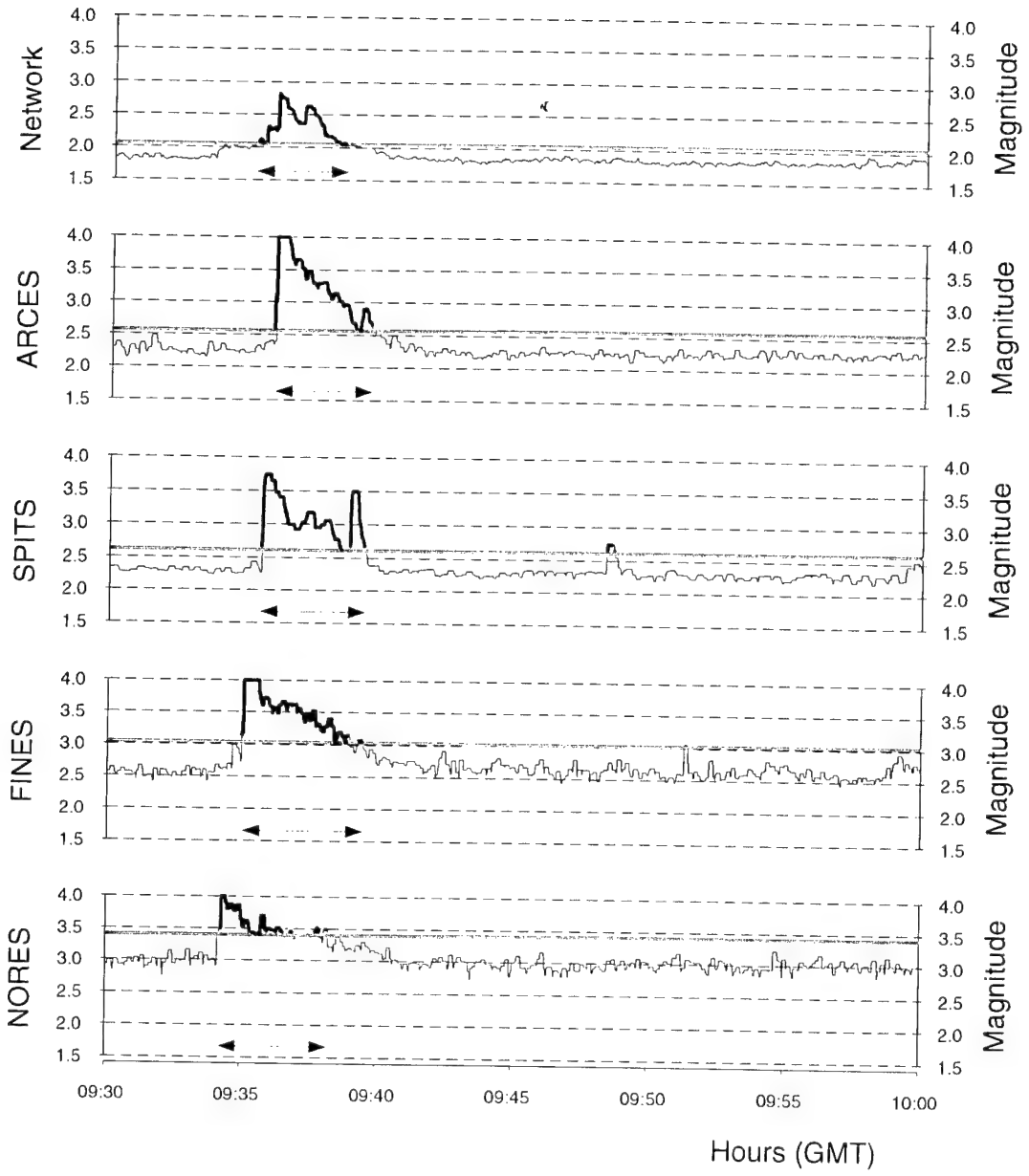

Figure 31. *Illustration of the procedure for defining the time intervals used for finding matching detections. For each station/phase considered, we find the peak detection intervals overlapping the peak detection intervals of the network threshold trace, and use the union as the time interval used for search for each station. When searching the detection lists for signals associated with the threshold peaks, we have to shift the detection times in accordance with the expected phase travel time from the NZ test site to the actual array.*

- From statistics on the distribution of slowness and azimuth estimates, we define for each phase a critical azimuth and slowness range for events in the vicinity of the NZ test site. The numbers used are given in **Table 12**. Detected signals with azimuth and slowness estimates falling outside the critical ranges are assumed to be caused by events located outside the NZ testing area, otherwise, further offline analysis will be required to determine the cause of the threshold peak. Examples of array signal detections associated with the network threshold peaks are shown in **Figure 32** and **Figure 33**.

Table 12. Definition of critical azimuth and slowness ranges for phases from events near the NZ test site.

Array	Phase	Expected Azimuth (degrees)	Lower Azimuth (degrees)	Higher Azimuth (degrees)	Expected Slowness (sec/deg)	Lower Slowness (sec/deg)	Higher Slowness (sec/deg)
ARCES	P	62.2	47.2	77.2	11.22	10.59	17.11
ARCES	S	64.3	49.3	79.3	23.21	19.86	31.77
SPITS	P	97.6	77.6	117.6	13.24	10.59	19.86
SPITS	S	97.6	77.6	117.6	23.16	19.86	34.75
FINES	P	29.6	11.6	47.6	11.63	10.59	14.83
NORES	P	33.6	18.6	48.6	10.85	9.27	14.26

- An overview of the results after associating the network threshold peaks to signals detected at each individual array is given in **Figure 34**. For each of the P-phase threshold traces we have only considered threshold peaks associated with a network threshold peak. In the four lower panels, green indicates that we have found no signal detections with azimuth and slowness estimates within the critical ranges. If one or more detections are found, the threshold peak is colored red. For the peaks of the network threshold trace shown on top of the figure, we have used a red color if at least one of the arrays has a detection with azimuth and slowness estimates within the critical ranges. Otherwise the peaks are colored green. The causes of the red threshold peaks have to be investigated in more detail, e.g. by comparing to existing event bulletins or by offline analysis of the raw seismic data.
- In order to investigate the threshold peaks having phase observations with slownesses and azimuths typical for NZ events, we have introduced the functionality of comparing the critical signals to phases associated to events reported in the NORSAR bulletin of events in northern Europe (Kværna et al., 1999). The critical threshold peak at 20:20 on 18 May 1999 (see **Figure 34**) is in this way found to be caused by an m_b 4.5 event located north of Severnaya Zemlya. For this location, P-phases observed at FINES and NORES have azimuths and slownesses comparable with P-phases from events at the NZ test site. Detailed information on the critical detections is given in **Table 13**.

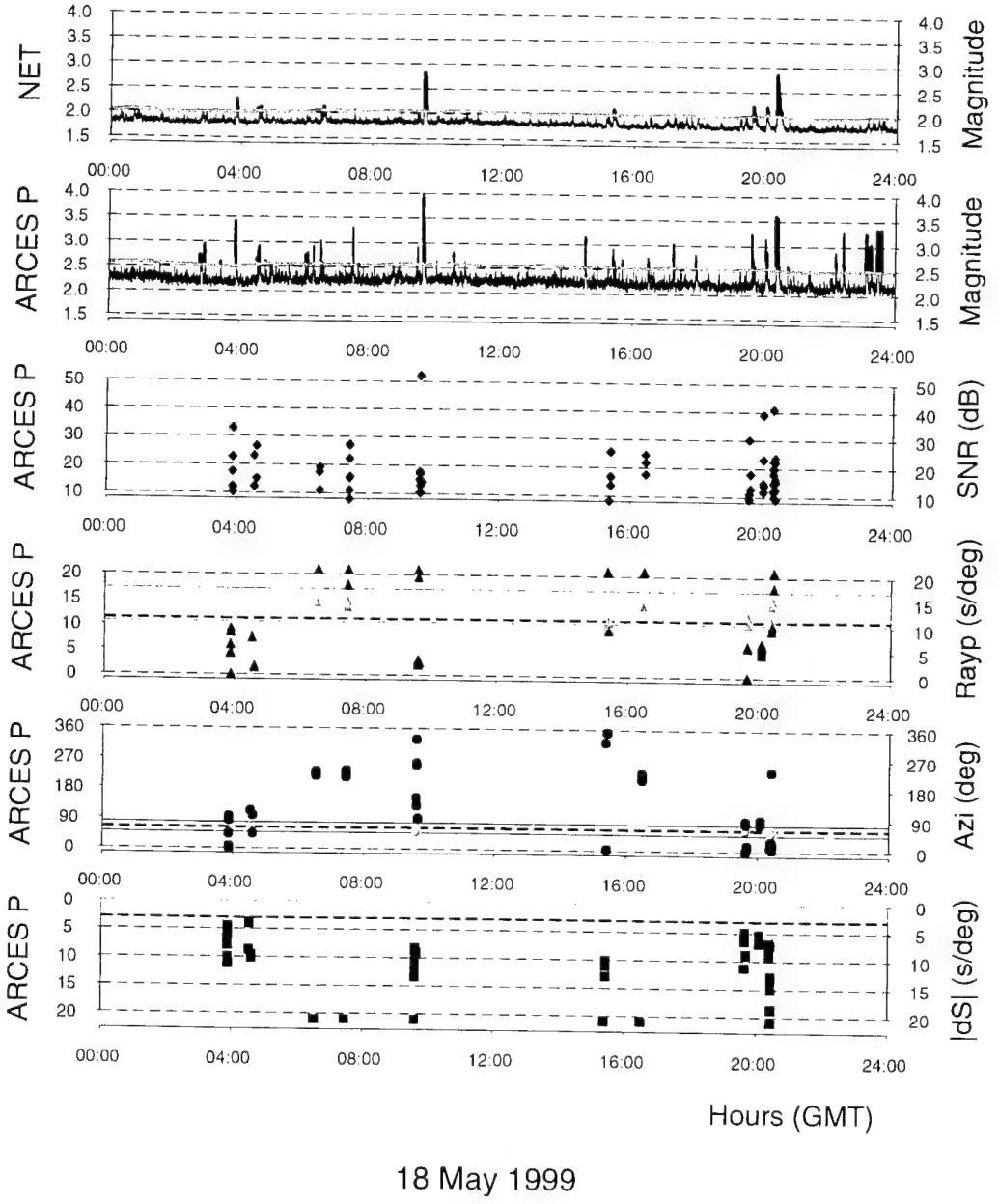

Figure 32. *Results from correlating peaks of the NZ magnitude thresholds (upper two panels) with information from the signal detector at ARCES (lower four panels). Threshold peaks exceeding the running magnitude limit (in blue) are red. The critical ranges of slowness (ray parameter) and azimuth are indicated in yellow, and the bold dashed lines indicate the expected values of P-phases from the NZ test site. The bottom panel indicates the differences in horizontal slowness between the detected and expected values (in s/deg), with the approximate range of interest for NZ P-phases shown in yellow. Signals falling within either the critical azimuth or the slowness ranges are shown in green. Signals satisfying both the azimuth and slowness criteria would be shown in red. Notice that no detections satisfies both the azimuth and slowness criteria.*

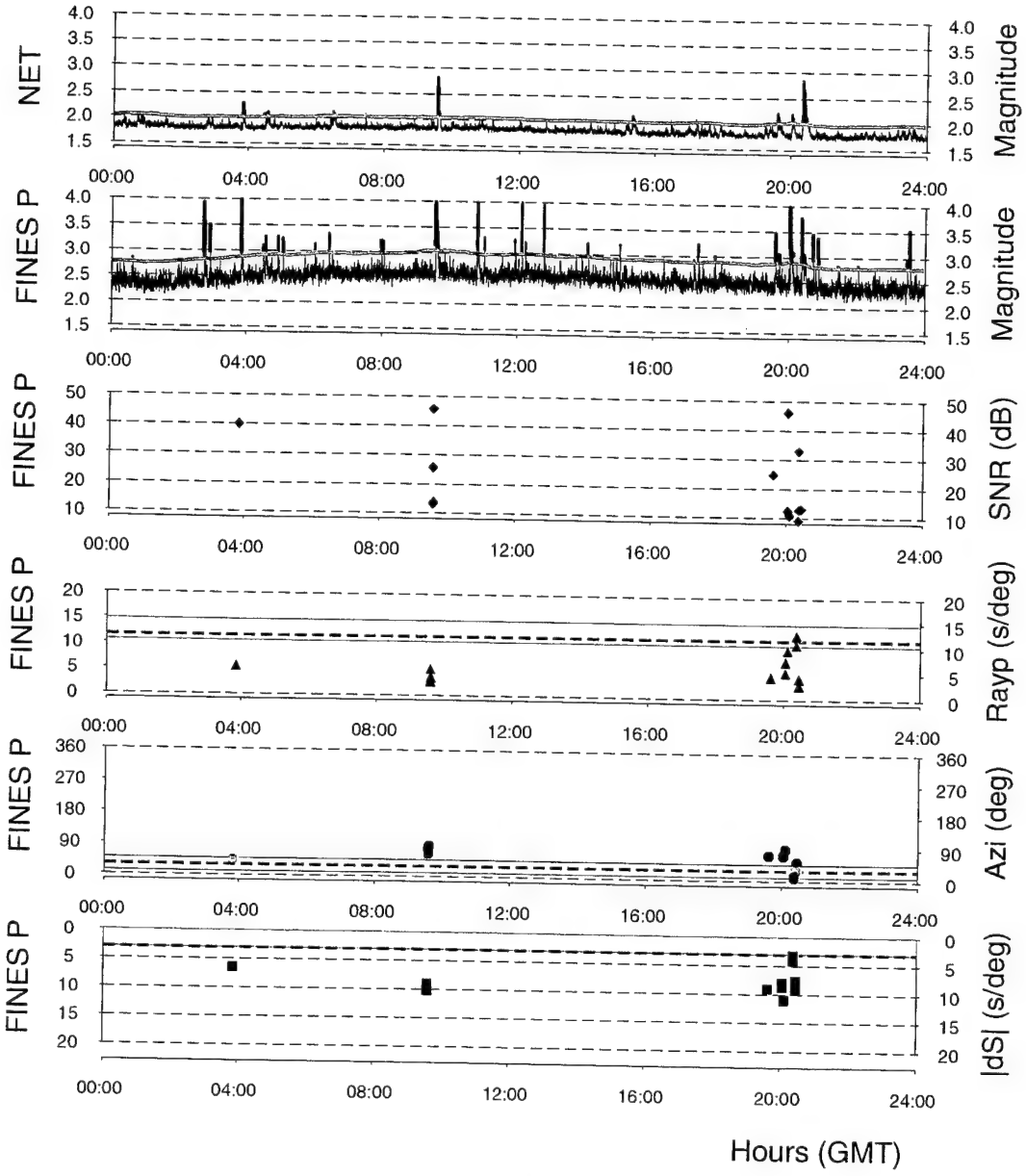

Figure 33. *Results from correlating peaks of the NZ magnitude thresholds with information from the signal detector at FINES. More details are given in the caption of* ***Figure 32****. Notice that for the network threshold peak around 8:20 p.m. there are two FINES detections with azimuth and slowness estimates that fall within the critical range for P-phases from NZ events (shown in red symbols).*

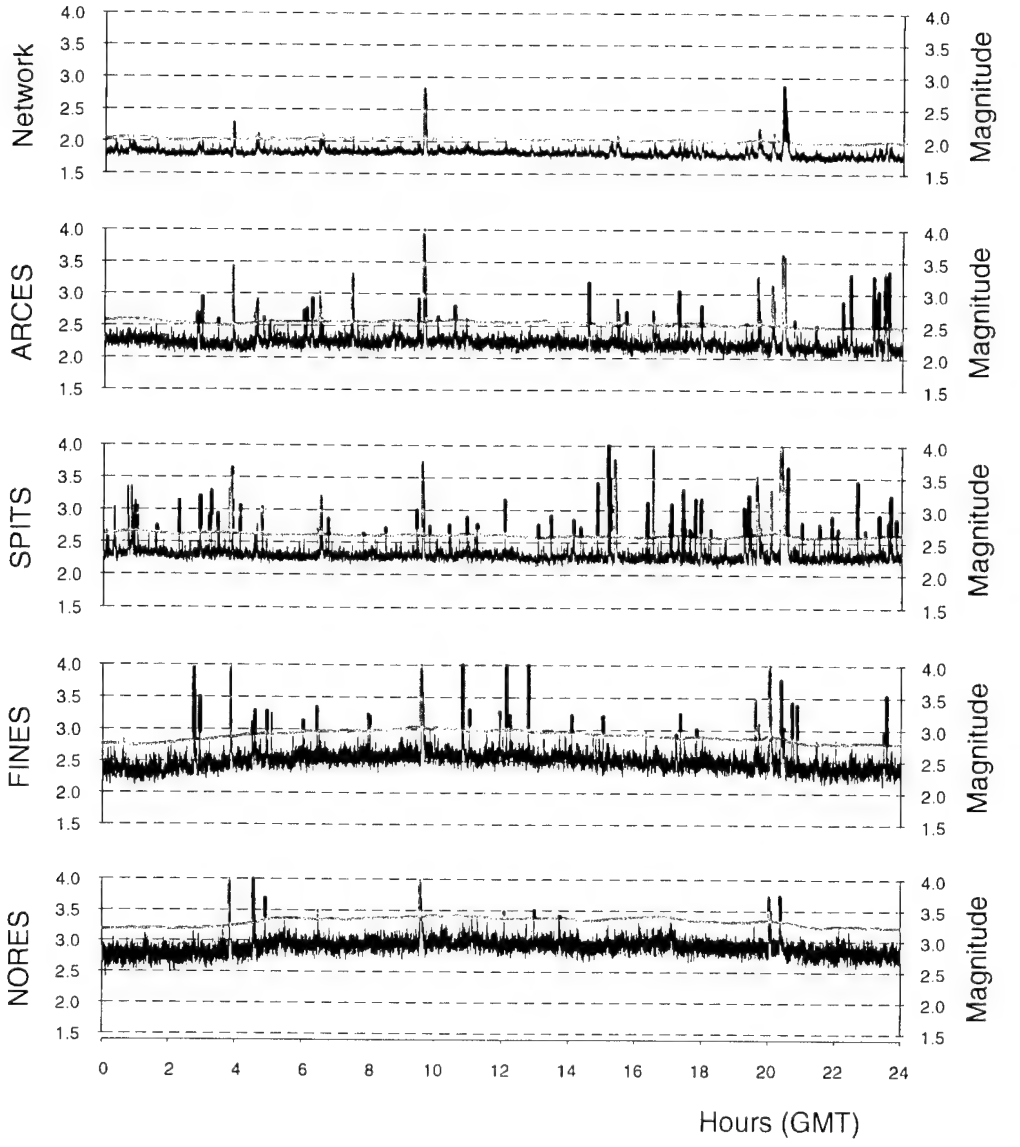

Figure 34. *This figure provides an overview of the results after associating the network threshold peaks to signals detected at each individual array. Red peaks indicate the presence of critical detections; green peaks indicate non-critical detections only (see text for details). After comparing the matching detections to the automatic NORSAR bulletin, we find that the red threshold peak at 20:20 is caused by an event north of Severnaya Zemlya. For this particular location, P-phases recorded at FINES and NORES have azimuth and slowness estimates comparable to the values from events at the NZ test site.*

Table 13. Definition of the critical threshold peaks shown in Figure 34. The phases with critical slownesses and azimuths are given in the lower part of the table. These phases are all associated with a magnitude 4.5 event located north of Severnaya Zemlya.

Configuration	Edge 1	Edge 2	Dura-tion (sec)	Max. mag.
Network	1999-138:20.21.28	1999-138:20.28.23	416	2.87
FINES P	1999-138:20.22.09	1999-138:20.28.16	367	3.78
NORES P	1999-138:20.21.27	1999-138:20.22.53	87	3.74

Station Phase	Arid	Arrival time (Origin time)	SNR	App. Vel. (km/s)	Azim. (deg)	R.pwr.	dS (s/deg)
FINES P	91336	1999-138:20.25.56.125 *(1999-138:20.22.11.925)*	45.1	10.3	12.7	0.98	3.40
FINES P	91339	1999-138:20.26.13.800 *(1999-138:20.22.29.600)*	2.9	8.7	15.9	0.97	3.13
NORES P	91473	1999-138:20.26.27.393 *(1999-138:20.21.45.993)*	3.0	11.6	23.3	0.93	2.22

There will still be a few situations when we have threshold peaks that cannot be explained by the procedures outlined above. In such situations we have to carry out additional manual analysis to determine the cause of the event. Typical situations may be signal detections in the coda of larger teleseismic events.

4.4 The 13 January 1996 Event.

At 17:17:23 GMT on 13 January 1996 there was an event located about 200 km north of the NZ test site (see **Figure 2**). Currently, the NZ monitoring region has a radius of 25 km, and the travel-time, azimuth and slowness tolerances are set accordingly. The same applies to the magnitude calibrations and the corresponding uncertainties. Because phases from the 13 Jan. 1996 event will have travel-times significantly different from those produced by events at the NZ test site, we expect a "smearing" of the corresponding network threshold peak. The result is shown in **Figure 35**, where the red peak around 17:17 GMT is caused by the actual event.

As an experiment we adjusted the TM processing parameters for the NZ test site to the location of the 13 January 1996 event. The travel-times derived for the NZ test site were recalculated for the new location using the travel-time model of Mykkeltveit and Ringdal (1981). The magnitude calibrations for SPITS, ARCES, and NORES remained unchanged, but for FINES the P magnitude calibration was reduced by 0.4 m_b units to compensate for a possible amplitude "bright spot" at the NZ test site. Comparisons between different events in the NZ region suggest that this is the case for FINES. The new result is shown in **Figure 36**, where the amplitude of the threshold

peak is increased as compared to **Figure 35**. The network peak around 13:00 GMT has changed color from green to red. The reason is that FINES has an associated detection where the azimuth and slowness match the critical range for the location 200 km north of the NZ test site.

From these results we propose to deploy a number of "small" monitoring areas covering the island of Novaya Zemlya and adjacent seas, and run threshold monitoring for each of these "small" areas. The automatic explanation facility will be activated for each of these areas, which will be deployed so as to provide a complete monitoring of the entire region.

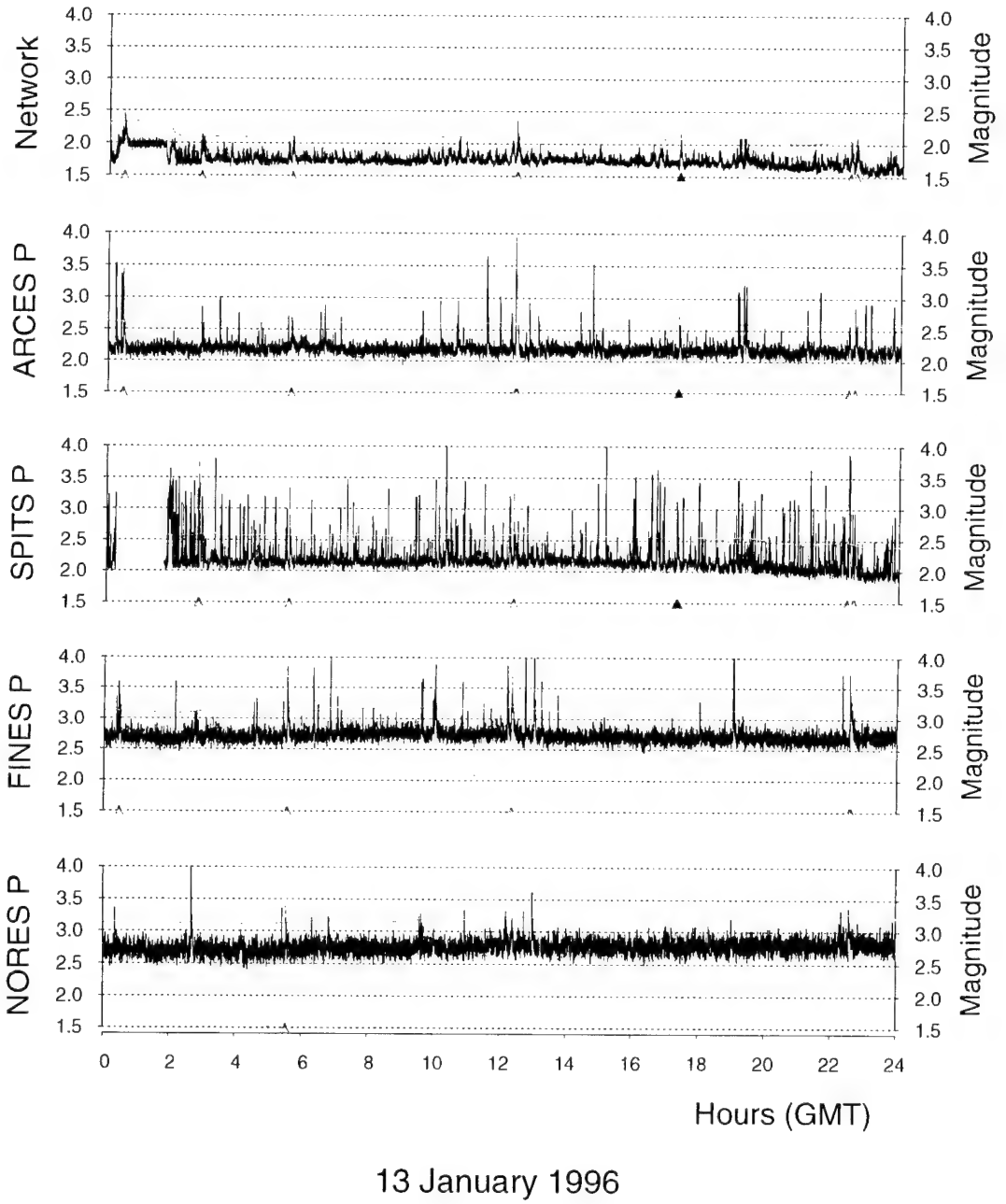

Figure 35. *Summary of threshold monitoring of the NZ test site for 13 January 1996. The red peak around 17:17 is caused by an event located about 200 km north of the test site. See text for interpretation of the figure.*

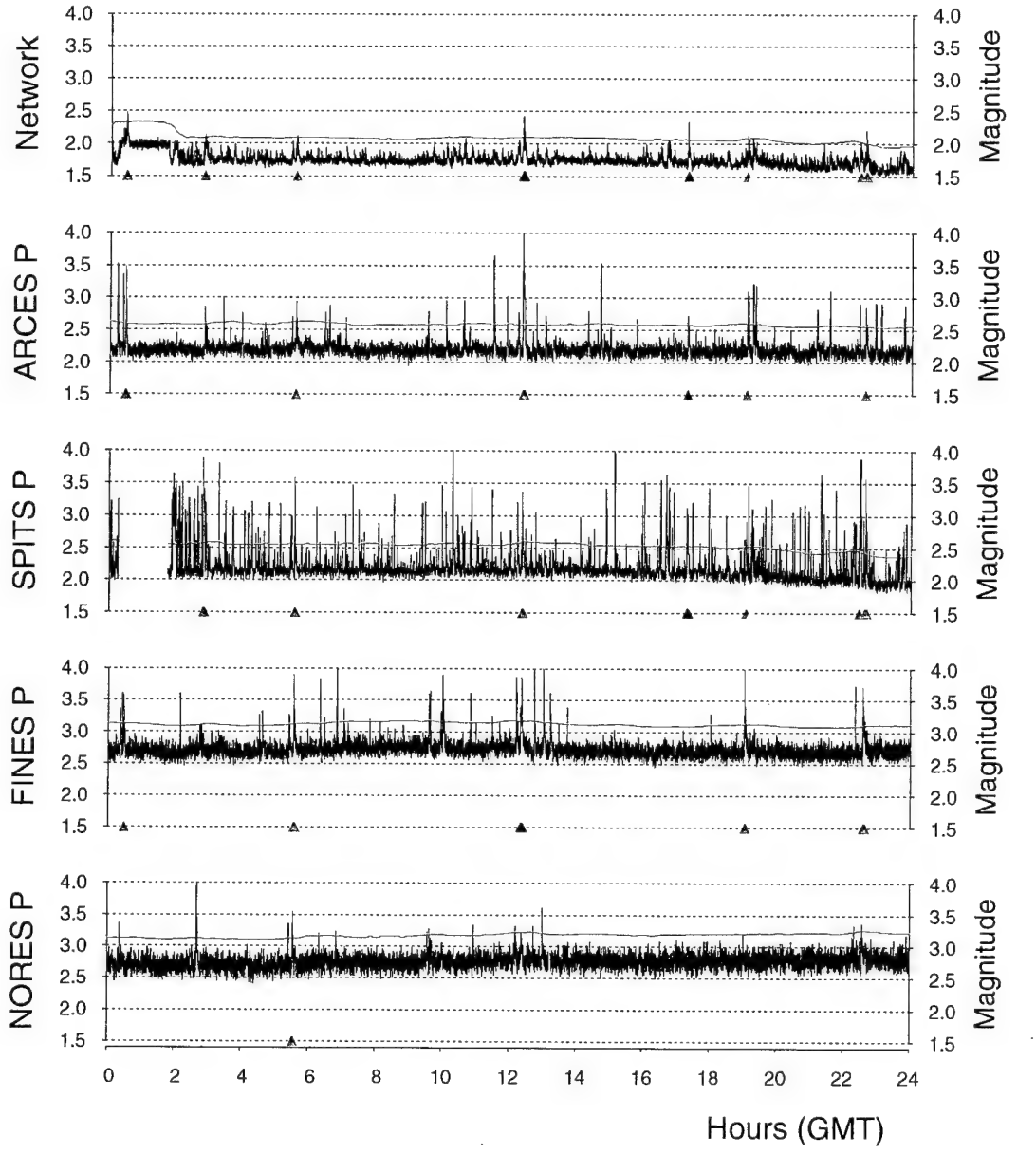

Figure 36. *Summary of threshold monitoring for the location of the event occurring at 17:17 GMT (about 200 km north of the NZ test site). See text for details. The network peak around 13:00 GMT is red because FINES has an associated detection where the azimuth and slowness match the critical range for this location.*

4.5 Discussion.

In our applications of the automatic explanation facility, we have chosen a very conservative approach to identify peaks on the threshold trace that could be subjected to further analysis. In effect, we mark a network peak as "red" if at least one phase from one station has a detection with azimuth and slowness consistent with the target site. In practice, it seems sufficient to make this requirement from one or two of the closest

and most sensitive network arrays (in the case of NZ, it would be ARCES and SPITS). By this alternative approach, the increased resolution of the closest arrays in terms of azimuth to the target site, could be more fully explored. Also, the higher SNR at these two arrays would make the azimuth and slowness estimates more reliable than for the arrays located further away.

A long-term study should be undertaken with the aim to determine the proper criteria for flagging threshold peaks, and in addition verifying the SNR threshold applied to the threshold trace. Time intervals of unusual noise conditions, or when one or several key stations have degraded capability need to be studied in particular detail. It would also be interesting to consider the use of possible available "local" seismic stations to supplement the TM process. This could be done either by including them continuously in the TM calculation, or perhaps more cost-efficiently, extract data from these stations only during times of threshold peaks or other time intervals of special interest.

The benefit of the latter approach was illustrated in **Section 3**, when we extracted 4 hours of data from the GSETT-3 auxiliary station NIL during the alleged time of the Indian nuclear explosions on 13 May 1998. In the case of the Novaya Zemlya test site, there are no readily available local seismic stations, although the AMD station in Northwest Russia could provide data to be used at least for research purposes in such a context.

We have so far not discussed "evasion" scenarios in the context of threshold monitoring. Our basic premise has been to determine the upper magnitude limit of the largest possible "hidden" seismic event, not to try to extract information that would single out such hidden events. Neither have we addressed the feasibility of actually carrying out a clandestine explosion at the time of the threshold peaks. Nevertheless, possible evasion scenarios are important, and it seems that three of these could be discussed in our context:

Hiding a nuclear explosion in the coda of a large earthquake.

In the case of NZ test site, there is essentially no active seismicity within almost 1000 km from the site. Therefore, such a scenario would only apply if a sufficiently large earthquake occurs at a large distance from the test site. The peaks on the TM traces that correspond to such "teleseismic" earthquakes are generally of very short duration, and this is to a large extent a consequence of the rapid drop-off in the earthquake coda at high frequencies. In fact, the short duration of significant energy from teleseismic earthquakes, when monitoring a site using a regional network, is an observation of major importance. Based on these considerations, it would seem unlikely that a potential evader could time the explosion accurately enough to escape detection. Additionally, the current state of "earthquake prediction" adds additional difficulties to this scenario.

Setting off a small nuclear explosion simultaneously (and co-located) with a large mining explosion.

Since there are no active mines at Novaya Zemlya, this scenario is not credible for the NZ test site. However, it is clearly feasible (at least in principle) for active mining areas. If the nuclear explosion is much smaller (in terms of magnitude) than the mining explosion, it would be difficult, if not impossible to identify it by seismic means. The threshold monitoring technique (when applied to the mining area as a "target site") would serve to give the upper limit on the size of such a potential nuclear explosion.

The automatic explanation facility would naturally flag the event as a potential event of interest for the target site, so that it would be subjected to further analysis.

Setting off a small nuclear explosion, with the intent that it would either not be detected, or go unnoticed.

This scenario would, in our opinion, be well handled by the TM technique, in combination with the automatic explanation facility. If the explosion was significant enough to cause a "peak" on the TM trace, it would be flagged as a potentially interesting event and subjected to analysis. If it was too small to cause a peak, the TM trace would provide an upper limit on its size.

Section 5
Continuous Assessment of Upper Limit M_S

5.1 Introduction.

The continuous seismic threshold monitoring technique (TM) is used to provide a continuous assessment of the size of events that may have occurred in a given geographical area. The main application of this technique has until now been restricted to short-period seismic data, both at regional and teleseismic distances.

We have recently initiated an effort to apply the continuous TM technique to long-period data, for the purpose of obtaining a continuous assessment of surface wave magnitude (M_S). In principle, this application is straightforward, but in practice one has to take into account many factors, not all of which apply to the short-period case, such as surface wave dispersion, oceanic versus continental propagation paths, the difficulties in calculating surface wave magnitudes at regional distances, regional calibration formulas for *log(A/T)* vs. *log(STA)* and so on.

Nevertheless, the TM application holds promise to significantly improve monitoring of surface waves. One of the main considerations of TM is that it provides a realistic estimate of network detection thresholds during "unusual" noise conditions, such as in the coda of a large earthquake or during a large aftershock sequence. In the short-period case, we have demonstrated that the global detection capability can deteriorate significantly for many tens of minutes following a large earthquake. In the long-period case, this situation could be expected to be far worse, since surface waves from a large earthquake can last for many hours.

We present initial results from investigating the relation between PIDC station magnitudes and STA based estimates calculated from bandpass filtered data, as well as a case study with monitoring of surface waves from a mining area on the Kola peninsula of Russia during and after a M_S 7.6 earthquake in Turkey.

5.2 TM Measurements of M_S.

When developing a strategy for threshold monitoring of surface waves, we have used the automatic surface wave measurements at the PIDC as the basis. Their procedure consists of the following steps:

- Shape Rayleigh wave observations to a common response type (KS36000)
- Search window for Rayleigh waves derived from regionalized group velocity models
- Measure largest *A/T* with periods between 18 and 22 seconds
- Calculate station magnitudes using the relation of Rezapour and Pearce (1998)

$$M_S = \log(A/T) + \frac{1}{3}\log(\Delta) + \frac{1}{2}\log(\sin(\Delta)) + 0.0046\Delta + 2.730$$

Our experience with threshold monitoring of body waves has shown that short-term averages (*STAs*) can efficiently be used to represent the traditional *A/T* measurements

used for magnitude estimation. We will therefore attempt to adopt a similar procedure for surface waves. Concerning the search window for Rayleigh waves, the PIDC calculate these from a regionalized group velocity model. Currently we do not have this utility at hand and we have therefore chosen to analyze surface wave travel-time observations available in the PIDC database to derive the STA search windows. For threshold monitoring of surface waves we have established the following procedure:

- Bandpass filter data between 17 and 24 seconds, using zero phase Butterworth filter of 2^{nd} order
- Generate short-term averages (*STAs*) with a window length of 30 seconds
- Measure largest *STA* within a search window derived from empirical PIDC data
- Derive *A/T* equivalent from the *STA* observation using station dependent empirical relations between $log(A/T)_{KS36000}$ and *log(STA)*
- Calculate station magnitudes using relation of Rezapour and Pearce (1998)

In **Figure 37** we show the travel-times and group velocities of PIDC M_S measurements at ARCES for continental propagations paths. Notice that a search window spanning the 2.5-3.3 km/s group velocity window covers all observations at ARCES.

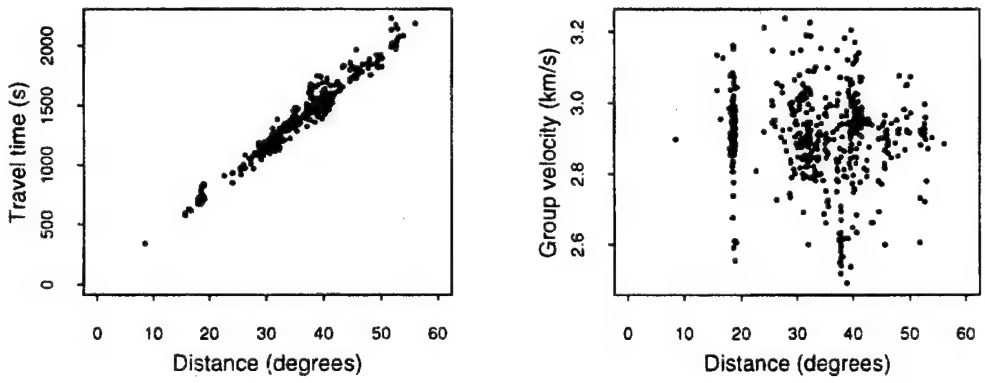

Figure 37. *Travel-times and group velocities of PIDC M_S measurements at ARCES for continental propagations paths.*

Figure 38 shows the relation between a small set of manual *log(A/T)* measurements made on the ARCES KS-36000 instrument, and *log(STA)* made on the same data filtered between 17 and 24 seconds. The difference between *log(A/T)* and *log(STA)* has a scatter with a standard deviation of 0.11 for this small data set, which is satisfactory in view of the scatter inherent in the magnitude-distance relation for surface waves (Rezapour and Pearce (1998)).

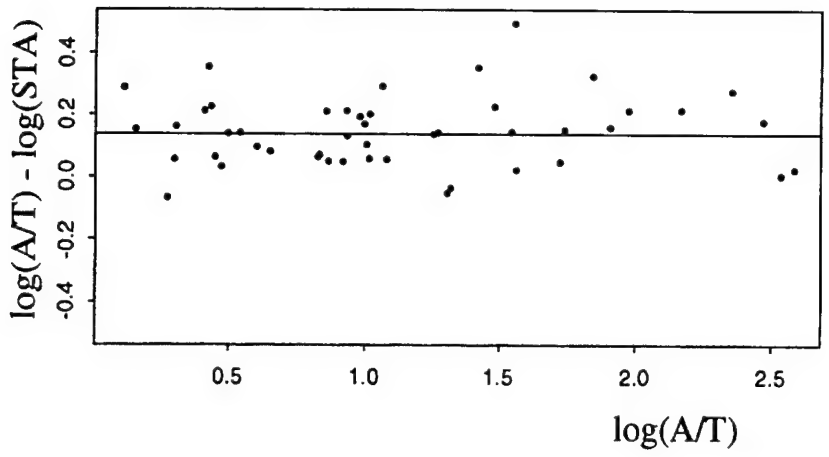

Figure 38. *Difference between manual log(A/T) measurements made on the ARCES KS-36000 instrument, and log(STA) made on the same data filtered between 17 and 24 seconds.*

X-axis: log (A/T). Y-axis: $log(A/T)_{KS36000} - log(\frac{\pi}{2} \cdot STA \cdot \frac{cal_{20}}{20})$*, where* cal_{20} *is the sensitivity in nm at 20 seconds.*

5.3 A First Surface Wave Threshold Monitoring Experiment.

As an example of TM processing of surface wave data, we have selected 17 August 1999, which was the day of the large Turkey earthquake (M_S=7.6). This earthquake was followed by numerous aftershocks, and therefore presents a good opportunity to assess the effects of such a situation on the surface wave detection capability. We focus our investigation on surface waves observed at the three Norwegian IMS stations NOA, ARCES and SPITS, as well as a TM trace based upon joint processing of the data from these three stations.

We have chosen to show a site-specific approach, with a TM beam focused towards the Lovozero Massif, Kola Peninsula. Our reason for selecting this target area is that on the same day, about 4 hours and 40 minutes after the Turkey earthquake, a moderate earthquake (m_b=4.2) occurred in this place. We will in the following show a number of figures illustrating the surface wave observations and the results from surface wave threshold monitoring using two different frequency bands.

Figure 39 shows the locations of the station network, and the locations of the Turkey and Lovozero events.

The seismograms of the Turkey event as recorded at NOA, ARCES and SPITS are shown in **Figure 40.** Different types of seismometers are used at these three stations; NOA - KS54000, ARCES - KS36000, SPITS - CMG-3T, and the epicentral distance to the three stations are 23.4, 28.9, and 37.9 degrees, respectively. Notice that the surface wave observations at ARCES are clipped.

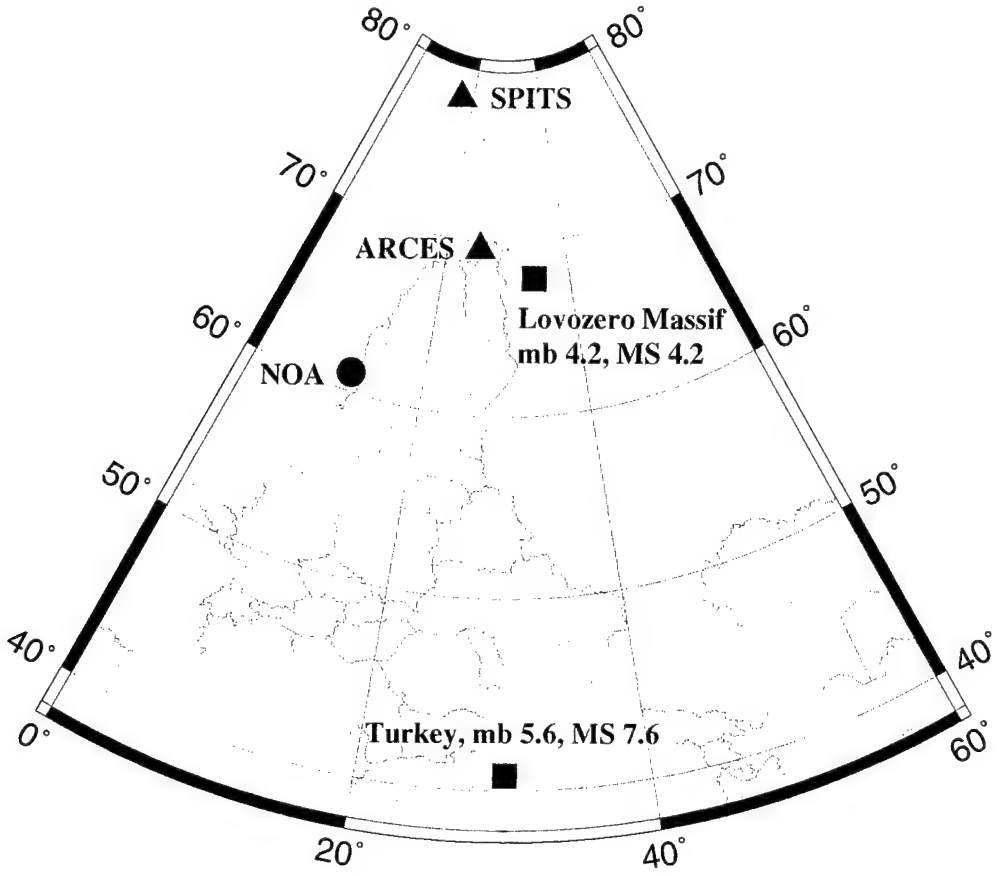

Figure 39. *Map showing the locations of the station network, and the Turkey and Lovozero events.*

Figure 41 shows the same time interval as in **Figure 40**, but now with simulated KS36000 traces at NOA and SPITS. These are the data used for magnitude estimation at the PIDC. Bandpass filtered recordings of the Lovozero event are shown in **Figures 42** and **43**. In the 17 - 24 s band (**Figure 42**), the Rayleigh waves have a low SNR and are only visible at ARCES and NOA. In contrast, clear Rayleigh waves are seen at all stations in the 8 - 12 s period band (**Figure 43**). The epicentral distance to ARCES, SPITS and NOA are 3.7, 11.5 and 12.1 degrees, respectively. Due to differences in the crustal and upper mantle structures, surface waves arrive later at SPITS than at NOA.

The NOA array consists of seven broad-band sensors deployed over an aperture of approximately 60 km. The surface waves from the Lovozero event arrive at NOA with an estimated back-azimuth of 42.4 degrees and an apparent velocity of 3.2 km/s. For the threshold monitoring experiment we beamform the NOA data using the estimated back-azimuth and slowness, resulting in improved SNR in both frequency bands. Based on 20 s Rayleigh wave observations at NOA and the ESDC array in Spain, we estimate a surface wave magnitude of 4.2 of the Lovozero event, using the relation of Rezapour and Pearce (1998).

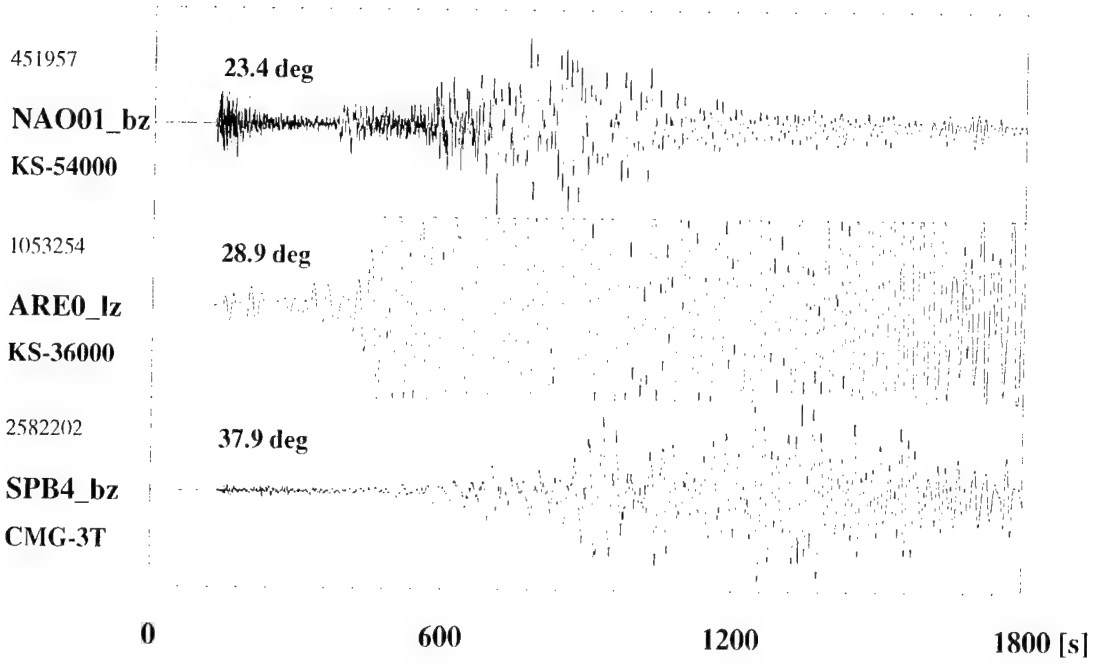

Figure 40. *NOA, ARCES and SPITS recordings of the Turkey event. Different types of seismometers are used: NOA - KS54000, ARCES - KS36000, SPITS - CMG-3T. The epicentral distances are given above each trace.*

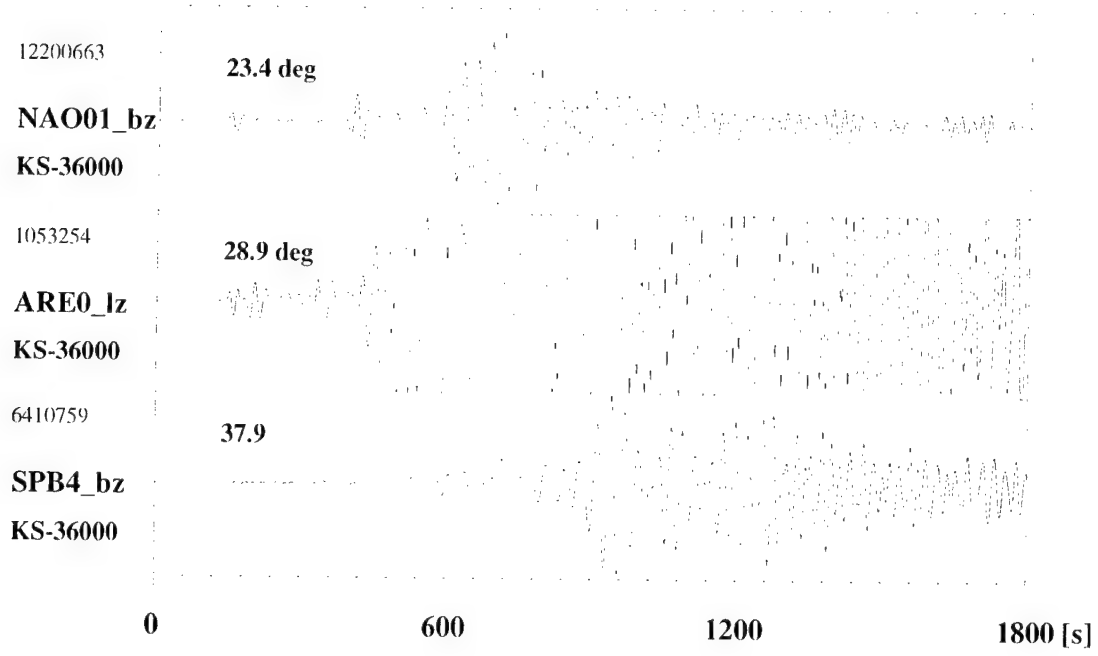

Figure 41. *Simulated KS36000 traces at NOA and SPITS for the Turkey event. The ARCES recording is shown in its original form (KS36000).*

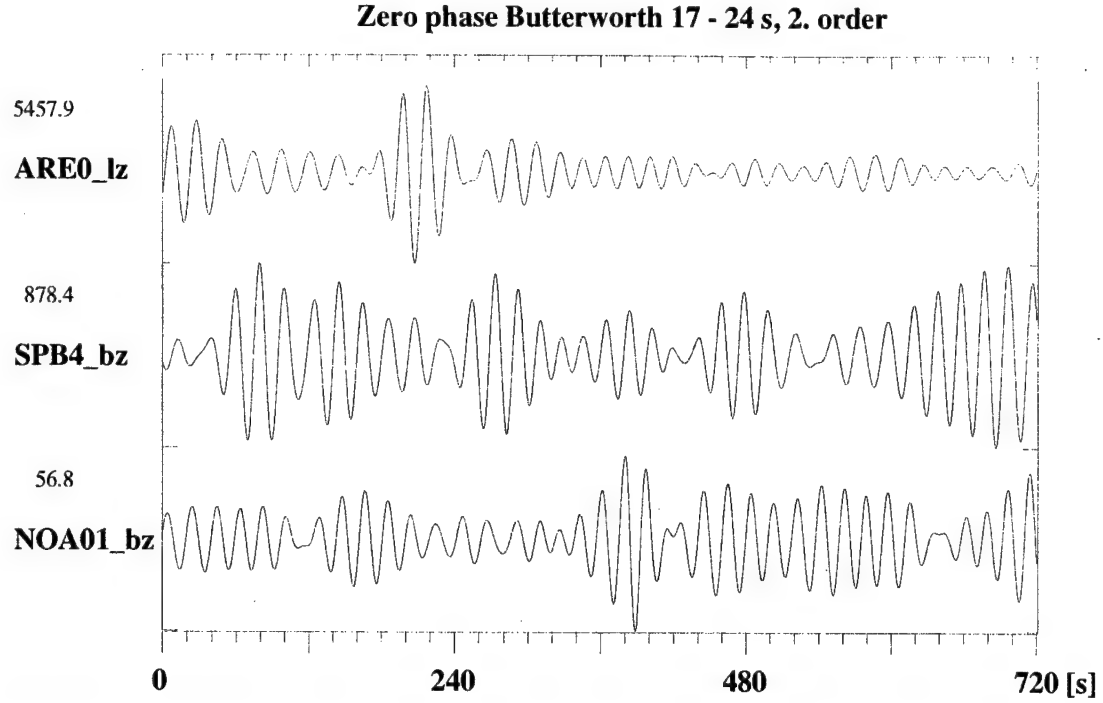

Figure 42. *Bandpass filtered (17 - 24 s) recordings of the Lovozero event.*

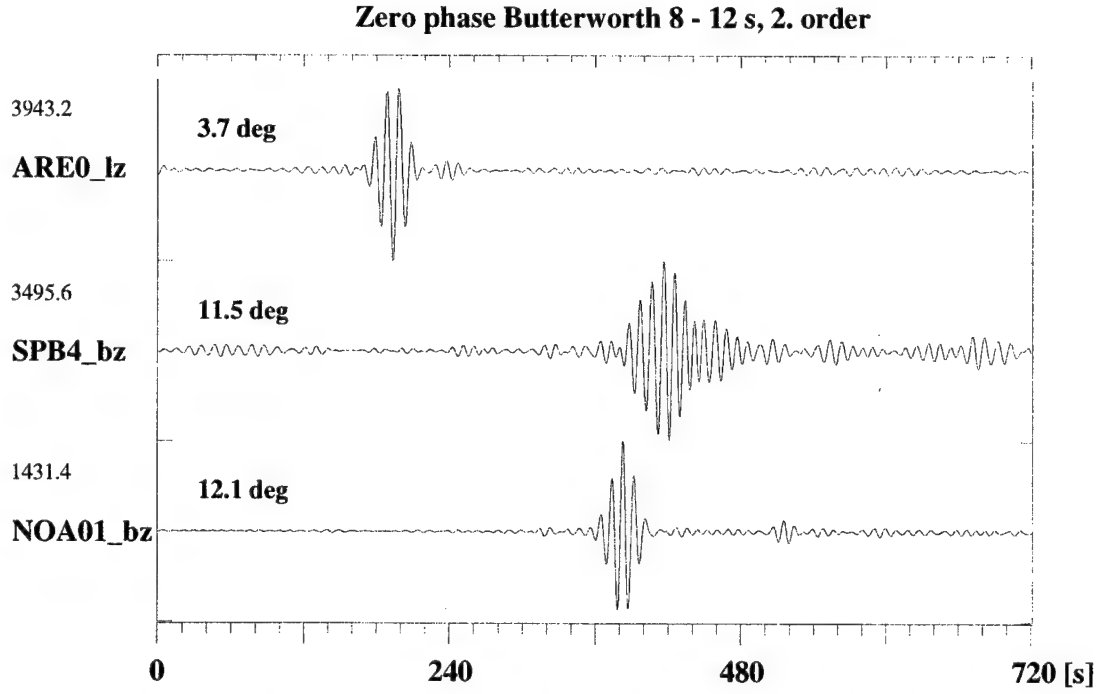

Figure 43. *Bandpass filtered (8 - 12 s) recordings of the Lovozero event. The epicentral distances are given above each trace.*

Using the site-specific threshold monitoring approach for the location of the Lovozero event, we have derived processing parameters such as travel-times, STA lengths, and amplitude-magnitude relations from the actual ARCES, SPITS and NOA observations. The threshold processing results in the "standard" PIDC frequency band (17-24 s) are

shown in **Figure 44**. We see that the surface waves from the Lovozero event are effectively masked by the coda/aftershocks of the Turkey earthquake

However, in a more "high frequency" filter band (8-12 s) the surface waves from the Lovozero event stand out very clearly, see **Figure 45**. This shows that "high frequency" processing of surface waves at regional distances can significantly improve detectability by suppressing the longer period energy from interfering distant earthquakes. **Figure 46** compares the threshold monitoring results for both frequency bands (17-24 and 8-12 s) for a 10 hour time period. This clearly illustrates that the amplitudes of the surface wave coda of the Turkey event decay much more rapidly at higher frequencies.

5.4 Discussion.

The continuous assessment of upper limits on surface wave magnitudes as described in this paper is an entirely new application of the Threshold Monitoring technique. Our results so far must be considered only as a preliminary indication of the potential of the method when applied to long-period seismic recordings, but it is already clear that there are significant possibilities for developing the TM process into a useful monitoring tool for surface waves.

In this study, we have used the three IMS arrays ARCES, NOA and SPITS, and applied a site-specific technique to investigate the threshold trace during a large earthquake sequence. A natural follow-up of this work would be to include additional long-period and broadband IMS stations for the same time interval, in order to assess the improvements in monitoring capability when using a network with better azimuthal coverage. It would also be interesting to steer the threshold beam to other sites, including the site of the earthquake sequence (Turkey), in order to assess the possibility for obtaining magnitude estimates (or upper limits) for individual aftershocks in the sequence.

An important result of this initial study is the demonstration of the significant benefits of using a shorter period band (8-12 seconds) instead of the traditional processing band (17-24 seconds) for processing surface waves at regional distances during an aftershock sequence. In future work, we will investigate further whether the use of this shorter period band could be applicable also during "normal" background noise conditions. In an operational setting, it is clearly an advantage to use a fixed frequency band for each station-site combination, but it requires a careful assessment of the relations between surface wave magnitudes calculated in different frequency bands.

As in the short period case, there is a tradeoff between optimizing the TM process for site-specific studies and developing a more general TM application for global surface wave monitoring. Among the main issues is the sharpness of the beam lobe, which depends upon the filter setting, the STA time windows and the tolerance for travel-time deviations. Another issue is the need for regional corrections, which may be greater than in the short-period case. For example, the significant difference between oceanic, continental and combined oceanic-continental paths are important for surface wave propagation, but have little or no counterpart in analyzing short-period P and S waves.

Since a main purpose of the MS measurements is to provide a basis for MS:mb screening (and discrimination), it is important to assess the effects of using shorter period

surface waves on the MS:mb discrimination potential. Recent studies in the European Arctic (Krementetskaya et. al. (1998)) have demonstrated some promising results using regional LP data from the Apatity long-period station for historic earthquakes and explosions in this region, including past nuclear explosions at Novaya Zemlya. This type of studies should be continued, using available regional recordings for earthquakes and underground nuclear explosions in various regions of the Earth.

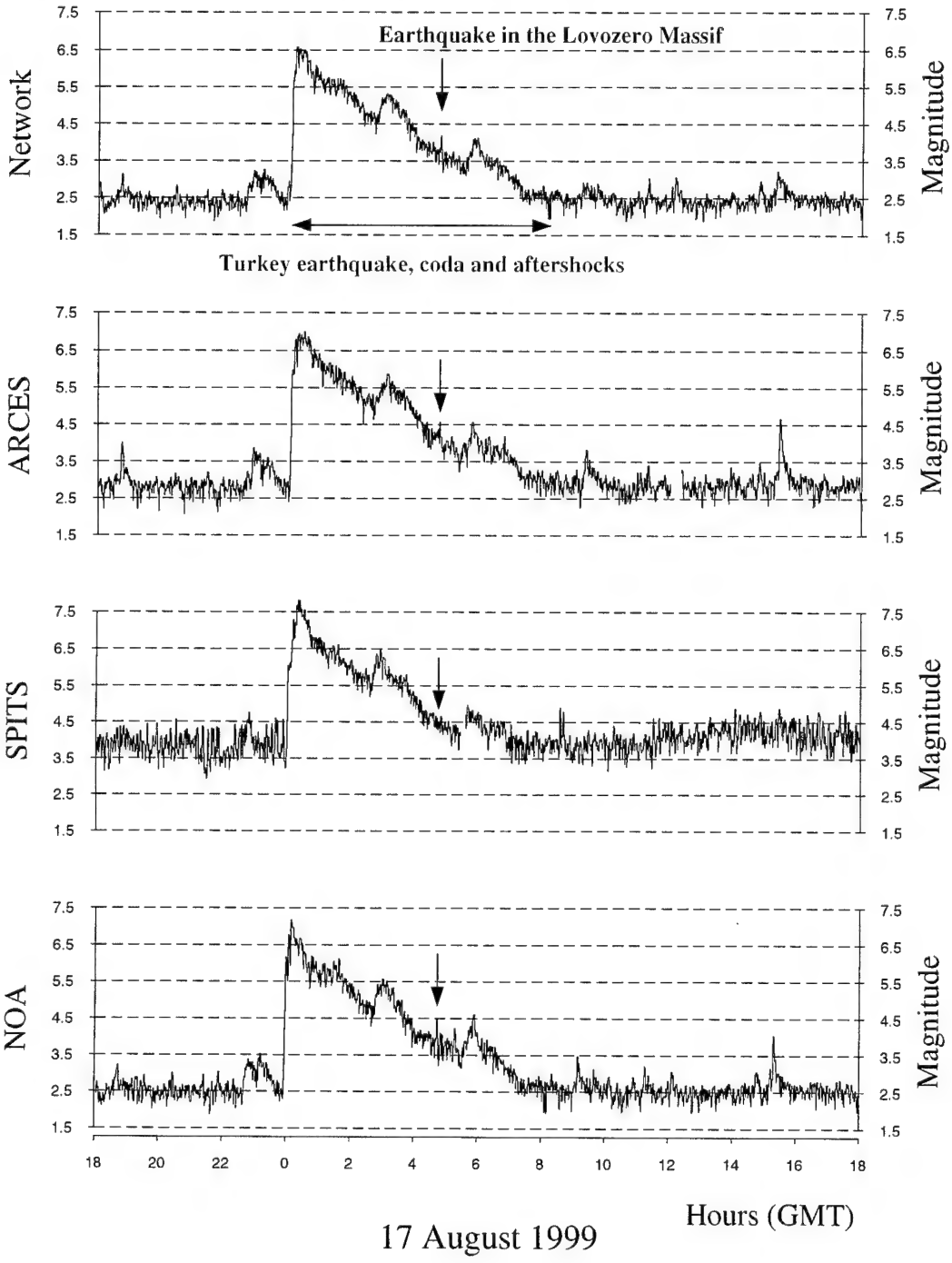

Figure 44. *Surface threshold monitoring for the location of the Lovozero event of17 August 1999, using data filtered between **17** and **24** s. The lower three traces represent thresholds (upper 90% magnitude limits) for each of the three stations; the top trace shows the combined network threshold. The peaks corresponding to the Lovozero event are indicated on each trace.*

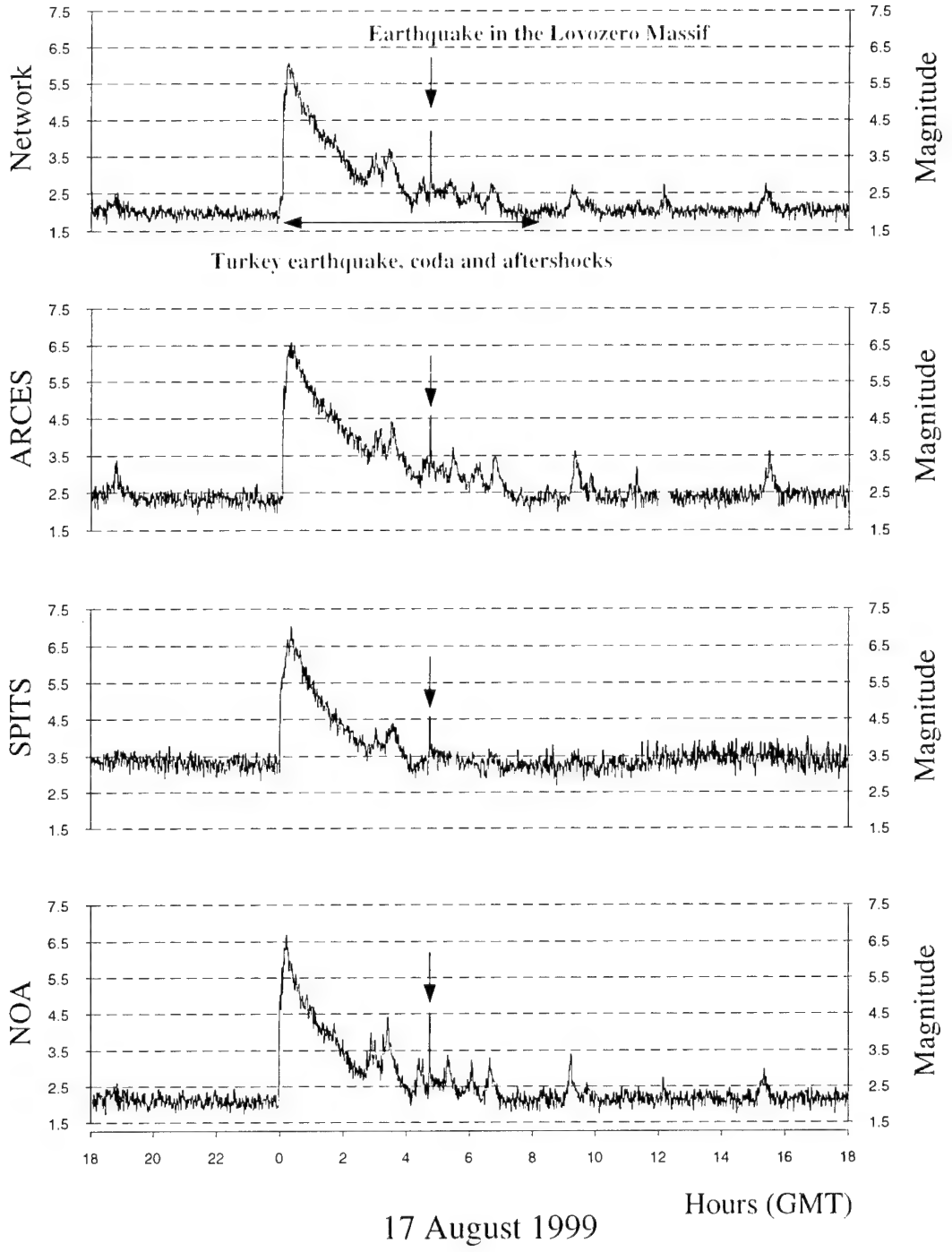

Figure 45. *Surface threshold monitoring for the location of the Lovozero event for 17 August 1999, using data filtered between* ***8*** *and* ***12*** *s. The lower three traces represent thresholds (upper 90% magnitude limits) obtained for each of the three stations, whereas the top trace shows the combined network thresholds. The peaks corresponding to the Lovozero event are indicated on each trace.*

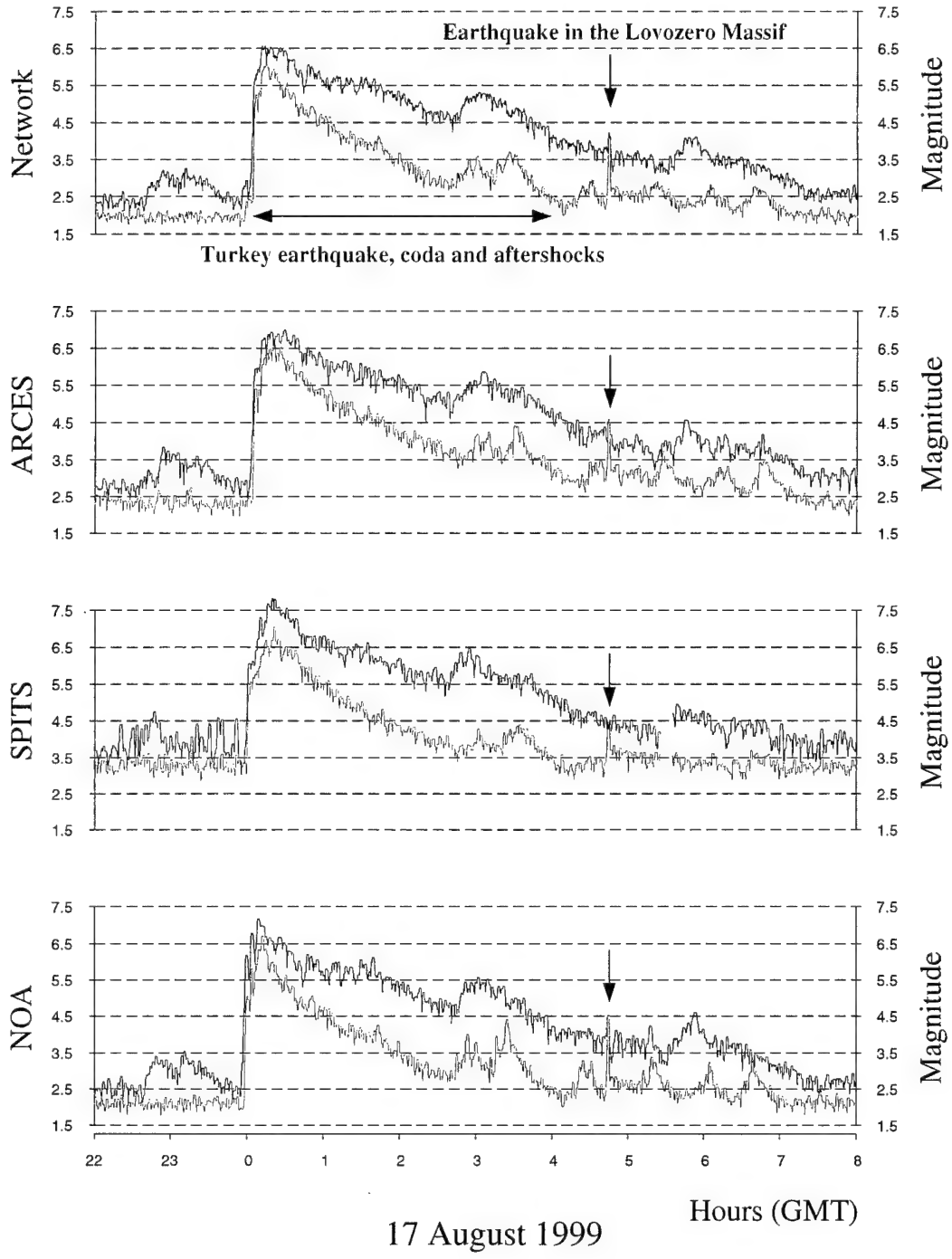

Figure 46. *Comparison between surface wave threshold monitoring using two different filter bands; red: 17 -24 s, green: 8-12 s. See captions of* ***Figure 44*** *and* ***45*** *for details.*

Section 6
CTBT Development

6.1 Introduction.

Experimental utilities for calculation of magnitude thresholds have been available at NORSAR for many years. However, these utilities are based on different types of available software (DP/EP, Splus) as well as experimental C and FORTRAN code, and do not conform with the structure of existing CTBT data processing pipelines.

In 1998 NORSAR released a global variant of the Threshold Monitoring (TM) method to be used for continuous assessment of event detection capability of the CTBT International Monitoring System (IMS). The system is currently running within the continuous processing pipelines at both the International Data Center (IDC) in Vienna, Austria, and the Prototype International Data Center (PIDC) in Arlington, VA, USA. For details on this system we refer to the Operations Manual by Taylor et. al (1998).

The methods developed under this contract are suitable for implementation in a CTBT environment, and we will in this section provide advice on how these could be integrated into the current PIDC processing pipeline. The proposed processing system will hereafter be referred to as the Optimized Site-Specific Threshold Monitoring (OSSTM) system.

6.2 Processing Flow.

Before starting any of the continuous processes within the OSSTM system, the processing environment has to be created. This is quite similar to what the program **CreateTMSession** is doing for the global TM system, and we propose to develop a similar functionality that creates a directory structure <*Session*> containing diskloops for storage of output from all continuous processes, as well as the necessary processing recipes.

The processing within the OSSTM system is logically divided into four parts:

1. Continuous calculation of short-term averages for the stations used for monitoring of the proposed target areas.
2. Continuous calculation of magnitude thresholds for the given target areas. A flowchart of processing steps 1) and 2) is given in **Figure 47**.
3. Analysis of threshold traces to automatically explain the cause of the threshold peaks.
4. Generation of products from the OSSTM system with subsequent presentation on the World-Wide Web.

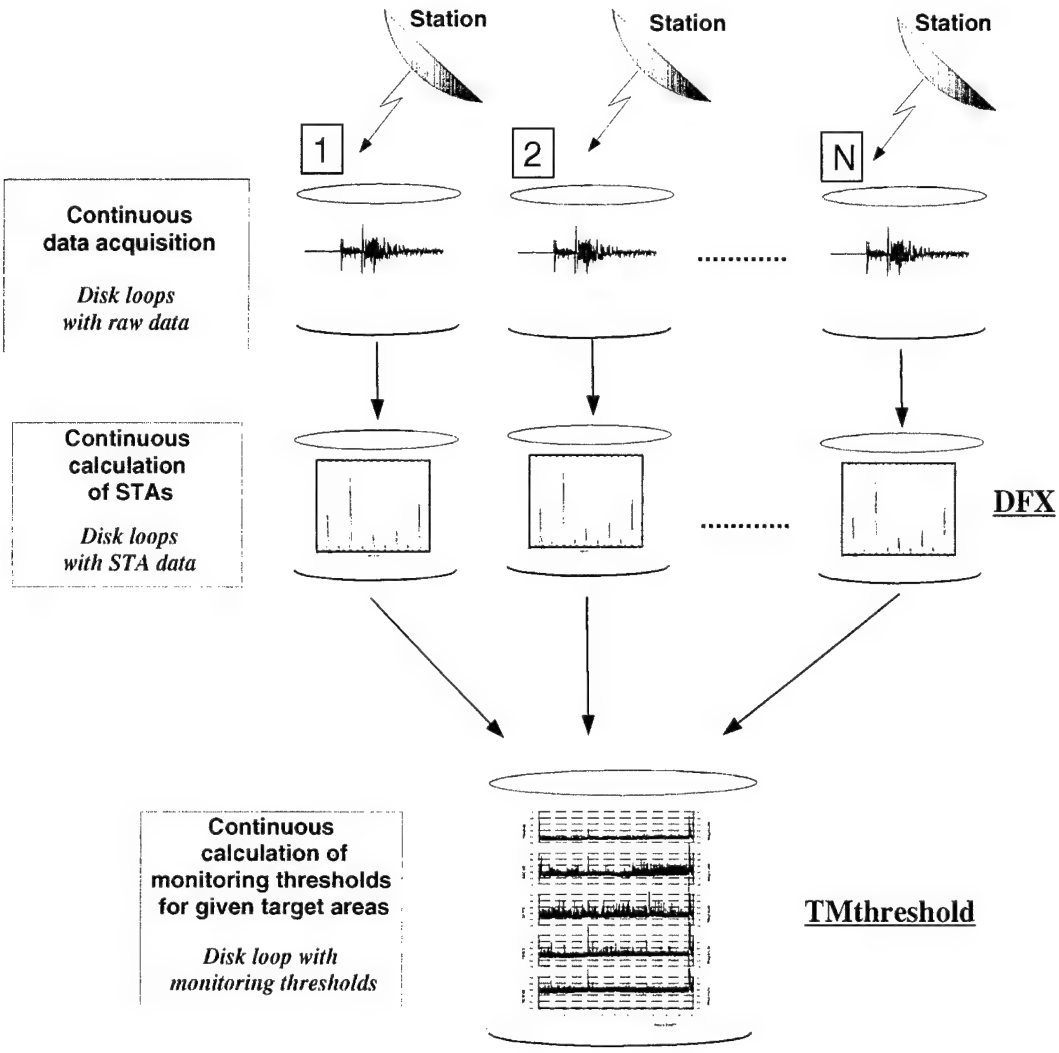

Figure 47. *Flowchart of processing within the proposed OSSTM system. Text in bold describes the different processes, whereas text in italic describes the results and the type of storage. The names of the different processes (programs) are underlined in the figure.*

6.2.1 Calculation of STA Traces.

The calculation of continuous STA traces can be done in parallel with the detection processing using the **DFX** program (*Detection and Feature Extraction*; Wahl (1996a,b)). The **DFX** program is run in the station processing pipeline at the IDC, typically initiating processing of 10 minutes long data segments as soon as complete segments are recorded and available at the IDC. For details on the overall IDC processing flow we refer to the current draft of the IDC operations manual (CTBT/PC/V/WGB/TL/44/Rev.2 (1998)).

In the context of the OSSTM system, **DFX** subjects the raw data to quality control, beamforming (arrays only), bandpass filtering, and short-term-average (STA) calculations. The continuous STA data are then stored onto new diskloops located within the OSSTM processing environment. The sampling interval of the STA diskloops is typi-

cally 1 second. Data gaps and processing gaps are identified by particular *null* values in the diskloops.

DFX must be configured to produce STA traces for the OSSTM system, and the parameter definitions are similar to those of the global TM system, as described by Taylor et. al (1998).

6.2.2 Calculation of MagnitudeThresholds.

The calculation of network magnitude thresholds can be done by the already existing **TMthreshold** program. This program reads the STA diskloops for each of the seismic stations, calculates the 90% magnitude thresholds for each of the selected target areas, and stores the results onto a new diskloop. For the global TM system, **TMthreshold** runs in the so-called SEL-3 pipeline, currently initiating processing of 20 minutes time segments with a time delay of 10 hours behind real-time.

For calculation of network magnitude thresholds for each target area, **TMthreshold** requires extensive information on how to combine the continuous STA data from each of the predefined seismic stations. These recipe files are created during the setup of the processing environment. In addition to the processing recipes, **TMthreshold** picks up a few input parameters either from the command line or from a parameter file. These are:

session_directory	Location of the OSSTM processing environment (required).	
t1	Start time of the processing segment (required).	
t2	End time of the processing segment (required).	
verbose	If present, diagnostics will be printed on stdout (optional).	
method	Processing method (required):	
	upplim	Calculate 90% upper magnitude limit for non-detected events
	detection	Calculate 90% detection threshold.

6.2.3 Automatic Explanation Facility.

A significant amount of coding would be required to develop an automatic explanation facility that can be implemented into the PIDC/IDC processing pipelines. The processing flow of such a program, e.g., called **TMexp**, is shown in **Figure 48**. The automatic explanation facility combines information from several sources to provide information on the cause of the threshold peaks. The input to **TMexp** would be:

- Parameter files and command line arguments
- Continuous magnitude thresholds, computed by **TMthreshold**
- Phase detection information, computed by **DFX**
- Event information found in the Reviewed Event Bulletin (REB)

The output from **TMexp** would typically be daily overviews of threshold levels and threshold peaks as shown in **Figure 34.** In addition, detailed information from the analysis of the threshold peaks as shown in **Figure 32**, **Figure 33** and **Table 13** would be made available.

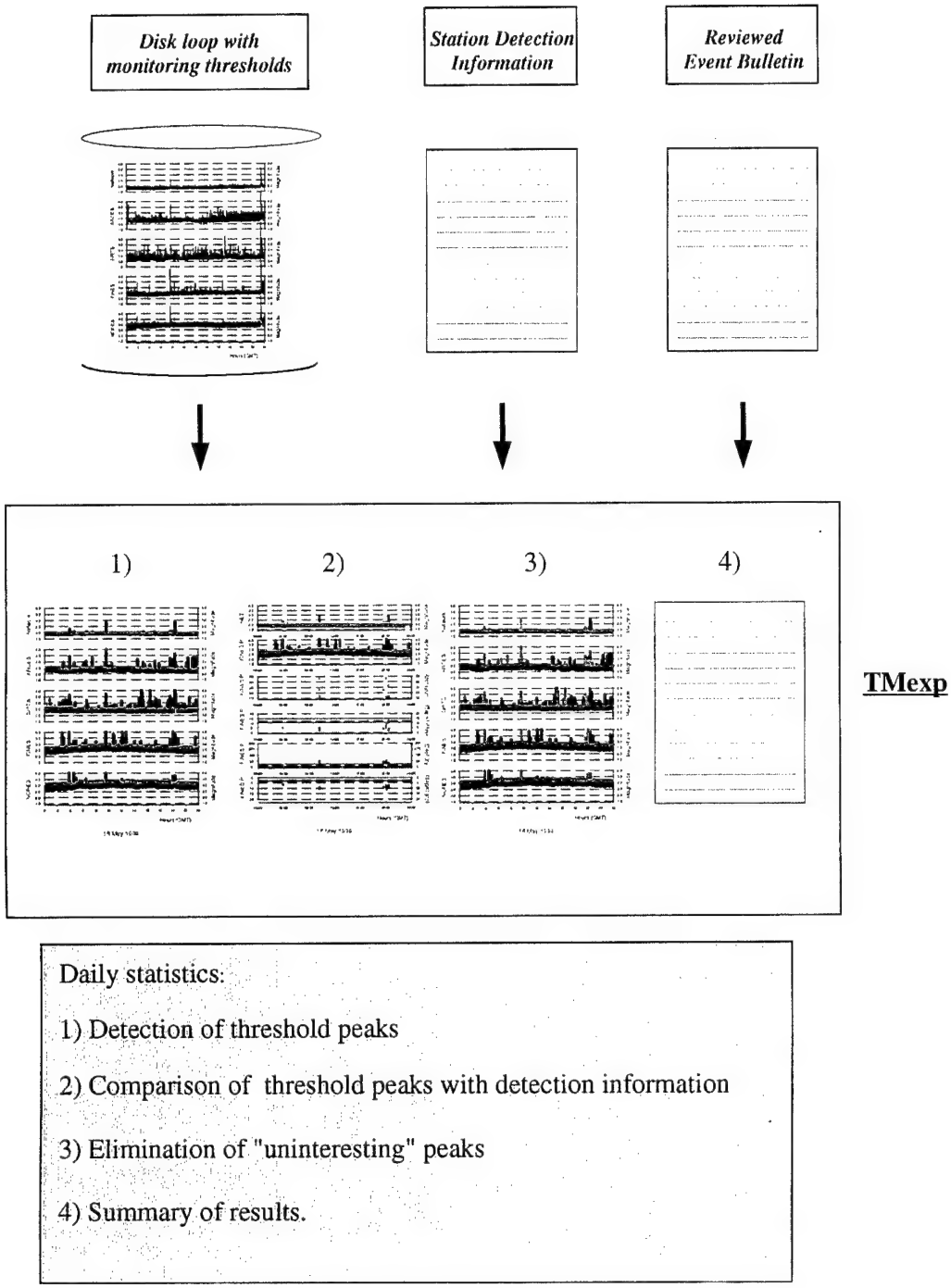

Figure 48. *Flowchart of the proposed process (TMexp) which produces daily statistics from the OSSTM system.*

6.2.4 Generation of Products.

Daily summaries of magnitude thresholds and results from the automatic explanation facility should be made available on the World-Wide Web. In order to accomplish this we need to include a process that converts the graphics from PostScript to a format (e.g., GIF) that is suitable for display using Internet browsers. This would be similar to the process used for the hourly displays of the existing global TM system.

6.3 Surface Wave Monitoring.

The development of surface wave threshold monitoring is still at a starting level, and a significant amount of research and experiments is necessary before the results should be made available as regular products. However, the building blocks described earlier in this section are quite general, and can therefore also be applied to surface waves.

6.4 Comments.

We emphasize that the OSSTM technique could in principle be applied to any target site on the globe. We are not suggesting any particular site to be selected for OSSTM processing in the CTBT environment. In practice, there are many interesting applications of this technique. It could, for example, be applied to monitor earthquake sequences, or to monitor mining sites of special interest. The main point of an operational implementation would be to introduce sufficient flexibility so that it would be a straightforward procedure to apply the technique to a specific target site and a specific time interval of interest.

Section 7
References

Bache, T. B., S. R. Bratt, J. Wang, R. M. Fung, C. Kobryn and J. W. Given (1990). The Intelligent Monitoring System, *Bull. Seism. Soc. Am.*, **80** Part B, 1833-1851. (UNCLASSIFIED)

Barker, B., M. Clark, P. Davis, M. Fisk, M. Hedlin, H. Israelsson, V. Khalturin, W.-Y. Kim, K. McLaughlin, C. Meade, J. Murphy, R. North, J. Orcutt, C. Powell, P. G. Richards, R. Stead, J. Stevens, F. Vernon and T. Wallace (1998). Monitoring Nuclear Tests, *Science* **281**, 1967-1968. (UNCLASSIFIED)

CTBT/PC/V/WGB/TL/44/Rev.2 (1998): Initial Draft of the Operational Manual for the International Data Centre. Preparatory Commision for the Comprehensive Nuclear-Test-Ban Organization, Vienna, 19-30 January 1998. (UNCLASSIFIED)

Hartse, H. E. (1998). The 16 August 1997 Novaya Zemlya Seismic Event as Viewed From GSN Stations KEV and KBS, *Seism. Res. Lett.*, Vol. **69**, No. 3, 206-215. (UNCLASSIFIED)

Kremenetskaya, E., V.Asming, Z. Jevtjugina and F. Ringdal (1998). Study of surface waves and Ms:mb using Apatity LP recordings. *Semiannual Technical Summary 1 April - 30 September 1998*, NORSAR Sci. Rep. 1-98/99, Kjeller, Norway. (UNCLASSIFIED)

Kværna, T., 1996. Tuning of processing parameters for Global Threshold Monitoring at the IDC. Semiannual Tech. Summary, 1 Apr-30 Sep 96, NORSAR Sci. Rep. 1-96/97, NORSAR, Kjeller, Norway. (UNCLASSIFIED)

Kværna, T. and F. Ringdal (1999). Seismic threshold monitoring for continuous assessment of global detection capability, *Bull. Seism. Soc. Am.*, **89**, No. 4, 946-959. (UNCLASSIFIED)

Marshall, P.D., R.C. Stewart and R. C Lilwall (1989). The seismic disturbance of 1986 August 1 near Novaya Zemlya, a source of concern? *Geophys. J. Int.*, **98**, 565-573. (UNCLASSIFIED)

Mykkeltveit, S. and F. Ringdal (1981). Phase identification and event location at regional distance using small-aperture array data.
In: Husebye, E.S. & Mykkeltveit, S. (eds.), 1981: Identification of seismic sources - earthquake or underground explosion. D. Reidel Publishing Company, 467 - 481. (UNCLASSIFIED)

Mykkeltveit, S., F. Ringdal, T. Kværna and R.W. Alewine (1990). Application of Regional Arrays in Seismic Verification Research, *Bull. Seism. Soc. Am.*, **80** Part B, 1777-1800. (UNCLASSIFIED)

Rezapour, M. and R.G. Pearce (1998): Bias in Surface-Wave Magnitude M_S due to Inadequate Distance Corrections. *Bull. Seism. Soc. Am.*, **88**, 43-61. (UNCLASSIFIED)

Richards, P. G. and W. -Y. Kim (1997). Testing the nuclear test ban treaty, *Nature*, **389**, 23 October 1997, 781-782. (UNCLASSIFIED)

Ringdal, F. (1977). P-Wave Amplitudes and Sources of Scattering in m_b-Observations. J. Geophys., 43, 611-622, 1977. (UNCLASSIFIED)

Ringdal,F. (1994). GSETT-3: a test of an experimental international seismic monitoring system, *Annali Geofis.*, **37**, 241-245. (UNCLASSIFIED)

Ringdal, F., 1996. Study of low-magnitude seismic events near the Novaya Zemlya nuclear test site. Semiannual Tech. Summary, 1 Apr-30 Sep 96, NORSAR Sci. Rep. 1-96/97, NORSAR, Kjeller, Norway. (UNCLASSIFIED)

Ringdal, F., 1997. P/S ratios for seismic events near Novaya Zemlya. Semiannual Tech. Summary, 1 Apr-30 Sep 97, NORSAR Sci. Rep. 1-97/98, NORSAR, Kjeller, Norway. (UNCLASSIFIED)

Ringdal, F. & T. Kværna (1989): A multichannel processing approach to real time network detection, phase association and threshold monitoring, *Bull. Seism. Soc. Am.*, 79, 1927-1940. (UNCLASSIFIED)

Ringdal, F. and T. Kværna (1992). Continuous seismic threshold monitoring, *Geophys. J. Int.*, **111**, 505-514. (UNCLASSIFIED)

Ringdal, F., T. Kværna, E. O. Kremenetskaya and V. E. Asming (1997). The seismic event near Novaya Zemlya on 16 August 1997, Semiannual Tech. Summ., 1 April - 30 September 1997, *NORSAR Sci. Rep. 1-97/98,* 110-119, NORSAR, Kjeller, Norway. (UNCLASSIFIED)

Schweitzer, J., F. Ringdal and J. Fyen (1998). The Indian nuclear explosions of 11 and 13 May 1998., Semiannual Tech. Summ., 1 October 1997 - 31 March 1998, *NORSAR Sci. Rep. 2-97/98,* 121-130, NORSAR, Kjeller, Norway. (UNCLASSIFIED)

Taylor, L., T. Kværna and F. Ringdal (1998). Threshold Monitoring Operations Manual, NORSAR Contribution No. 639, NORSAR, Kjeller, Norway. (UNCLASSIFIED)

Veith, K. F., and G. E. Clawson (1972). Magnitude from short-period P-wave data, *Bull. Seism. Soc. Am.*, **62**, 1927-1940. (UNCLASSIFIED)

Wahl, D. (1996a): User's Manual for the Detection and Feature Extraction program (**DFX**). SAIC-96/1098. (UNCLASSIFIED)

Wahl, D. (1996b): Programmer's Guide for the Detection and Feature Extraction program (**DFX**). SAIC-96/1069. (UNCLASSIFIED)

Wallace, T. C. (1998). The May 1998 Indian and Pakistan Nuclear Tests, *Seism. Res. Lett.*, Vol. **69**, No. 5, 386-393. (UNCLASSIFIED)

DISTRIBUTION LIST

DEPARTMENT OF DEFENSE

BALLISTIC MISSILE DEFENSE OFFICE
7100 DEFENSE PENTAGON
WASHINGTON, DC 20301-7100
ATTN: GTS, CAPT S. LEVINSON

DIRECTOR
DEFENSE RESEARCH & ENGINEERING
WASHINGTON, DC 20301-3110
ATTN: DDR&E

DEFENSE TECHNICAL INFORMATION CENTER
8725 JOHN J. KINGMAN ROAD, SUITE 0944
FORT BELVOIR, VA 22060-6218
ATTN: DTIC/OCP

DEFENSE THREAT REDUCTION AGENCY
44965 AVIATION DRIVE
DULLES, VA 20166-7517
ATTN: TDCN, DR A. DAINTY

DEFENSE THREAT REDUCTION AGENCY
6801 TELEGRAPH ROAD
ALEXANDRIA, VA 22310-3398
ATTN: CSOB, P. HEBERT
ATTN: TD, DR D. LINGER
ATTN: TDANP, TRC
ATTN: TDC, M. SHORE
ATTN: TDCN, R. JIH
ATTN: TDS, DR C. GALLAWAY

OASD (C3I)
WASHINGTON, DC 20301
ATTN: MS D. ROSELL, ROOM 1E814

DEPARTMENT OF DEFENSE CONTRACTORS

ACIS
6T11 NHB
WASHINGTON, DC 20505
ATTN: LAWRENCE TURNBULL
ATTN: NTMT, MS TARA HARDIMAN

BATTELLE MEMORIAL INSTITUTE
MUNITIONS & ORDNANCE CTR
505 KING AVENUE
COLUMBUS, OH 43201-2693
ATTN: TACTEC

BBN CORPORATION
1300 N. 17TH STREET, SUITE 1200
ARLINGTON, VA 22209
ATTN: H. FARRELL
ATTN: J. PULLI

BDM CORPORATION OF SAUDI ARABIA
12150 EAST MONUMENT DRIVE, SUITE 501
FAIRFAX, VA 22033-4050
ATTN: J. STOCKTON, JB 4C22
ATTN: R. FINNO, JB 4C15

CALIFORNIA, UNIVERSITY AT SAN DIEGO
SCRIPPS INSTITUTION OF OCEANOGRAPHY
P. O. BOX 6049
SAN DIEGO, CA 92166-6049
ATTN: C. DEGROOT-HEDLIN
ATTN: DR M. A. H. HEDLIN
ATTN: PROF F. VERNON
ATTN: PROF J. A. ORCUTT
ATTN: PROF J. BERGER

CENTER FOR MONITORING RESEARCH
1300 N, 17TH STREET, SUITE 1450
ARLINGTON, VA 22209
ATTN: DR K. L. MCLAUGHLIN
ATTN: DR R. NORTH
ATTN: LIBRARIAN
ATTN: V. RYABOY

CTB TREATY MANAGER
ROSSLYN GATEWAY
1901 N. MOORE STREET, SUITE 609
ARLINGTON, VA 22209
ATTN: DR R. W. ALEWINE, III

ENSCO, INC
445 PINEDA COURT
MELBOURNE, FL 3940
ATTN: DR D. TAYLOR

ENSCO, INC.
P. O. BOX 1346
SPRINGFIELD, VA 22151-0346
ATTN: D. BAUMGARDT
ATTN: Z. DER

GEOPHEX, LTD.
WESTON GEOPHYSICAL
325 WEST MAIN STREET
NORTHBOROUGH, MA 01532
ATTN: DR D. REITER
ATTN: MR J. LEWKOWICZ

ITT INDUSTRIES
ITT SYSTEMS CORPORATION
ATTN: AODTRA/DTRIAC
1680 TEXAS STREET, SE
KIRTLAND AFB, NM 87117-5669
ATTN: DTRIAC
ATTN: DTRIAC/DARE

JAYCOR
1410 SPRING HILL ROAD, SUITE 300
MCLEAN, VA 22102
ATTN: DR C. P. KNOWLES

LOGICON RDA
6940 S. KINGS HIGHWAY, SUITE 202
ALEXANDRIA, VA 22310
ATTN: T. SANDIN

MAXWELL LABORATORIES, INC.
S-CUBED WASHINGTON RESEARCH OFFICE
11800 SUNRISE VALLEY DRIVE, SUITE 1212
RESTON, VA 22091
ATTN: DR T. J. BENNETT

MAXWELL TECHNOLOGIES INC
SYSTEMS DIVISION
9210 SKY PARK COURT
SAN DIEGO, CA 92123-4302
ATTN: DR J. L. STEVENS
ATTN: DR G. E. BAKER

MISSION RESEARCH CORPORATION
8560 CINDERBED ROAD, SUITE 700
NEWINGTON, VA 22122
ATTN: DR M. FISK

MULTIMAX, INC
1441 MCCORMICK DRIVE
LANDOVER, MD 20785
ATTN: DR I. N. GUPTA
ATTN: DR W. CHAN
ATTN: MS L. GRANT

NORSAR
POST BOX 51
N-2027 KJELLER, NORWAY
ATTN: DR T. KVAERNA

PACIFIC NORTHWEST LABORATORIES
A DIV OF BATTELLE MEMORIAL INST
P O BOX 999
RICHLAND, MA 99352
ATTN: TECHNICAL STAFF, MS K5-12

S-CUBED
A DIVISION OF MAXWELL LABS, INC
11800 SUNRISE VALLEY DRIVE, SUITE 1212
RESTON, VA 22091
ATTN: J. MURPHY

SCIENCE APPLICATION INT'L CORPORATION
3309 NW GOLDEN PLACE
SEATTLE, WA 98117
ATTN: A. RATLETON

SCIENCE APPLICATIONS INT'L CORPORATION
10260 CAMPUS POINT DRIVE
SAN DIEGO, CA 92121-1578
ATTN: DR T. C. BACHE, JR.
ATTN: DR T. J. SERENO, JR.

SOUTHERN METHODIST UNIVERSITY
DEPT OF GEOLOGICAL SCIENCE
P. O. BOX 395
DALLAS, TX 75275-0395
ATTN: DR B. STUMP
ATTN: E. HERRIN

ST LOUIS UNIVERSITY
P. O. BOX 8148
PIERRE LACLEDE STATION
ST LOUIS, MO 63156-8148
ATTN: PROF B. HERRMANN
ATTN: PROF B. J. MITCHELL

TEXAS, UNIVERSITY AT AUSTIN
P. O. BOX 7726
AUSTIN, TX 78712
ATTN: C. A.. FROELICH

WOODWARD-CLYDE CONSULTANTS
566 EL DORADO STREET
PASADENA, CA 91109-3245
ATTN: DR B. B. WOODS
ATTN: DR C. K. SAIKIA

DEPARTMENT OF ENERGY

DEPARTMENT OF ENERGY
1000 INDEPENDENCE AVENUE SW
WASHINGTON, DC 20585
ATTN: NN-42, MR A. SCHEINMANN

UNIVERSITY OF CALIFORNIA
LAWRENCE LIVERMORE NATIONAL LAB
P. O. BOX 808
LIVERMORE, CA 94551-9900
ATTN: K. NAKANISHI
ATTN: W. J. HANNON, JR, L-103
ATTN: DR J. ZUCCA, L-205
ATTN: M. DENNY, L-205
ATTN: J. SWEENEY, L-208
ATTN: TECHNICAL STAFF, MS L-200
ATTN: TECHNICAL STAFF, MS L-208
ATTN: TECHNICAL STAFF, MS-205

LOS ALAMOS NATIONAL LABORATORY
P. O. BOX 1663
LOS ALAMOS, NM 87545
ATTN: F. CHAVEZ, MS-D460
ATTN: D STEEDMAN MS-F 607
ATTN: TECHNICAL STAFF, MS C335
ATTN: TECHNICAL STAFF, MS D460
ATTN: TECHNICAL STAFF, MS F665

PACIFIC NORTHWEST NATIONAL
LABORATORY
P. O. BOX 999
BATTELLE BOULEVARD
RICHLAND, WA 99352
ATTN: D. N. HAGEDORN, MS K5-12

SANDIA NATIONAL LABORATORIES
ATTN: MAIL SERVICES
P. O. BOX 5800
ALBUQUERQUE, NM 87185-0459
ATTN: DR R. GOUGH, MS 0419
ATTN: TECHNICAL STAFF, DEPT 5704, MS 0655
ATTN: TECHNICAL STAFF, DEPT 5704, MS 0979
ATTN: TECHNICAL STAFF, DEPT 5736, MS 0655
ATTN: TECHNICAL STAFF, DEPT 9311, MS 1159

SEISMOLOGICAL LABORATORY 252-21
CALIFORNIA INSTITUTE OF TECHNOLOGY
PASADENA, CA 91125
ATTN: T. AHERNS

UNIVERSITY OF CALIFORNIA
EARTH SCIENCE DIVISION
479 MCCONE HALL, LBNL, 90-2106
BERKELEY, CA 94720
ATTN: LANE JOHNSON, MS 90-1116

DEPARTMENT OF THE AIR FORCE

HEADQUARTERS
AFTAC/TTR
1030 SOUTH HIGHWAY A1A
PATRICK AFB, FL 32925-3002
ATTN: V. HSU

AIR FORCE RESEARCH LABATORY
29 RANDOLPH ROAD
HANSCOM AFB, MA 01731-5000
ATTN: DR D. HARKRIDER
ATTN: DR D. REITER
ATTN: GPE, J. LEWKOWICZ

AIR FORCE RESEARCH LABORATORY
5 WRIGHT STREET
HANSCOM AFB, MA 01731-3004
ATTN: RESEARCH LIBRARY/TL

AIR FORCE TECHNICAL APPLICATIONS
CENTER
1300 17TH STREET, SUITE 1450
ARLINGTON, VA 22209
ATTN: R. BLANDFORD

AIR FORCE TECHNICAL APPLICATIONS CTR/TT
1030 S. HIGHWAY AIA
PATRICK AFB, FL 32925-3002
ATTN: CA/STINFO
ATTN: DR B. KEMERAIT
ATTN: DR D. RUSSELL
ATTN: G. ROTHE, TTR
ATTN: MR M. SIBOL

DIRECTORY OF OTHER (LIBRARIES AND UNIVERSITIES)

UNIVERSITY OF ARIZONA
DEPARTMENT OF GEOSCIENCES/SASO
TUCSON, AZ 85721
ATTN: PROF T. C. WALLACE

BOISE STATE UNIVERSITY
GEOSCIENCES DEPARTMENT
1910 UNIVERSITY DRIVE
BOISE, ID 83725
ATTN: J. E. ZOLLWEG

BOSTON COLLEGE
INSTITUTE FOR SPACE RESEARCH
140 COMMONWEALTH AVENUE
CHESTNUT HILL, MA 02167
ATTN: PROF L. SYKES

CALIFORNIA INSTITUTE OF TECHNOLOGY
DIVISION OF GEOLOGY &
PLANETARY SCIENCES
PASADENA, CA 91125
ATTN: PROF D. V. HELMBERGER

UNIVERSITY OF CALIFORNIA - DAVIS
DAVIS, CA 95616
ATTN: R. H. SHUMWAY, DIV STATISTICS

UNIVERSITY OF CALIFORNIA - SANTA CRUZ
INSTITUTE OF TECTONICS
SANTA CRUZ, CA 95064
ATTN: DR. R. S. WU
ATTN: PROF T. LAY

UNIVERSITY OF COLORADO - BOULDER
BOULDER, CO 80309
ATTN: M. RITZWOLLER, CAMPUS BOX 390
ATTN: PROF C. ARCHAMBEAU

UNIVERSITY COLUMBIA
LAMONT-DOHERTY EARTH OBSERVATORY
PALISADES, NY 10964
ATTN: DR L. R. SYKES
ATTN: DR J. XIE
ATTN: PROF P. G. RICHARDS

UNIVERSITY OF CONNECTICUT
DEPARTMENT OF GEOLOGY & GEOPHICS
STOORS, CT 06269-2045
ATTN: PROF V. F. CORMIER, U-45,
ROOM 207

CORNELL UNIVERSITY
DEPARTMENT OF GEOLOGICAL SCIENCES
3126 SNEE HALL
ITHACA, NY 14853
ATTN: PROF M. BARAZANGI

HARVARD UNIVERSITY
HOFFMAN LABORATORY
20 OXFORD STREET
CAMBRIDGE, MA 02138
ATTN: PROF A. DZIEWONSKI
ATTN: PROF G. EKSTROM

IRIS
1200 NEW YORK AVENUE, NW, SUITE 800
WASHINGTON, DC 20005
ATTN: DR D. SIMPSON
ATTN: DR G. E. VAN DER VINK

MASSACHUSETTS INSTITUTE
OF TECHNOLOGY
EARTH RESOURCES LABORATORY
42 CARLETON STREET
CAMBRIDGE, MA 02142
ATTN: PROF M. N. TOKSOZ

MICHIGAN STATE UNIVERSITY LIBRARY
450 ADMINISTRATION BUILDING
EAST LANSING, MI 48824
ATTN: K. FUJITA

NEW MEXICO STATE UNIVERSITY
DEPARTMENT OF PHYSICS
LAS CRUCES, NM 88003
ATTN: PROF J. NI
ATTN: PROF T. HEARN

PENNSYLVANIA STATE UNIVERSITY
GEOSCIENCES DEPARTMENT
403 DEIKE BUILDING
UNIVERSITY PARK, PA 16802
ATTN: PROF C. A. LANGSTON
ATTN: PROF S. ALEXANDER

SAN DIEGO STATE UNIVERSITY
DEPARTMENT OF GEOLOGICAL SCIENCES
SAN DIEGO, CA 92182
ATTN: PROF S. M. DAY

SOUTHERN METHODIST UNIVERSITY
FONDREN LIBRARY
DALLAS, TX 75275
ATTN: B. STUMP
ATTN: G. MCCARTOR,
DEPARTMENT OF PHYSICS
ATTN: H. L. GRAY,
DEPARTMENT OF STATISTICS

UNIVERSITY OF COLORADO
CAMPUS BOX 583
BOULDER, CO 80309
ATTN: DR A. L. LEVSHIN

UNIVERSITY OF SOUTHERN CALIFORNIA
520 SEAVER SCIENCE CENTER
UNIVERSITY PARK
LOS ANGELES, CA 90089-0483
ATTN: PROF C. G. SAMMIS

FOREIGN

AUSTRALIAN GEOLOGICAL SURVEY
ORGANIZATION
CORNER OF JERRAGOMRRRA &
NINDMARSH DRIVE
CANBERRA, ACT 2609
AUSTRALIA
ATTN: D. JEPSON

GEOPHYSICAL INSTITUTE OF ISRAEL
HAMASHBIR STREET, 1
HOLON, 58122 ISRAEL
ATTN: DR Y. GITTERMAN

I.R.I.G.M. - B.P. 68
38402 ST. MARTIN D'HERES
CEDEX, FRANCE
ATTN: DR M. BOUCHON

MINISTRY OF DEFENSE/
PROCUREMENT EXECUTIVE
ALACKNESS, BRIMPTON
READING FG7-4RS ENGLAND
ATTN: DR P. MARSHALL

NTNF/NORSAR
P. O. BOX 51
N-2007 KJELLER, NORWAY
ATTN: DR F. RINGDAL
ATTN: T. KVAERNA

OBSERVATOIRE DE GRENOBLE
I.R.I.G.M. - B.P. 53
38041 GRENOBLE, FRANCE
ATTN: DR M. CAMPILLO

RESEARCH SCHOOL OF EARTH SCIENCES
INSTITUTE OF ADVANCES STUDIES
G. P. O. BOX 4
CANABERRA 2601, AUSTRALIA
ATTN: PROF B. L. N. KENNETT

RUHR UNIVERSTY/BOCHUM
INSTITUTE FOR GEOPHYSIK
P. O. BOX 102148
463 BOCHUM 1, GERMANY
ATTN: PROF H. P. HARJES

SEISMOLOGICAL DIVISION
IRPG
P.O. BOX 2286
HOLON 58122
ISRAEL
ATTN: A. SHAPIRA

SOCIETE RADIOMANA
27 RU CLAUDE BERNARD
75005 PARIS, FRANCE
ATTN: DR B. MASSINON
ATTN: DR P. MECHLER

UNIVERSITY OF BERGEN
INSTITUTE FOR SOLID EARTH PHYSICS
ALLEGATION 40
N-5007 BERGEN, NORWAY
ATTN: R. E. HUSEBYE

UNIVERSITY OF CAMBRIDGE
DEPARTMENT OF EARTH SCIENCES
MADINGLEY RISE, MADINGLEY ROAD
CAMBRIDGE CB3 0EZ, ENGLAND
ATTN: PROF K. PRIESTLEY

OTHER GOVERNMENT

NATIONAL ARCHIVES & RECORDS
ADMINISTRATION
8601 ADELPHI ROAD, ROOM 3360
COLLEGE PARK, MD 20740-6001
ATTN: USER SERVICE BRANCH

U.S. DEPARTMENT OF STATE
OFFICE OF VERIFICATION AND COMPLIANCE
BUREAU OF ARMS CONTROL
2201 C. STREET, NW
WASHINGTON, DC 20520
ATTN: MA, G. CHAVETZ
ATTN: MR G. SATEIA

US GEOLOGICAL SURVEY
ADVANCED SYSTEMS CENTER
MS 562
RESTON, VA 20192
ATTN: DR J. FILSON
ATTN: W. LEITH